Numerical Study of Aerosol Deposition in a Realistic Human Lung in Different Body Orientations

A thesis submitted in partial fulfillment of the requirements for the degree of

Master of Science in Mechanical Engineering



By

Turag Dev

22MME026F

Supervised by

Dr. Prasanjit Das

Professor, Dept. of ME, CUET

APPROVAL

The thesis titled "**Numerical Study of Aerosol Deposition in a Realistic Human Lung in Different Body Orientations**" submitted by **Turag Dev (ID:22MME026)** has been accepted as satisfactory by the dissertation committee for the partial fulfillment of the requirement for the degree of Master of Science (M.Sc.) in Mechanical Engineering, dated on 23rd July 2025.

Dissertation Committee	
_____ Dr. Prasanjit Das Professor, Department of Mechanical Engineering, CUET.	Chairman (Supervisor)
_____ Dr. Tilok Kumar Das Professor, Department of Mechanical Engineering, CUET.	Member (Co-Supervisor)
_____ Head, Department of Mechanical Engineering, CUET.	Member (Ex-Officio)
_____ Dr. Mahbubul Alam Professor, Department of Mechanical Engineering, CUET.	Member (Internal)
_____ Dr. Md. Mamunur Roshid Professor, Department of Mechanical Engineering, CUET.	Member (Internal)
_____ Dr. A. B. M. Toufique Hasan Professor, Department of Mechanical Engineering, BUET.	Member (External)

Declaration

I hereby declare that the work in this thesis has not been previously submitted to meet the requirements for an award at this or any other higher education institution. To the best of my knowledge and belief, the thesis contains no material previously published or written by another person except where due reference is cited. Furthermore, the thesis complies with the PLAGIARISM and ACADEMIC INTEGRITY regulations of CUET.

Turag Dev

(ID:22MME026F)

Department of Mechanical Engineering

Chittagong University of Engineering & Technology (CUET)

Copyright © Turag Dev, 2025

This work may not be copied without permission of the author or

Chittagong University of Engineering & Technology.

Approval by the Supervisor

This is to certify that Turag Dev (ID:22MME026F) has carried out this work under my supervision, and he has fulfilled the relevant academic ordinances of the Chittagong University of Engineering and Technology and is therefore qualified to submit the following thesis in application for the degree of Master of Science in Mechanical Engineering. Furthermore, the thesis complies with the plagiarism and academic integrity regulations of CUET.

Dr. Prasanjit Das

Professor

Department of Mechanical Engineering

Chittagong University of Engineering & Technology

Abstract

The success of targeted drug delivery through inhalation largely depends on the efficient deposition of aerosols across different regions of the human lung. Factors such as particle size, airflow dynamics, lung geometry, and body posture have a significant influence on aerosol transport and deposition. This computational fluid dynamics (CFD)-based study investigates the combined effects of body orientation and particle size on aerosol deposition using a realistic lung geometry reconstructed from computed tomography (CT) images and a realistic aerosol breathing profile derived from patient data. Simulations were conducted in ANSYS Fluent using the Discrete Phase Model (DPM) for five particle sizes (3, 5, 7, 9, and 10 μm) across three body orientations: upright, dorsal, and lateral.

Results showed that total deposition efficiency increased with particle size, while regional deposition varied noticeably with posture. The right lung consistently exhibited higher deposition than the left, and the upper lobes of both lungs received the majority of particles, particularly for larger aerosols. Although overall deposition efficiency remained similar across orientations, regional redistribution was evident. These findings highlight how body posture influences aerosol transport within the lungs and offer valuable insights for optimizing posture-based inhalation strategies and improving targeted drug delivery.

সারসংক্ষেপ

প্রশ্বাসের মাধ্যমে ফুসফুসের নির্দিষ্ট স্থানে ঔষধ প্রেরণের সাফল্য বহুলাংশে নির্ভর করে অ্যারোসলের কণিকাগুলোর ফুসফুসের বিভিন্ন অঞ্চলে যথাযথভাবে পৌঁছানো এবং সেখানে অবক্ষিপ্ত হওয়ার উপর। কণার আকার, শ্বসনজনিত বায়ুপ্রবাহের গতি, ফুসফুসের গঠন এবং ব্যক্তির শারীরিক ভঙ্গির মতো বিষয়গুলো অ্যারোসলের পরিবহন এবং অবক্ষেপনের উপর উল্লেখযোগ্য প্রভাব ফেলে। কম্পিউটেশনাল ফ্লুইড ডাইনামিক্স ভিত্তিক এই গবেষণাটি কম্পিউটেড টমোগ্রাফি (সিটি) চিত্র থেকে পুনর্গঠিত বাস্তবানুগ মানব ফুসফুসের ত্রিমাত্রিক মডেল এবং অ্যারোসল শ্বসনের বাস্তবানুগ বায়ুপ্রবাহের মডেল ব্যবহার করে, এবং ফুসফুসে অ্যারোসল অবক্ষেপনের উপর ব্যবহারকারীর শারীরিক ভঙ্গি এবং অ্যারোসল কণিকার আকারের সম্মিলিত প্রভাব নিরীক্ষণ করে। এনসিস সফটওয়্যারের ফ্লুয়েন্ট মডিউল ব্যবহার করে ডিসক্রিট ফেইজ মডেল প্রয়োগের মাধ্যমে পাঁচটি ভিন্ন আকারের কণিকা (৩,৫,৭,৯ ও ১০ মাইক্রোমিটার আকারের) এবং তিনটি ভিন্ন ভিন্ন দেহ ভঙ্গি - উলম্ব, পৃষ্ঠীয় এবং পার্শ্বীয় অবস্থার জন্য সিমুলেশন পরিচালিত হয়েছে। ফলাফল থেকে দেখা যায় যে, কণার আকার বৃদ্ধির সঙ্গে সঙ্গে মোট অবক্ষেপনের হার বৃদ্ধি পেয়েছে, তবে আঞ্চলিক অবক্ষেপনের পার্থক্য লক্ষণীয় হয়েছে কণার আকারের পাশাপাশি দেহভঙ্গির পরিবর্তনের জন্যও। ডান ফুসফুসে প্রায় প্রতিটি ক্ষেত্রেই বাম ফুসফুসের তুলনায় অধিক অবক্ষেপন লক্ষ্য করা গেছে, এবং উভয় ফুসফুসের উপরের খন্ডে তুলনামূলক বেশি কণা জমা হতে দেখা গেছে, বিশেষত তুলনামূলক বড় আকারের কণাগুলোর ক্ষেত্রে এটি অধিকমাত্রায় পরিলক্ষিত হয়েছে। যদিও ভিন্ন ভিন্ন দেহ ভঙ্গির জন্য মোট অবক্ষেপনের হার প্রায় একই ছিল, তবুও বিভিন্ন অঞ্চলে কণার বন্টনে স্পষ্ট পার্থক্য দেখা গেছে। প্রাপ্ত ফলাফলগুলো দেখায় কীভাবে শারীরিক ভঙ্গি ফুসফুসের ভেতরে অ্যারোসলের পরিবহনকে প্রভাবিত করে এবং কীভাবে শারীরিক ভঙ্গির মাধ্যমে ফুসফুসের নির্দিষ্ট স্থানে ঔষধ প্রেরণের কৌশলকে উন্নত করা যায় ও অ্যারোসল গ্রহণের সর্বোত্তম ফল পাওয়া যায় সেই বিষয়ে গুরুত্ববহ সূক্ষ্ম ধারণা দেয়।

Acknowledgement

I am deeply indebted to my respected supervisor, **Dr. Prasanjit Das**, Professor, Department of Mechanical Engineering, Chittagong University of Engineering and Technology, for his invaluable support, guidance, and encouragement throughout this research. His insightful suggestions and constant motivation have been instrumental in the successful completion of this thesis. I will always remain grateful for the time and knowledge he generously shared with me.

I would also like to express my sincere gratitude to the **Department of Mechanical Engineering** for providing the necessary facilities, academic environment, and support that enabled me to carry out this work effectively.

My heartfelt thanks go to my **parents**, whose unwavering support, patience, and faith in me have been a constant source of strength throughout this journey.

Special thanks are due to **Eshrak Jamil** and **Ammara Al Jabin** for being there during moments of need, offering help, encouragement, and companionship whenever I required it.

To all who have been a part of this journey in any form, I extend my deepest appreciation.

Table of Contents

APPROVAL ii
Declaration iii
Approval by the Supervisor iv
Abstract v
সারসংক্ষেপ vi
Acknowledgement vii
Chapter 01 1
Introduction 1
1.1 Background and Motivation 1
1.2 Anatomical Structure of the Lung Model 2
1.3 Influence of Body Orientation 3
1.4 Objective of the study 6
1.5 Structure of the Thesis 6
Chapter 02 8
Literature Review 8
2.1 Historical Perspective and Background 8
2.2 Lung Anatomy and Its Role in Aerosol Transport 9
2.2.1 Airway branching, asymmetry, and lobar anatomy 9
2.2.2 Physiological features influencing deposition 9
2.2.3 Right versus left lung and flow implications 10
2.3 Modeling Approaches 11
2.3.1 Symmetric versus Asymmetric Bifurcations 11
2.3.2 Multi-bifurcation versus Full-tree Models 12
2.3.3 Three-dimensional Reconstructions from CT or MRI 13
2.3.4 Advantages of Realistic Lung Models in CFD-Based Aerosol Deposition 14
2.3.5 Mesh Generation Practices in Literature 15
2.4 Numerical Methods and Simulation Tools in Pulmonary CFD 17
2.4.1 Use of ANSYS Fluent, OpenFOAM, and COMSOL in Pulmonary CFD 17
2.4.2 Numerical Solvers in Pulmonary CFD 18
2.4.3 Steady and Transient Flow Simulations in Pulmonary CFD 20
2.4.4 Grid Independence and Convergence Practices in Pulmonary CFD 21

2.4.5 Validation Strategies in Pulmonary CFD Simulations 23
2.5 Particle Dynamics and Transport Mechanisms 24
2.5.1 Primary Aerosol Deposition Mechanisms 24
2.5.2 Influence of Particle Size on Aerosol Deposition in the Human Lung 26
2.5.3 Particle Tracking Approaches in CFD 27
2.5.4 Coupling Strategies and Forces 29
2.6 Influence of Airflow Patterns on Deposition 30
2.6.1 Steady versus Unsteady Airflow Conditions in Aerosol Deposition 30
2.6.2 Sinusoidal Versus Realistic Inhalation Profiles: Impacts on Aerosol Deposition 31
2.6.3 Effects of Airflow Changes on Aerosol Particle Transport in the Lung 33
2.6.4 Comparative Studies of Aerosol Deposition Under Different Inhalation Waveforms 34
2.7 Role of Body Orientation and Gravity 35
2.7.1 Gravity Vector Effects on Aerosol Transport 35
2.7.2 Effect of Body Posture on Aerosol Deposition 36
2.7.3 Experimental Studies on Gravity and Posture Effects 37
2.7.4 Limitations of Past CFD Studies on Body Orientation 38
2.8 Drug Delivery and Clinical Relevance 39
2.8.1 Applications in Asthma, COPD, and Cystic Fibrosis 39
2.8.2 Challenges in Targeting Specific Lung Regions 40
2.8.3 Device-Based Studies 41
2.8.4 Personalized Aerosol Therapy Approaches 42
2.9 Summary of Gaps in the Literature 43
2.9.1 Posture-Insensitive Use of Realistic Lung Geometry in Aerosol CFD Studies 43
2.9.2 Lack of Posture-Integrated Studies with Realistic Aerosol Breathing Profiles 44
2.9.3 Lack of Integrated Models Combining Anatomy, Breathing Pattern, and Body Orientation 45
Chapter 03 47
Methodology 47
3.1 Reconstruction of the Realistic Lung Model 47
3.2 Governing Equations and Physical Models 49
3.2.1 Mathematical Formulation of Continuous-Phase Airflow 49
3.2.2 Finite Volume Discretization and Numerical Implementation in ANSYS Fluent 51
3.2.3 Turbulence Modeling 52

3.2.4 Discrete Phase Model (DPM): Particle Tracking 54
3.2.5 Coupling Between Phases 54
3.3 Mesh Generation and Grid Independence Study 54
3.4 Numerical Setup and Boundary Conditions 57
3.4.1 Solver Settings 57
3.4.2 Continuous Phase Boundary Conditions 58
3.4.3 Realistic Breathing Profile 58
3.4.4 Particle Properties and Injection Settings 61
3.4.5 Discrete Phase Boundary Conditions 61
3.4.6 Modeling Body Orientations 62
3.5 Post-Processing and Deposition Analysis 65
Chapter 04 66
Results and Discussion 66
4.1 Overview of Regional Deposition Data 66
4.2 Influence of Particle Size on Deposition Behavior 67
4.3 Regional Distribution Patterns under Different Body Orientations 71
4.4 Differences in Deposition Efficiency Across Body Orientations 77
4.5 Dominant Orientation for Regional Deposition 83
4.6 Discussion 84
Chapter 05 86
Conclusion 86
References 87
Publications 94

List of Figures

Figure 1.1: Segmented Lung Model 3
Figure 1. 2: Upright orientation 4
Figure 1. 3: Dorsal orientation 5
Figure 1. 4: Lateral orientation 5
Figure 3. 1: Reconstructed model of human lung using CT scan images.....48
Figure 3. 2: Sample CT image slices in MIMICS during lung model reconstruction 49
Figure 3. 3: Computational mesh of the reconstructed lung model 56
Figure 3. 4: Variation of average velocity with number of cells 57
Figure 3.5: Realistic aerosol breathing pattern for female (Volume flow rate vs. normalized time, t/T) 60
Figure 3. 6: Velocity profile vs. time for Realistic Aerosol Breathing.....60
Figure 3. 7: Upright orientation (gravity applied along -Z direction).....63
Figure 3. 8: Dorsal orientation (gravity applied along +Y direction) 64
Figure 3. 9: Lateral orientation (gravity applied along +X direction) 64
Figure 4.1: Deposition efficiency variation with particle size (upright position).....69
Figure 4.2: Deposition efficiency variation with particle size (Dorsal position).....70
Figure 4.3: Deposition efficiency variation with particle size (Lateral Position).....71
Figure 4.4: Regional aerosol deposition at different body orientations for particle Size 3 µm 72
Figure 4.5: Regional aerosol deposition at different body orientations for particle size 5 µm 73
Figure 4.6: Regional aerosol deposition at different body orientations for particle size 7 µm 74
Figure 4.7: Regional aerosol deposition at different body orientations for particle Size 9 µm 76
Figure 4.8: Regional aerosol deposition at different body orientations for particle size 10 µm 77
Figure 4.9: Heatmap of absolute differences in deposition efficiency from upright to dorsal orientation across lung lobes and particle sizes 78
Figure 4.10: Heatmap of relative differences in deposition efficiency from upright to dorsal orientation across lung lobes and particle sizes 79

Figure 4.11: Heatmap of absolute differences in deposition efficiency from upright to lateral orientation across lung lobes and particle sizes 80
Figure 4.12: Heatmap of relative differences in deposition efficiency from upright to lateral orientation across lung lobes and particle sizes 81
Figure 4.13: Heatmap of absolute differences in deposition efficiency from dorsal to lateral orientation across lung lobes and particle sizes 82
Figure 4. 14: Heatmap of relative differences in deposition efficiency from upright to lateral orientation across lung lobes and particle sizes 82
Figure 4. 15: Dominant body orientation for maximum deposition efficiency across lung lobes and particle sizes 84

List of Tables

Table 2.1: Summary of mesh generation techniques used in lung CFD.....16
Table 2.2: Comparison of particle tracking methods in pulmonary 28
Table 3.1: Grid independence study results and mesh quality parameters 56
Table 3. 2: Parameters of the first 10 harmonics for female realistic breathing.....59
Table 4.1: Deposition efficiency in upright position 66
Table 4. 2: Deposition efficiency in dorsal position 67
Table 4.3: Deposition efficiency in lateral position.....67

Chapter 01

Introduction

1.1 Background and Motivation

The efficiency of aerosol-based drug delivery or inhalation exposure assessment largely depends on how accurately we can predict particle transport and deposition throughout the human respiratory tract. Since direct observation of aerosol behavior within living lungs is practically unfeasible, researchers have long relied on both experimental surrogates and computational models to explore the complex dynamics of airflow and particle transport. Among these methods, computational fluid dynamics (CFD) has emerged as a particularly powerful approach, enabling detailed simulations of airflow and aerosol behavior across a wide range of physiological conditions and particle sizes.

Early studies in this field often employed simplified, idealized lung geometries, typically based on symmetric branching models. While mathematically convenient, these models fall short in representing the anatomical asymmetry, lobar distinctions, and irregular branching that characterize the actual human lung. More recently, advancements in medical imaging and segmentation techniques have enabled the development of anatomically realistic models. These more detailed reconstructions incorporate critical features such as lobe-specific bronchial pathways, nonuniform cross-sections, and natural curvatures, providing a more accurate foundation for studying how aerosols distribute across different regions of the lungs.

Despite these advancements, several important physiological variables remain insufficiently explored. One such variable is body orientation, which alters the gravitational direction acting on inhaled particles without changing the lung structure itself. Gravity plays a crucial role in deposition, especially for particles commonly used in therapeutic delivery, where sedimentation is a dominant mechanism. Yet, most simulation studies assume a default upright posture, overlooking the variety of orientations patients naturally or clinically assume—during sleep, intensive care ventilation, rehabilitation exercises, or postural drainage therapy. Moreover, from a therapeutic standpoint, if a particular body posture enhances overall deposition or targets a specific lung lobe more effectively, that posture could be intentionally adopted during inhalation to improve treatment efficacy and minimize drug waste.

In this context, a focused investigation that isolates the effect of body orientation—using a consistent, anatomically accurate lung model and controlled breathing profile—offers both

novelty and clinical relevance. This study employs a high-resolution, patient-based lung geometry segmented into five lobes: right upper lobe (RUL), right middle lobe (RML), right lower lobe (RLL), left upper lobe (LUL), and left lower lobe (LLL), along with the trachea and first-generation bronchus (G1). The geometric segmentation, as illustrated in ***Figure 1.1***, allows for lobar-level analysis of how posture-induced changes in gravity influence deposition distribution.

To explore this effect, the same lung model is simulated under three distinct body orientations: upright, dorsal, and lateral. These orientations are incorporated by altering the gravitational vector in the simulation environment while maintaining consistent geometry and boundary conditions. This approach ensures that the only changing variable is the direction of gravity, allowing a clean assessment of how posture alone reshapes aerosol deposition patterns.

By addressing the combined impact of anatomical realism and posture-aware modeling under realistic breathing conditions, this research fills an important gap in the literature. It provides practical insights that could inform optimized strategies for inhalation therapy, with potential applications in both clinical and home-care settings. Beyond identifying general trends, this work opens up the possibility of tailoring inhalation posture to maximize regional deposition or therapeutic targeting—an aspect that could lead to more personalized and effective respiratory treatments.

1.2 Anatomical Structure of the Lung Model

The lung geometry employed in this study was reconstructed from high-resolution CT scan data to preserve anatomical accuracy and branching asymmetry. The model includes the trachea, the Generation 1 (g1) bronchial branch, and five lobes—three on the right and two on the left. This segmentation enables regional deposition analysis at the lobar level while maintaining consistency across different simulation conditions. The anatomical regions are shown in ***Figure 1.1***.

The trachea serves as the primary airway, guiding inhaled air from the external environment toward the lungs. It bifurcates into the first-generation bronchus (g1)**,** which splits into the left and right main bronchi. This bifurcation represents the entrance to the lobar bronchi and plays a critical role in dividing airflow between the two lungs.

The lung consists of five lobes:

- **Right Upper Lobe (RUL):** Positioned superiorly, it branches with minimal angular deviation from the right main bronchus, allowing direct airflow and resulting in relatively high deposition, especially under upright posture.

- **Right Middle Lobe (RML):** Located centrally, the RML branches at a sharper angle and is narrower in volume. It often receives less deposition due to its recessed orientation and flow shielding by surrounding branches.
- **Right Lower Lobe (RLL):** Extending downward, the RLL follows a longer, more curved path. Its deposition is sensitive to gravity-driven mechanisms and varies significantly across body orientations.
- **Left Upper Lobe (LUL):** It branches steeply from the left main bronchus and has a wide inlet. Due to its upward orientation and exposure to the main flow path, it frequently receives high deposition in all postures.
- **Left Lower Lobe (LLL):** This lobe is anatomically deep, with a narrow entrance. It typically experiences reduced deposition, particularly in upright conditions, due to longer flow paths and geometric shielding.

The airway geometry was kept fixed throughout all simulations, with only the gravitational direction adjusted to simulate different body postures. This consistent anatomical structure ensures that observed changes in deposition arise purely from posture-induced variations.

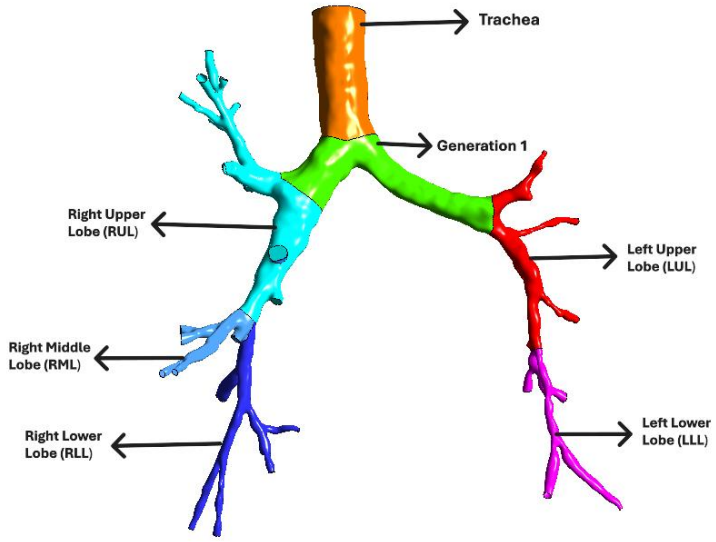


***Figure 1.2**: Segmented Lung Model*

1.3 Influence of Body Orientation

Inhalation studies often assume that individuals are in an upright position. However, in many real-world scenarios—including sleep, clinical care, and drug delivery in bedridden patients—the human body may be in dorsal or lateral positions, altering how gravity acts on inhaled

particles. Since gravitational sedimentation plays a significant role in aerosol deposition, body posture becomes a critical but often overlooked variable in deposition analysis. This study addresses this gap by simulating three distinct body orientations: upright, dorsal, and lateral, each modeled by changing the direction of gravitational acceleration in the computational domain while keeping the airway geometry unchanged.

In the upright orientation**,** gravity is applied in the negative Z-direction (–Z**)** to simulate a standing or seated posture. This configuration aligns the lung vertically with respect to gravity, a condition under which most traditional inhalation studies are conducted.

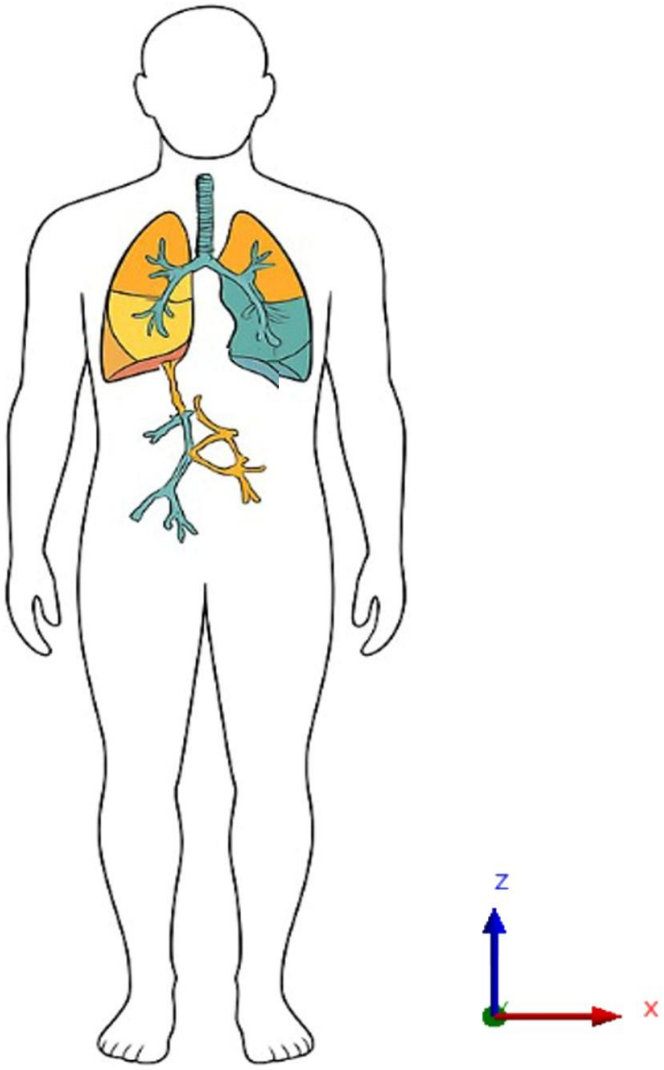


Figure 1.3*: Upright orientation*

In the dorsal orientation**,** the body is modeled as lying on its back, with gravity directed along the positive Y-direction (+Y)**.** This simulates a supine posture commonly encountered during sleep or clinical treatment. In this setup, the gravitational vector is orthogonal to the vertical

lung axis, redistributing particle settling toward the posterior regions of the lungs. The shift in gravitational alignment alters the regional flow dynamics and affects where inertial and gravitational forces combine to drive deposition.

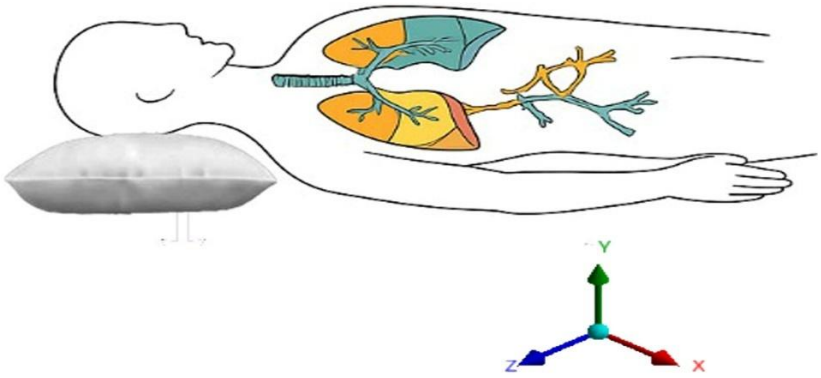


Figure 1.4: *Dorsal orientation*

In the lateral orientation**,** the model simulates a person lying on one side, with gravity applied in the positive X-direction (+X)**.** This setup rotates the lung horizontally relative to gravity, making the lateral sides of the airways the primary targets of gravitational settling. Asymmetry between the right and left lungs, particularly in airway branching angles and cross-sectional area, becomes even more influential in this posture. As a result, lateral orientation introduces a unique deposition pattern that differs significantly from both upright and dorsal positions.

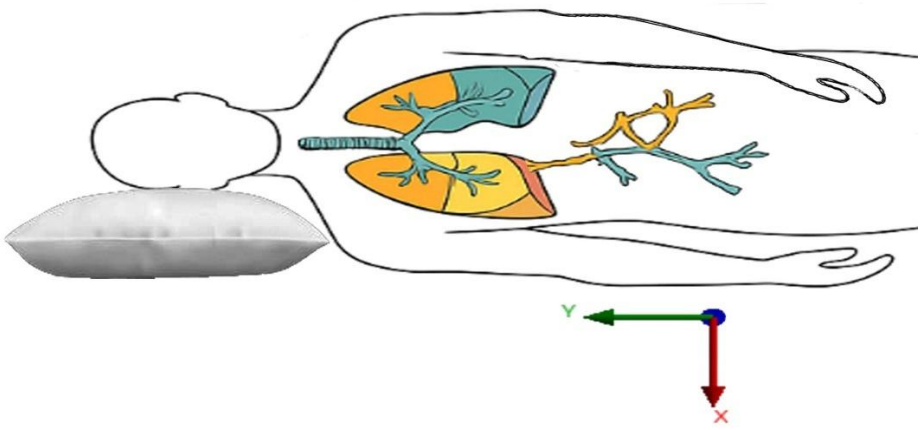


Figure 1.5: *Lateral orientation*

In all three cases, the magnitude of gravitational acceleration was fixed at 9.8 m/s^2**,** ensuring that only the direction of gravity was varied, not its strength. This approach isolates the influence of posture on particle behavior, allowing for a controlled and systematic comparison of regional deposition across orientations.

1.4 Objective of the study

The objective of this study is to improve targeted drug delivery by identifying how different body postures during inhalation influence regional aerosol deposition in the human lung. Specifically, the study aims to determine the effect of gravity direction on particle transport and deposition patterns within distinct lobes of the lung. Although factors such as airway geometry, particle size, and airflow profile are widely recognized to influence deposition behavior, the role of body orientation remains poorly understood. This is especially true when considering how changes in body posture affect the direction of gravity and its impact on particle deposition at the level of individual lung lobes.

To achieve this, the study aims:

- To simulate aerosol transport in a realistic human lung model under a realistic aerosol breathing profile for dry powder inhalers
- To investigate the effect of upright, dorsal and lateral postures on deposition trends
- To quantify deposition across different lung lobes under each posture
- To identify the posture that enhances targeted drug delivery
- To improve understanding of how gravity influences aerosol behavior in the lung

This approach utilizes a three-dimensional lung model reconstructed from computed tomography data, accurately segmented into five lobes, and including the trachea and the first-generation bronchus. This geometry enables precise tracking of deposition in clinically relevant lung regions. A realistic aerosol breathing profile was applied, characteristic of the inhalation phase during dry powder inhaler use.

The study focuses exclusively on the inhalation phase, with particle diameters ranging from three to ten micrometers. By maintaining a consistent geometry and breathing condition across all simulations and varying only the direction of gravity to represent different postures, the specific influence of body orientation on deposition can be clearly identified.

The findings aim to offer practical guidance on posture selection during inhalation therapy. Additionally, the results contribute to a deeper understanding of how gravity interacts with lung anatomy and particle dynamics, relevant to both clinical applications and inhalation exposure studies.

1.5 Structure of the Thesis

This thesis is organized into five chapters. Following the introduction, **Chapter 2** presents a comprehensive review of existing literature on aerosol transport and deposition in the human respiratory system, highlighting key factors, modeling approaches, and knowledge gaps. **Chapter 3** outlines the methodology, including geometry reconstruction, numerical modeling,

governing equations, boundary conditions, and simulation setup. **Chapter 4** discusses the results of the simulations, with a focus on regional deposition patterns across different body orientations and particle sizes. Finally, **Chapter 5** summarizes the main findings, discusses their implications, and suggests directions for future research.

Chapter 02

Literature Review

2.1 Historical Perspective and Background

The study of lung structure and airflow dynamics was revolutionized by Ewald R. Weibel's 1963 morphometric model of the human bronchial tree. His "Morphometry of the Human Lung" introduced a symmetric, dichotomously branching system comprising 23 generations of airways, paving the way for analytical approximations in respiratory mechanics and aerosol transport [1]. Although Weibel's model lacks anatomical irregularities, its simplicity facilitated analytical models of deposition mechanisms such as inertial impaction, sedimentation, and diffusion.

Numerous simplified derivatives such as one-dimensional flow models and triple bifurcation structures, were developed throughout the 1970s–1990s to allow easier integration into analytical and early computational simulations [2]. However, these models could not capture inter-individual anatomical variability or nonlinear airflow patterns resulting from asymmetry and airway curvature.

In parallel with modeling, in vitro experiments and radioactive tracer studies played a crucial role in understanding aerosol deposition. Early techniques included casting physical replicas of bronchial segments and using gamma scintigraphy or autoradiography to track aerosol paths. These studies helped validate the role of gravity, airway geometry, and breathing patterns on deposition but were limited to upper airways due to imaging constraints.

Modern in vitro systems like the Dosimetric Aerosol in Vitro Inhalation Device (DAVID) now offer spatially resolved deposition control for nanoparticle toxicity studies, mimicking real-world deposition heterogeneity [3]. Likewise, wind tunnel testing and tracer-labeled aerosols have been used to validate deposition under controlled airflow and particle size conditions in simplified and complex airway geometries [4].

With the rise of Computational Fluid-Particle Dynamics (CFPD), validated against these empirical setups, simulation of entire airway trees became feasible culminating in anatomically realistic, patient-specific lung models reconstructed from CT data.

The motivation for studying aerosol dynamics is deeply rooted in clinical medicine, particularly in pulmonary drug delivery. Inhalation therapy offers direct access to lung tissues, enabling rapid drug action with minimal systemic exposure, which is ideal for diseases like asthma, COPD, and cystic fibrosis.

Historical use of inhalation therapy began with nebulized bronchodilators in the early 20th century, followed by the development of metered-dose inhalers (MDIs) in the 1950s. Today, cutting-edge delivery methods include high-flow nasal cannula (HFNC) systems and dry powder inhalers (DPIs), each optimized through aerosol deposition studies [5].

Emerging technologies even explore aerosolized gene delivery systems, offering hope for genetic lung diseases and infections like SARS-CoV-2 and tuberculosis [6]. These therapies depend critically on our understanding of where and how aerosols deposit under various breathing and disease conditions.

2.2 Lung Anatomy and Its Role in Aerosol Transport

A thorough understanding of lung anatomy is essential for analyzing aerosol transport and deposition. The structural complexity of the pulmonary system, from airway branching patterns to the segmentation of lobes, plays a significant role in determining how inhaled particles move through the respiratory tract. This section explores the anatomical and physiological features that influence aerosol dynamics, with particular attention to asymmetry, lobar differences, and the importance of using accurate geometrical models.

2.2.1 Airway branching, asymmetry, and lobar anatomy

The architecture of the human lung is defined by a branching network that originates from the trachea and divides into progressively smaller airways. This branching is dichotomous in nature but rarely symmetrical. Variations in branching angles, airway diameters, and lengths create asymmetric flow distributions. These differences are particularly important because they affect the regional patterns of aerosol transport and deposition.

Asymmetry in airway structure contributes to spatial differences in particle retention across lung lobes. Subramaniam et al. conducted image-based simulations to study airflow and particle behavior in realistic airway geometries [7]. Additionally, Bennett et al. used shallow inhaled bolus tracers to investigate deposition patterns in different lung regions [8].

This tendency is influenced by anatomical constraints such as the position of the heart, diaphragm asymmetry, and volume differences between lobes [9].

2.2.2 Physiological features influencing deposition

The distribution of aerosol particles is shaped by several anatomical and physiological factors including airway diameter, surface area, and the nature of the airway lining. In the central conducting airways, which are larger in diameter, flow tends to be more turbulent, increasing the likelihood of deposition by inertial impaction. In contrast, peripheral bronchioles are smaller and associated with lower velocities, making them more susceptible to gravitational sedimentation and diffusion-based deposition [2].

In addition, the mucosal lining of the airway introduces another layer of complexity. The mucus layer can trap inhaled particles and facilitate mucociliary clearance. Computational models suggest that the interaction between particle inertia and mucus distribution at airway bifurcations leads to localized deposition hotspots [10].

Furthermore, asymmetry in branching may have evolved as a biological mechanism to enhance airway defense. A study by Mahesh V. Panchagnula proposed that structural asymmetry increases filtration efficiency in upper airway generations, thus acting as a protective feature against inhaled pathogens [11].

2.2.3 Right versus left lung and flow implications

The right and left lungs differ in both shape and structure. The right lung has three lobes while the left has two. The bronchial branches leading into these lobes are not mirror images, and this anatomical divergence affects how air and particles are distributed. Several imaging and simulation studies report that more particles tend to deposit in the left lung for small particles, particularly in posterior regions. This is attributed to the more horizontal orientation of the left main bronchus and the position of the heart which modifies thoracic geometry [9].

In contrast, for larger particles, deposition trends reverse. Using computational fluid dynamics simulations, Zhou et al. demonstrated that under strong inspiratory flow conditions, particles in the range of five to ten micrometers showed preferential deposition in the right upper lobe [12]. Similarly, Winkler-Heil and Hofmann, employing stochastic lung modeling, reported increased particle deposition in the bronchial regions of the right lung for large particles due to the effects of airway geometry and inertial impaction [13].

Understanding this variation is important when considering how diseases such as asthma, chronic obstructive pulmonary disease, and pneumonia manifest differently between the two lungs. It also underscores the need for models that can distinguish between left and right lung behavior.

2.2.4 Relevance for accurate geometrical modeling

Given that airway branching asymmetry, lobar anatomy, and individual physiological differences all contribute to heterogeneous particle distribution, it is critical that simulation models incorporate realistic geometries. Symmetric or idealized models do not account for variations in curvature, lobe volume, and airway angle, which can lead to significant errors in estimating deposition efficiency. Anatomically correct models allow for accurate mapping of deposition patterns and improve predictions for site-specific drug delivery and exposure risk [14].

2.3 Modeling Approaches

Accurate modeling of aerosol transport in the respiratory system requires careful consideration of anatomical geometry, physiological conditions, and computational strategies. Over the years, various modeling approaches have been developed to balance anatomical fidelity, computational feasibility, and simulation accuracy. This section reviews key strategies used in lung modeling, including symmetric and asymmetric bifurcation structures, multi-bifurcation versus full-tree models, image-based reconstructions, and mesh generation practices for computational fluid dynamics simulations.

2.3.1 Symmetric versus Asymmetric Bifurcations

The modeling of pulmonary airflow and aerosol transport has its conceptual foundation in the symmetric branching framework introduced by Ewald R. Weibel in 1963. Weibel's model described the human lung as a regular dichotomously branching structure consisting of twenty three generations of airways, each daughter branch dividing at a fixed angle and maintaining a uniform geometric ratio relative to its parent [1].

To address this limitation, researchers have introduced mathematical models to modify and adapt geometries.

This morphometric representation allowed for tractable mathematical modeling of airflow, gas exchange, and particle deposition and served as the basis for early analytical and semi empirical models of lung physiology. However, one of the major limitations of the Weibel model is its assumption of perfect symmetry. Real human airways deviate significantly from this idealized configuration. Branching angles, airway diameters, and generation lengths vary across individuals and even between lobes within the same lung.

Later studies demonstrated that such anatomical asymmetry plays a critical role in shaping regional ventilation and deposition patterns. In particular, asymmetric bifurcation geometries have been shown to promote flow skewing, non uniform particle distribution, and increased filtering efficiency in upper bronchial generations [15].

Computational models using asymmetric airway segments, such as those designed by Combs and colleagues in a neonatal lung geometry, have further revealed that branching asymmetry alters surfactant and aerosol distribution across lung regions [16].

These insights have prompted a shift in the field from simplified, symmetric representations toward anatomically accurate reconstructions that reflect individual variability. While symmetric models continue to offer computational efficiency and pedagogical clarity, their limitations in predicting spatially resolved deposition patterns, especially in the context of therapeutic aerosol delivery, have become increasingly evident.

2.3.2 Multi-bifurcation versus Full-tree Models

Lung models used in computational studies of aerosol transport can be broadly categorized into two types based on the extent of airway generations they represent: multi-bifurcation segmental models and full-tree airway models. Multi-bifurcation models typically consist of two to eight branching generations and are designed to study localized airflow and deposition dynamics. These are computationally efficient and are often used to test effects of airway geometry, flow regime, or aerosol properties within specific lung regions. However, their limited depth and artificial outlet conditions reduce their ability to capture global deposition patterns or predict dose distributions across the entire respiratory tract.

In contrast, full-tree models aim to replicate the entire bronchial hierarchy, sometimes including up to 23 generations from the trachea to the terminal bronchioles. These anatomically comprehensive models are often reconstructed from imaging data and account for asymmetric branching, lobar volume distribution, and individual variability. Their primary advantage lies in the ability to simulate spatially resolved aerosol behavior, assess lobe-specific delivery, and identify distal airway deposition—a critical factor for evaluating inhalation therapies and pollutant exposure.

Xiao et al. proposed a multi-scale modeling approach that integrates a full-tree structure with extended boundary conditions to mimic physiologically realistic inhalation. By comparing a full-tree mouth-to-bronchi model using a lobar network boundary method to a simplified truncated model with uniform pressure outlets, they observed up to 93 percent difference in particle penetration into deep lobes depending on particle size and flow rate [17].

Aboelezz et al. similarly examined simplified versus complex airway models for dust particle deposition using computational fluid dynamics and wind tunnel testing. Their findings revealed that simplified bifurcation models failed to capture realistic velocity gradients and turbulence behavior, which led to substantial underestimation of deposition hotspots in upper lobes [18].

These comparisons demonstrate that although multi-bifurcation models are valuable for focused mechanistic analysis, full-tree models are necessary for any clinically or environmentally relevant simulation that involves deposition across a wide range of particle sizes and airway generations. They allow for personalized drug delivery predictions, cumulative dose assessments, and evaluation of disease-specific airflow obstructions.

2.3.3 Three-dimensional Reconstructions from CT or MRI

The shift from idealized lung models to anatomically realistic simulations has been made possible by advances in three-dimensional reconstruction techniques from clinical imaging data. High-resolution computed tomography (CT) and magnetic resonance imaging (MRI) are the most commonly used modalities for extracting structural information of the pulmonary system. These imaging techniques enable the visualization of airways at submillimeter resolution, allowing researchers to build subject-specific airway geometries for computational simulations of airflow and aerosol deposition.

The typical workflow begins with lung segmentation, where software algorithms or manual corrections isolate the air-conducting regions of the respiratory tract from surrounding tissues. Segmentation accuracy plays a pivotal role in determining the fidelity of reconstructed geometries. Zhang et al. proposed an enhanced segmentation approach based on an improved UNet++ architecture tailored for lung CT slice processing. Their method achieved an accuracy of 98.03 percent and addressed common pitfalls like overfitting in small medical datasets [19].

After segmentation, the next step involves mesh generation for computational fluid dynamics (CFD) simulations. However, this process is complicated by irregular airway shapes, partial volume effects, and image artifacts. Moreover, while CT offers high spatial resolution for larger bronchial generations, it is less effective in visualizing peripheral airways beyond the seventh or eighth generation. MRI, though non-ionizing and safe for repeated imaging, typically provides lower spatial resolution and is more commonly used in functional studies such as ventilation mapping.

Even with complete CT-derived geometries, generating a usable three-dimensional mesh for numerical simulation remains a non-trivial task. Manual or semi-automated smoothing, surface remeshing, and artificial extension of peripheral branches are often employed to ensure flow stability and reduce computational load. Gouveia et al. compared two-dimensional and three-dimensional feature extraction methods on CT datasets, emphasizing the superior spatial context preserved in volumetric reconstructions despite higher computational costs [20].

Furthermore, the computational demand of simulating airflow in full airway trees reconstructed from imaging data is a significant barrier. Meshes derived from CT scans often contain over one million elements, especially when modeling airflow under transient breathing conditions. These challenges have motivated recent efforts to integrate machine learning into reconstruction workflows. For instance, new 3D networks like Fast3R allow rapid rendering of thousands of airway images in a single computational pass, potentially enabling large-scale modeling of population variability [21].

In summary, while the use of CT or MRI-derived geometries significantly enhances anatomical accuracy, challenges remain in segmentation precision, peripheral airway capture, mesh generation, and computational scalability. Despite these hurdles, three-dimensional reconstructions are now considered essential for studies aiming to evaluate subject-specific deposition or to develop personalized inhalation therapies.

2.3.4 Advantages of Realistic Lung Models in CFD-Based Aerosol Deposition Studies

The incorporation of realistic anatomical geometries into computational fluid dynamics (CFD) simulations marks a pivotal advancement in aerosol deposition research. Unlike symmetric, idealized models which simplify the bronchial tree into uniform branching structures, realistic models derived from CT or MRI data capture anatomical heterogeneity such as lobar asymmetry, airway curvature, irregular diameters, and subject-specific features. This fidelity is essential for accurately predicting regional and local deposition patterns of inhaled particles.

One of the primary benefits of realistic models is their improved alignment with in vivo data. For example, Sadafi et al. compared aerosol deposition predictions from CFD simulations using patient-specific airway geometries against single-photon emission computed tomography (SPECT) data in asthmatic patients. Their model, which incorporated inspiratory and expiratory CT images and anatomical upper airway reconstructions, achieved a mean error of just 2.1 percent in lobar deposition prediction [22].

Validation studies have consistently shown that simplified models often fail to replicate physiological deposition profiles. Tian et al. demonstrated that CFD models using stochastic individual pathways and realistic mouth-throat geometries predicted total and regional lung deposition of pharmaceutical aerosols with less than 10 percent relative error across multiple inhalers and particle sizes [23].

Another key advantage is the ability to simulate segmental or lobar-specific deposition**,** especially relevant for targeted drug delivery. Ma and Lutchen, using an anatomically accurate model from mouth to generation 10, found that particle retention varied significantly across lobes depending on particle size and inhalation flow rate. Idealized geometries could not capture these inter-lobar variations, often averaging out clinically important deposition differences [24].

Furthermore, realistic models enable dynamic simulations across breathing cycles. A recent study by Laycock et al. simulated particle deposition under normal and surfactant-deficient conditions. Their work showed that realistic surface interactions and branching complexity significantly influenced deposition of gold nanoparticles in knockout mice, especially under transient airflow [25].

These models also accommodate pathological variations**.** CFD simulations by Koullapis et al. evaluated the effect of COPD-induced airway narrowing on deposition. Their large-eddy simulations revealed altered deposition zones and enhanced filtration at stenosed sites—trends that would be entirely missed in idealized models [26].

Moreover, realistic models support multi-scale coupling**,** connecting regional transport with alveolar processes. This is vital in evaluating exposure risks and systemic absorption, as highlighted by Oldham, who cautioned that accurate local deposition predictions require validated geometries and boundary conditions. His work also emphasizes the complexity of true CFD validation, advocating for rigorous comparison with both experimental and imaging datasets [27].

In summary, realistic lung models in CFD simulations offer multiple advantages over idealized models. These include greater accuracy in replicating experimental data, capability to simulate lobar-specific and pathological conditions, and support for dynamic, transient inhalation patterns. These strengths have made anatomically accurate models indispensable in drug delivery, occupational exposure assessment, and respiratory disease modeling.

2.3.5 Mesh Generation Practices in Literature

Once a segmented airway geometry is obtained from CT or MRI data, the next critical step for computational simulations is the generation of a high-quality mesh. This mesh discretizes the 3D volume into elements, allowing numerical solutions to the governing fluid dynamics and particle transport equations. The accuracy and stability of simulations in lung models are highly dependent on mesh quality, especially at bifurcations and in distal regions where flow gradients can be steep.

Mesh generation in the context of pulmonary modeling presents several challenges. The bronchial tree contains sudden changes in diameter, tight curvatures, and tapering branches, all of which can produce numerical instabilities if not meshed properly. Studies have shown that coarse meshes may fail to resolve secondary flow structures or underpredict deposition at branching sites. To address these limitations, researchers commonly apply unstructured tetrahedral or polyhedral meshes in combination with surface smoothing and local refinement. Zhang et al. proposed an enhanced mesh-ready CT segmentation pipeline using an optimized version of the UNet++ network. Their model produced smoothed boundary contours suitable for surface remeshing, while significantly minimizing oversegmentation artifacts commonly seen in deep airway generations [19].

Beyond segmentation quality, mesh resolution is frequently tailored to the simulation objectives. In models targeting the upper airways or tracheobronchial region, local mesh

refinement is applied around bifurcation zones to capture vortices and deposition gradients. For full-tree simulations, mesh sizes often exceed one million elements, necessitating parallel computing strategies and mesh partitioning.

Advanced mesh handling methods are also being integrated with machine learning frameworks. For instance, Tian et al. implemented a multilevel support-based architecture that generates lesion-sensitive CT segmentations optimized for mesh compatibility. Their model adapts resolution levels based on lesion complexity and spatial curvature, improving both anatomical fidelity and simulation performance [28].

Furthermore, there is growing interest in meshless or hybrid mesh approaches, especially for very small airways where standard tetrahedral meshing becomes unstable or overly memory-intensive. Mesh-free particle methods and lattice-Boltzmann solvers are being explored as alternatives in distal lung simulations. While these remain experimental, they offer potential to overcome resolution limitations in terminal bronchioles and alveolar regions.

In summary, the evolution of mesh generation practices in pulmonary modeling reflects a trade-off between anatomical accuracy, numerical stability, and computational cost.

Table 2.1 shows the advantages and limitations of different types of mesh along with their area of applications in previous computational fluid dynamics studies.

Table2.1: Summary of mesh generation techniques used in lung CFD

Mesh Type	Use Case	Advantages	Limitations
Tetrahedral Mesh	Full-tree airway models, upper airway CFD	Flexible for complex geometry, widely supported	May require high resolution near bifurcations
Polyhedral Mesh	Segmental bifurcation studies	Reduces cell count, good for capturing gradients	Complex to generate from segmented data
Hexahedral Mesh	Idealized symmetric models	High numerical accuracy	Poor adaptability to real anatomy
Adaptive Mesh Refinement	Local deposition studies, vortical flow zones	Focuses resolution where needed	Complex implementation, higher memory cost
Hybrid Mesh	CT-based full tree with tracheal extensions	Balances efficiency and detail	Mesh transition zones require careful smoothing
Meshless Methods	Peripheral airway and alveolar flow modeling.	Avoids complex meshing in tiny airways	Still experimental; computationally intensive

2.4 Numerical Methods and Simulation Tools in Pulmonary CFD

Accurate simulation of pulmonary airflow and particle dynamics requires appropriate numerical schemes, solver settings, and modeling assumptions. The following sections outline commonly used CFD tools, solver approaches, and modeling practices relevant to lung airflow and aerosol deposition.

2.4.1 Use of ANSYS Fluent, OpenFOAM, and COMSOL in Pulmonary CFD

Over the past two decades, computational fluid dynamics (CFD) has become indispensable in simulating airflow and aerosol deposition in the human lung. Among the most commonly employed simulation platforms are ANSYS Fluent, OpenFOAM, and COMSOL Multiphysics. Each has unique strengths and limitations regarding accuracy, scalability, customization, and multiphysics integration.

ANSYS Fluent is widely used in pulmonary research due to its robustness, pre-built solvers, and commercial support. It applies the finite volume method and supports a wide array of turbulence models, discrete phase tracking (Lagrangian and Eulerian), and multiphase flow schemes. Its graphical interface simplifies model setup, mesh refinement, and solver configuration. Fluent has been extensively validated against experimental data. For example, Rahman et al. used ANSYS Fluent to study particle transport in realistic lungs with and without airway stenosis, observing accurate deposition trends across particle sizes ranging from 5 nm to 10 μm [29].

Earlier studies also relied on Fluent for its mature discrete phase modeling. López et al. compared Fluent's Lagrangian particle tracking capabilities with OpenFOAM's in a submerged jet impingement setup, validating Fluent's accuracy for transient particle-wall interactions [30].

OpenFOAM, an open-source CFD platform, has gained popularity due to its transparency, cost-free licensing, and customizability. Unlike Fluent, OpenFOAM allows users to modify solver algorithms directly, which is beneficial for research in emerging areas such as dynamic boundary conditions, subject-specific geometries, and multi-breath-cycle simulations. Pandal-Blanco et al. (2019) demonstrated that with customized boundary conditions and solvers, OpenFOAM could outperform commercial solvers in representing airflow in a simplified Weibel-based lung model [31].

OpenFOAM has also been used in direct comparisons with Fluent. Welahettige and Vaagsaether found OpenFOAM delivered more diffusive species transport in gas-gas mixing problems, whereas Fluent yielded stronger convective dominance. Their findings underscore

the importance of solver settings and turbulence models in reproducing realistic flow profiles [32].

COMSOL Multiphysics offers an integrated modeling environment especially suited for simulations involving heat, mass transfer, and electrochemical reactions. While not as commonly used for high-resolution airflow simulations, it is valuable in multiphysics scenarios such as gas exchange modeling, pulmonary drug delivery involving phase change, and membrane interaction studies.

In general, ANSYS Fluent is preferred for well-supported, commercially validated simulations and is ideal for anatomically realistic airway geometries. OpenFOAM is more suited for academic environments and exploratory modeling, offering maximum solver flexibility and scalability, particularly in full-lung or multibreath simulations. COMSOL**,** while less common in mainstream pulmonary CFD, is highly effective in coupled physics environments and small-scale alveolar or membrane transport models.

Ultimately, the choice of platform depends on the project goals, computational resources, licensing availability, and the user's technical expertise. Cross-validation between platforms, as shown in comparative studies, also remains essential for assessing model reliability.

2.4.2 Numerical Solvers in Pulmonary CFD

The choice of numerical solver in computational fluid dynamics (CFD) is fundamental to the accuracy, stability, and computational efficiency of airflow and aerosol simulations in the human respiratory system. In pulmonary CFD, the solvers used must handle low-Mach number, unsteady, laminar-to-transitional flows in highly irregular, branching geometries. The governing equations typically involve the continuity equation, Navier–Stokes momentum equations, and energy conservation (for heat or mass transfer when necessary). To solve these, solvers are broadly categorized into pressure-based**,** density-based, and hybrid approaches, each with specific applications and computational strategies.

Pressure-based solvers are the most commonly used in lung modeling due to their stability and suitability for incompressible or low-speed compressible flows (Mach number < 0.3), which characterize normal breathing. These solvers discretize the pressure-velocity coupling either through segregated (e.g., SIMPLE, PISO, SIMPLEC) or coupled algorithms. In segregated solvers, the continuity and momentum equations are solved separately with pressure corrections iteratively adjusting the velocity field to enforce mass conservation. This approach is employed in many commercial codes including ANSYS Fluent, COMSOL, and in the OpenFOAM solver simpleFoam.

Fully coupled pressure-based solvers, on the other hand, solve the momentum and continuity equations simultaneously. Xiao et al. presented a fully coupled pressure-based finite volume solver capable of simulating subsonic and transonic flows across structured and unstructured grids, enhancing convergence in complex geometries such as bifurcated airways [33].

These solvers are known for their robustness in transient simulations and have been validated extensively in aerosol deposition research. For instance, ANSYS Fluent's pressure-based solvers have been used by Rahman et al. (2021) to evaluate particle deposition in both normal and obstructed lungs, demonstrating strong agreement with imaging data [29].

Originally developed for high-speed, compressible flow simulations in aerospace applications, density-based solvers solve the continuity, momentum, and energy equations as a coupled system, using the equation of state to link pressure and density. These solvers are generally inappropriate for pulmonary simulations due to their sensitivity to numerical stiffness at low Mach numbers and higher computational cost.

However, with the development of preconditioning techniques and improved time integration schemes, density-based solvers have been adapted for use in biomedical flows under special circumstances, such as shock-tube simulations, gas exchange models, or high-frequency ventilation studies. Cheng et al. (2005) explored both density- and pressure-based approaches for compressible and incompressible CFD models, emphasizing that pressure-based solvers outperformed in subsonic regimes with high mesh quality [34].

In a benchmarking study, Mangani et al. (2016) compared a pressure-based solver developed in OpenFOAM (couple foam) with a density-based solver (LINARS) for turbomachinery applications. Although not lung-specific, their results reaffirmed that pressure-based solvers were more efficient and accurate in low-speed applications typical of respiratory simulations [35].

Recent work has introduced hybrid solver strategies that merge the numerical stability of pressure-based schemes with the conservation strengths of density-based methods. These solvers dynamically switch between formulations based on local flow conditions or user-defined Mach number thresholds. For example, some customized OpenFOAM solvers use implicit coupling schemes for the pressure–velocity–energy field, enabling more accurate modeling of unsteady compressible flows in lung airways during coughing or forced expiration.

Further, high-order discontinuous Galerkin (DG) solvers have been developed for next-generation pulmonary simulations. Kronbichler et al. designed a scalable DG solver capable of handling incompressible Navier–Stokes equations in lung geometries, integrating both pressure–velocity coupling and turbulence modeling with adaptive mesh refinement [36].

Such solvers are particularly useful in large-scale simulations involving patient-specific full-lung geometries and realistic breathing cycles, where traditional finite-volume solvers may become inefficient or unstable.

In conclusion, pressure-based solvers remain the dominant approach in pulmonary CFD due to their balance of stability, computational efficiency, and applicability to low-speed airway flows. Density-based solvers are rarely used outside specialized cases but offer valuable insight into coupled compressible phenomena when carefully implemented. Hybrid and high-order solvers, though computationally intensive, represent the future of lung modeling as the field moves toward real-time, patient-specific simulation and multi-physics coupling.

2.4.3 Steady and Transient Flow Simulations in Pulmonary CFD

Accurately simulating the transport and deposition of inhaled aerosols in the respiratory system requires careful selection of the temporal profile of the airflow. Broadly, CFD simulations use either steady-state or transient (time-dependent) breathing profiles. Each has implications for computational cost, simulation realism, and predictive power regarding deposition efficiency and distribution.

Steady-state simulations assume a constant flow rate and ignore time variations in airflow, representing a snapshot or average of the breathing process. These are commonly used in early-stage modeling due to their lower computational demands and simplified setup. For many applications, such as baseline comparisons or general trends in deposition under controlled conditions, steady-state simulations are adequate.

Studies such as that by Koullapis et al. employed steady-state flows to examine the impact of airway narrowing on particle deposition under different physical activity levels. Their simulations across air flow rates (15.2, 30, and 60 L/min) revealed consistent deposition patterns, particularly for particles above 2.5 μm [37].

However, multiple studies caution against over-reliance on steady-state models for predicting regional or deep lung deposition. Nowak et al. found that time-independent simulations over-predicted upper airway deposition and under-predicted deposition in distal generations, leading to inaccuracies when compared to in vivo data [38].

Transient simulations incorporate the natural variation in breathing, including acceleration and deceleration phases. Transient flows are typically modeled using sinusoidal, spirometry-derived, or patient-specific waveforms. These simulations are essential for capturing the full dynamic behavior of inhaled flows and particles, especially for applications involving therapeutic aerosols or environmental exposures.

Ryusei Kizuka et al. compared deposition patterns under steady and transient conditions using a realistic upper respiratory model. Their study revealed significantly higher deposition efficiency in the nasal and tracheal regions during transient inhalation, especially for particles below 2 μm, due to variable inertial impaction and secondary flow structures [39].

Similarly, Kiasadegh et al. used transient UDF-based simulations in ANSYS Fluent to evaluate fibrous particle deposition. They reported that while total deposition agreed with steady-state approximations, regional deposition—particularly penetration to the lower airways—was significantly underestimated by steady models [40].

From an anatomical perspective, Wedel et al. demonstrated using transient OpenFOAM simulations that subject-specific laryngeal geometry and dynamic flow conditions substantially influence local deposition intensity and pattern. These effects were muted in steady-state equivalents [14].

Comparative studies have shown that while steady-state simulations are often sufficient for approximating overall or total aerosol deposition within the lung, they fall short when accurate prediction of regional or lobar deposition is required. In contrast, transient simulations are better suited for capturing dynamic respiratory phenomena such as vortex shedding, inertial lag of particles, and flow reversals—especially within bifurcations and distal airway generations. These time-dependent effects significantly influence the trajectory and eventual deposition site of inhaled particles, making transient modeling essential for detailed and physiologically realistic analysis of aerosol transport.

The choice between steady and transient should be guided by study objectives: drug targeting, toxicology, or airflow obstruction studies benefit more from transient modeling. In conclusion, while steady-state simulations offer a valuable first approximation with reduced computational cost, transient breathing models are essential for capturing physiologically accurate particle behavior and should be prioritized in clinical or safety-critical CFD applications.

2.4.4 Grid Independence and Convergence Practices in Pulmonary CFD

Grid independence and convergence testing are essential steps in the validation of computational fluid dynamics simulations. In the context of pulmonary modeling, where anatomical complexity and physiological accuracy are critical, ensuring that results are not influenced by the mesh resolution or numerical artifacts is necessary for achieving reliable predictions of airflow and particle behavior.

Grid independence refers to the condition in which further refinement of the computational mesh does not cause significant changes in the simulation output. A simulation is considered

grid independent when key variables such as airflow velocity, wall shear stress, pressure drop, and regional or total deposition stabilize across progressively finer mesh configurations.

This step is particularly important in lung simulations, as critical flow features including vortices and separation zones occur near bronchial bifurcations and sharply curved airways. Many studies employ localized mesh refinement in the upper airway, carina, and branching points to improve resolution where deposition is most sensitive. Zhang and Kleinstreuer demonstrated that inadequate resolution in the laryngeal region could lead to substantial underprediction of localized aerosol deposition [41].

Typical mesh sizes range from a few hundred thousand cells in simplified models to over ten million in full airway geometries derived from imaging data. Unstructured tetrahedral and polyhedral meshes are commonly used for anatomically realistic models, while structured hexahedral grids remain popular in idealized simulations.

Convergence refers to the stability and accuracy of numerical solutions to the governing flow equations. It is generally evaluated by monitoring the residuals of continuity, momentum, and scalar transport equations, which should drop by at least three to six orders of magnitude. However, in simulations of respiratory flow where time dependence, secondary flows, and particle transport are involved, residual norms alone may not reflect true physical convergence. Best practices include tracking both numerical residuals and physical output parameters such as pressure loss, outlet mass flow balance, and total deposition. Kiasadegh et al. highlighted that even when residuals reached acceptable levels, variation in deposition results across time steps required additional refinement to ensure temporal convergence [40].

In transient simulations, time step sensitivity analysis is also necessary. Just as mesh refinement establishes spatial convergence, repeating simulations with smaller time increments ensures that unsteady features such as vortex formation and particle tracking remain consistent. A common practice is to reduce the time step until changes in monitored outputs fall below one percent.

Best practices for ensuring grid and temporal convergence in pulmonary CFD simulations include simulating with at least three different levels of mesh density and comparing the results for key variables of interest. Particular attention should be given to wall resolution near airway surfaces, which is especially important when employing turbulence models or simulating particle-wall interactions. Convergence assessment should go beyond monitoring residuals by incorporating additional indicators such as mass conservation and deposition efficiency. When quantitative accuracy is critical, the Grid Convergence Index method can be applied to estimate numerical uncertainty. Overall, rigorous testing for both grid and convergence independence

enhances the reliability and scientific credibility of simulation results, which is particularly important when the findings are intended to guide therapeutic strategies or assess respiratory exposure risks.

2.4.5 Validation Strategies in Pulmonary CFD Simulations

Validation is a critical step in computational fluid dynamics modeling, serving as the bridge between theoretical simulation and experimental or clinical reality. In pulmonary CFD, validation ensures that the predicted airflow and particle deposition patterns accurately represent physiological phenomena. The main strategies for validation include in vitro experiments**,** in vivo measurements, and medical imaging techniques**,** each contributing unique strengths and constraints to the validation process.

In vitro validation uses physical replicas of the human airway—often constructed from CT scans via 3D printing, to experimentally observe airflow patterns or particle deposition. These models provide high spatial resolution, reproducibility, and the ability to test under controlled conditions.

A prominent study by Ahookhosh et al. used a CT-derived model of the tracheobronchial tree up to the fourth generation to validate CFD predictions for dry powder inhalers at varying inhalation flow rates. Their results demonstrated strong agreement between deposition fractions obtained experimentally and through simulation, especially in regions like the trachea and main bronchi [42].

Holbrook and Longest further validated CFD models by comparing local deposition patterns in a double bifurcation airway model under steady flow using fluorescent microscopy. Their findings confirmed that realistic surface properties and wall roughness must be incorporated to achieve meaningful agreement with experiments [43].

In vivo validation involves comparing CFD predictions to data collected from human or animal subjects. This typically includes deposition measurements using radioactive tracers, spirometry, or pharmacokinetic outcomes.

Tian et al. performed extensive validation by comparing CFD predictions of pharmaceutical aerosol deposition against human in vivo data across multiple aerosol types and delivery devices. Their stochastic individual pathway (SIP) model showed less than 10 percent relative error in both central and peripheral deposition metrics [28].

Further extending this approach, Longest et al. used whole-airway CFD models to predict dry powder inhaler deposition at different inhalation waveforms, comparing results to gamma scintigraphy data. The model successfully captured the effects of variable flow rates on both central and peripheral deposition.

Functional imaging techniques such as SPECT (Single Photon Emission Computed Tomography)**,** PET, and gamma scintigraphy are increasingly used to validate regional deposition predictions from CFD. These methods allow for non-invasive visualization of aerosol distribution within the lung in living subjects.

Sadafi et al. conducted a landmark study comparing CFD predictions of lobar deposition to SPECT imaging data in asthmatic patients. Using subject-specific airway geometries and boundary conditions from inspiratory and expiratory CT scans, they achieved a mean error of only 2.1 percent in regional deposition prediction [22].

In another effort, Ma and Lutchen (2009) used deposition metrics from multi-detector CT-based geometries to cross-validate large and medium airway CFD predictions, showing high consistency with earlier imaging studies on micrometer-scale aerosols [24].

In summary, validation of CFD models in pulmonary applications is a multi-tiered process involving physical models, biological experiments, and advanced imaging. Each method supports specific aspects of model reliability—from geometric representation to flow-field realism and particle behavior. A combination of these strategies is essential to ensure that CFD models can be confidently used in clinical decision-making, drug delivery optimization, and exposure risk assessments.

2.5 Particle Dynamics and Transport Mechanisms

The transport and deposition of aerosol particles within the human respiratory tract are governed by a complex interplay of physical forces, particle characteristics, and anatomical features. Understanding these dynamics is critical for predicting how inhaled particles behave under various physiological conditions. This section outlines the primary deposition mechanisms—including inertial impaction, gravitational sedimentation, and Brownian diffusion—and examines how particle size and breathing patterns influence transport behavior. It also discusses computational modeling strategies used to simulate particle trajectories, highlighting key numerical approaches such as the Discrete Phase Model, Lagrangian particle tracking, and Eulerian field methods.

2.5.1 Primary Aerosol Deposition Mechanisms

Aerosol deposition in the human respiratory tract is governed by three primary physical mechanisms: inertial impaction, gravitational sedimentation, and Brownian diffusion**.** Each plays a dominant role depending on particle size, airflow velocity, and airway geometry. Understanding how these mechanisms operate is essential for predicting where particles deposit and how efficiently therapeutic or harmful aerosols penetrate the lungs.

Inertial impaction occurs when particles cannot follow the curved streamlines of the airflow due to their momentum, causing them to impact onto airway walls. This mechanism dominates for larger particles (above 5 micrometers) and is most significant in regions of high velocity and rapid directional change, such as the mouth-throat, trachea, and early bronchial generations.

Nicolaou demonstrated through direct numerical simulations that in the upper airway and carinal ridge, impaction dominates especially at high Stokes numbers, with particle inertia overwhelming drag forces [44].

Sedimentation refers to the settling of particles under the force of gravity, particularly as airflow slows down in the deeper regions of the lungs. This mechanism is most important for intermediate particle sizes (0.5 to 5 micrometers) under slow flow conditions, such as during resting breathing.

Chantal Darquenne performed experiments during parabolic flights and found that particle deposition in the lower lung lobes was significantly reduced under microgravity, confirming the importance of gravity in deposition of mid-sized particles [45].

Chen et al. further confirmed that under low flow rates, sedimentation contributes to particle capture along airway walls and is enhanced in horizontal orientations of daughter branches [46].

Brownian diffusion results from random collisions between aerosol particles and gas molecules, causing erratic movement and deposition. This mechanism dominates for ultrafine particles (below 0.5 micrometers) and becomes particularly important in the alveolar region and small bronchioles.

Yu et al. conducted analytical studies in circular tubes and showed that diffusion-driven deposition varies with transport distance and becomes more significant when gravitational forces are negligible [47].

Wu et al. (2022) used a 3D Monte Carlo model to simulate Brownian and gravitational contributions to deposition morphology. Their findings showed distinct deposition patterns depending on the Peclet number, which captures the ratio of advective to diffusive transport [48].

In real-world breathing conditions, these mechanisms often act simultaneously. Tsuda et al. highlighted that in alveolated ducts, gravitational and inertial effects cannot be simply added. In fact, particle inertia can suppress gravitational deposition by preventing particles from crossing streamlines, creating complex, flow-dependent interactions [49].

In conclusion, the interplay between impaction, sedimentation, and diffusion depends on the local flow regime, particle size, and anatomical location. A robust CFD model must capture all three processes to accurately predict regional deposition and inform drug delivery or inhalation risk assessments.

2.5.2 Influence of Particle Size on Aerosol Deposition in the Human Lung

Particle size is one of the most influential parameters in determining where and how aerosol particles deposit within the human respiratory tract. The aerodynamic diameter of a particle dictates which transport mechanism—impaction, sedimentation, or diffusion—dominates its trajectory and influences whether the particle reaches the upper airways, the bronchial tree, or the alveolar region.

Particles larger than 5 micrometers tend to deposit in the upper airway and early bronchial generations due to their high inertia. During inhalation, these particles are unable to follow the rapidly curving streamlines at bifurcations, causing them to impact on airway walls. In a numerical simulation of micron-sized particles (5, 10, and 20 micrometers), Rahman et al. showed that nearly all 20 micrometer particles deposited in generations G0 to G5, and none reached beyond generation G7 [29].

Similarly, in a study by Ou et al. particles of 10 micrometers exhibited intense inertial deposition in the proximal airways, particularly near carinal ridges and primary bifurcations [50].

Particles between 1 and 5 micrometers demonstrate mixed behavior. While still subject to impaction in upper airways, they can also undergo sedimentation in slower-moving distal airways. Particle transport studies under various activity levels indicate that increased flow rates shift the deposition of 5 micrometer particles toward upper generations due to stronger impaction forces.

A study by Rahman et al. revealed that approximately 48 percent of 5 micrometer particles could penetrate to generation G14, indicating their ability to reach the deeper lung under low-flow conditions. These particles are often used in inhalation therapies targeted at central-to-peripheral airways due to their deposition flexibility depending on inhalation waveform and orientation [29].

Particles smaller than 0.5 micrometers primarily deposit via Brownian diffusion, driven by random molecular collisions. These particles can reach the alveoli and even cross into systemic circulation under certain physiological conditions. In a CFD study analyzing particles from 5 nanometers to 10 micrometers, Rahman et al. reported that over 90 percent of 5 nanometer

particles avoided deposition in upper airways and reached the deep lung, a behavior consistent with their extremely low inertia and high diffusivity [29].

The same study also emphasized that increasing flow rate significantly decreased deposition for ultrafine particles by reducing their residence time and limiting their chance to diffuse toward the airway wall.

Under realistic breathing conditions, particles of varying sizes experience temporal changes in deposition behavior due to fluctuating flow velocities. A recent study on multiple breathing cycles by researchers in the Journal of Pharmaceutical Sciences revealed that 2 micrometer particles had lower deposition during light activity but showed increased efficiency during heavier inhalation due to enhanced impaction and secondary flows [51].

In summary, large particles are filtered primarily in the upper airway through inertial impaction, mid-sized particles exhibit both inertial and gravitational deposition, and ultrafine particles reach deep regions via diffusion. The choice of particle size in therapeutic aerosols must therefore be matched to the intended deposition site, taking into account patient-specific breathing conditions, posture, and disease state.

2.5.3 Particle Tracking Approaches in CFD

Accurate simulation of particle behavior in pulmonary computational fluid dynamics models requires appropriate numerical representation of the dispersed phase. The three main frameworks used for tracking aerosols are the Discrete Phase Model (DPM)**,** Lagrangian particle tracking**,** and Eulerian field methods. Each has specific assumptions, computational demands, and use cases, especially in relation to particle concentration, coupling effects, and desired resolution.

The DPM, widely available in commercial solvers like ANSYS Fluent, treats particles as point masses tracked individually within a continuous fluid. It is a Lagrangian-based approach where each particle is subjected to external forces including drag, gravity, Brownian motion, and thermophoresis. The governing equations integrate Newton's second law to resolve trajectories under a given flow field.

DPM is especially suited for low particle concentrations (dilute regime), where inter-particle collisions and feedback effects on the fluid are negligible. Mohammad S. Islam et al. used DPM to study diesel exhaust nanoparticle transport across 17 airway generations. Their simulation revealed that DPM could capture complex flow-dependent deposition patterns, particularly for Brownian and inertial transport [52].

Lagrangian tracking explicitly calculates the path of each particle over time, accounting for individualized interactions with the fluid and boundaries. While DPM is a form of Lagrangian

modeling, advanced Lagrangian methods incorporate effects such as particle clustering, wall adhesion, and detachment from carrier particles.

Sommerfeld et al. highlighted the power and limitations of Lagrangian modeling in dry powder inhalers, stressing its ability to simulate drug detachment, particle break-up, and wall rebound effects. They found that although computationally expensive, Lagrangian approaches could simulate polydisperse and agglomerated particles more realistically than field-based methods [53].

Eulerian methods treat the particulate phase as a continuous concentration field, governed by scalar transport equations similar to fluid species transport. These methods are computationally efficient for dense aerosol flows but assume continuum behavior of the particle phase, which may not hold for low concentration or large particle size applications.

Saidi et al. directly compared Lagrangian and Eulerian approaches in alveolar modeling and found that Eulerian results deviated significantly from Lagrangian solutions when particle number density was below a threshold, especially in short-time exposure scenarios [54].

For long-duration exposure or in high particle number environments, Eulerian methods provide a good approximation and are preferred for bulk deposition estimation.

Table2.2: Comparison of Particle Tracking Methods in Pulmonary

Method	**Strengths**	**Limitations**	**Recommended Use Cases**
DPM	Efficient, widely available, supports Brownian and drag	Limited inter-particle dynamics, assumes dilute flow	Therapeutic aerosol transport
Lagrangian	High-resolution particle behavior, good for clusters	High computational cost, needs large sample size	DPI simulation, deposition hotspots
Eulerian	Fast for large-scale modeling, suited for steady states	Poor accuracy at low particle counts or short exposure	Pollution modeling, long-term exposure

In summary, particle tracking strategies in CFD should be selected based on particle concentration, size distribution, exposure duration, and computational resources. A

combination of DPM for regional prediction and Lagrangian modeling for local analysis is often the most effective approach.

2.5.4 Coupling Strategies and Forces

Accurate particle transport simulations in the lung require thoughtful modeling of both fluid-particle interactions and external forces acting on aerosol particles. Two key assumptions govern these simulations: the type of phase coupling (one-way versus two-way) and the set of forces included in the particle motion equations. The combination of these assumptions determines the realism, computational demand, and applicability of the model for drug delivery or toxicological prediction.

One-way coupling assumes that the airflow field influences the motion of particles, but the reverse effect is negligible. This simplification is valid for dilute suspensions, such as in pharmaceutical aerosol delivery, where particle volume fractions are low. It reduces computational complexity and is the most widely used coupling strategy in lung CFD simulations.

For example, in the study by Xiao et al. (2013), one-way coupling using a Lagrangian model was implemented to simulate droplet transport in reactor containment environments. Their approach showed that particle feedback had minimal effect on flow field accuracy for low volume fractions [55].

Two-way coupling**,** on the other hand, accounts for the momentum exchange between the dispersed and continuous phases. This becomes essential when particles are dense or large enough to alter the flow field. Two-way coupling adds source terms for momentum (and sometimes energy) into the Navier-Stokes equations, increasing both complexity and fidelity.

Venditti et al. (2022) used a two-way coupling model to investigate particle transport through confined geometries with hydrodynamic chromatography. Their study demonstrated that neglecting two-way effects led to overestimation of particle separation efficiency [56].

Although not lung-specific, these findings stress the importance of coupling strategy selection in particle-laden flows.

Aerosol particles in the lung are subject to multiple forces beyond drag and gravity. Accurate trajectory prediction requires modeling these forces with consideration of particle size, density, and surrounding flow conditions.

- **Drag Force**: This is the dominant force opposing particle motion, often modeled using Stokes or Cunningham-corrected drag laws depending on the Reynolds number and Knudsen regime.

- **Gravitational Force**: Gravity drives particle sedimentation in horizontal or inclined airways. Its importance increases for particles above 1 micrometer and is especially relevant in lower lung regions.
- **Brownian Force**: For particles smaller than 0.5 micrometers, random molecular impacts lead to Brownian diffusion, significantly affecting deposition in alveoli.
- **Lift Forces**: In regions with high shear, especially near curved walls, Saffman or Magnus lift forces may contribute to lateral displacement of particles. These are less commonly implemented due to lack of empirical constants for lung environments.
- **Thermophoretic and Electrostatic Forces**: While rare in conventional respiratory studies, these may be relevant for nanoparticle research or heated inhalation devices.

In comprehensive models, these forces are summed into the Newtonian equation of motion for each particle or group of particles. The decision on which forces to include depends on particle characteristics and the simulation's resolution.

Including or excluding physical forces such as gravity or Brownian motion should be informed by particle size, airway region, and breathing rate. Failure to do so may result in significant underestimation or mislocation of deposition sites.

2.6 Influence of Airflow Patterns on Deposition

Airflow patterns within the respiratory tract play a crucial role in determining the transport and deposition of inhaled aerosols. The nature of the airflow, whether steady or unsteady, idealized or based on actual breathing data, directly affects how long particles stay in the airways, the paths they follow, and where they eventually settle. To make accurate predictions in computational simulations, especially for drug delivery or inhalation risk assessment, it is important to reflect the true dynamics of breathing. This section examines how different assumptions about airflow, including constant versus time-varying conditions and simplified versus realistic breathing profiles, influence deposition efficiency and spatial distribution within the lungs.

2.6.1 Steady versus Unsteady Airflow Conditions in Aerosol Deposition

The simulation of respiratory airflow can be conducted under two main conditions: steady and unsteady (time-varying or transient). This choice significantly influences the accuracy of predicted particle transport and deposition patterns in the lung.

In steady-state models, the flow velocity is held constant, simplifying the governing equations and significantly reducing computational time. These models are often used for initial estimates or in studies focused on general trends rather than precise regional deposition.

For example, B. Soni and Shahrouz Aliabadi (2013) used a ten-generation idealized bronchial model to simulate both steady and unsteady inhalation. They found that steady simulations offered a good approximation of bulk flow behavior but failed to capture local variations in deposition that occur due to time-dependent vortices and flow reversals in deeper generations [57].

Unsteady simulations incorporate the natural fluctuations in flow associated with real breathing cycles, typically modeled as sinusoidal or patient-specific waveforms. This is crucial for accurately resolving dynamic features such as acceleration, deceleration, and flow reversal, which directly impact particle residence time and deposition efficiency.

Farghadan et al. (2020) conducted CFD simulations using both steady and unsteady inspiratory profiles across six patient-specific airway trees. They showed that transient flow led to more complex and physiologically realistic shear stress distributions and significantly altered deposition patterns, especially for inertial particles [58].

Kakade et al. (2002) further demonstrated that steady models could closely approximate deposition under uniform inhalation conditions, but time-varying models were required to predict deposition variability during exhalation or irregular breathing [59].

Key Comparisons:

- Steady flow assumptions typically overestimate upper airway deposition and underestimate distal deposition for particles in the 1–5 micrometer range.
- Unsteady flows reveal phase-dependent deposition, where particles entering the airways at different points in the inhalation cycle follow significantly different trajectories.
- The deposition efficiency under unsteady flow may show asymmetric behavior during inspiration and expiration due to airway compliance and vortex dynamics.

Ryusei Kizuka et al. (2023) evaluated the effect of unsteady breathing on deposition of nano-to-microscale particles in a realistic nasal airway. They found that transient simulations predicted deeper particle penetration and more uniform lobar deposition compared to steady models [60].

2.6.2 Sinusoidal Versus Realistic Inhalation Profiles: Impacts on Aerosol Deposition

Respiratory CFD studies have traditionally used idealized sinusoidal inhalation profiles to represent the time-dependent nature of breathing. While sinusoidal functions offer mathematical simplicity and reasonable approximation for tidal breathing at rest, realistic inhalation profiles, derived from spirometry or in vivo data, better reflect variability in respiratory flow dynamics. The differences between these profiles can significantly alter

particle transport behavior and deposition outcomes, especially for clinical drug delivery or exposure modeling.

Sinusoidal flow profiles are mathematically defined, continuous, and symmetrical, mimicking tidal breathing with smooth acceleration and deceleration. These models are often used in preliminary simulations because they offer control over breathing frequency and amplitude, reducing computational cost and complexity.

For example, Esmaeili et al. (2020) used a sinusoidal waveform with a maximum flow rate of 20 liters per minute in a 3D nasal geometry to evaluate deposition of ellipsoidal particles. They found that although sinusoidal profiles could approximate average flow rates, they underestimated deposition during rapid flow changes, especially in the acceleration phase of inhalation [61].

Kakade et al. (2002) similarly found that sinusoidal waveforms led to smoother particle distribution patterns in comparison to time-varying real flows, especially under low activity conditions [59].

Realistic profiles are derived from actual breathing data recorded using spirometry or imaging-based lung function analysis. These profiles include asymmetric phases of inspiration and expiration, irregular accelerations, flow pauses, and often show a sharp rise to peak inspiratory flow followed by a gradual decay.

Longest et al. (2020) used realistic inhalation waveforms in combination with aerosol synchronization techniques to optimize nose-to-lung delivery. Their study demonstrated that realistic waveforms improved distal deposition targeting and reduced nasal loss by over 60 percent compared to sinusoidal models. They also confirmed that synchronizing aerosol delivery with realistic flow peaks allowed for more efficient deposition across both central and peripheral airways, especially for small-particle therapies administered through nasal cannula systems [62].

Mirzaaghaian et al. (2024) developed aerosol breathing profiles based on measured transient inhalation data—reporting peak flow rates up to 263 L/min for males and 161.6 L/min for females—and incorporated these into CFD simulations using realistic human lung geometries. They observed significantly altered deposition efficiencies in upper and mid-airway regions compared with simulations using steady flow, highlighting the critical impact of realistic waveforms on targeted drug delivery [63]. The differences between sinusoidal and realistic inhalation profiles influence aerosol deposition in several important ways, as outlined below:

- **Deposition Efficiency**

  Realistic profiles generate sharper and more pronounced deposition peaks in key airway regions due to rapid inhalation phases that sinusoidal models smooth over.
- **Phase-Dependent Behavior**

  Particles entering the airway during early acceleration phases (just after the onset of inhalation) show deeper penetration and more targeted deposition than those inhaled later.
- **Flow Magnitude and Timing**

  Real breathing profiles capture high peak flows and dynamic acceleration rates that significantly influence inertial impaction and sedimentation—factors essential for therapeutic or toxicological relevance.

These distinctions highlight the importance of using realistic inhalation waveforms in CFD studies when accurate regional deposition predictions are necessary, such as in inhaler design, environmental exposure modeling, or targeted respiratory treatments.

2.6.3 Effects of Airflow Changes on Aerosol Particle Transport in the Lung

Variations in respiratory airflow due to activity level, posture, lung health, or waveform dynamics profoundly influence the transport and deposition of aerosol particles in the human lung. These changes can alter particle residence time, affect secondary flow development, and shift the dominant deposition mechanisms from diffusion to impaction or sedimentation, depending on particle size and airway region.

Higher flow rates, often associated with physical activity or deep inhalation, increase airflow velocity and Reynolds number, enhancing inertial impaction. This results in greater deposition in the upper airways and reduces particle penetration to distal regions. For example, Rahman et al. (2021) showed that as inspiratory flow increased from 15 to 60 liters per minute, the deposition of 10 micrometer particles increased significantly in the tracheobronchial region, reducing the likelihood of distal delivery [29].

Similarly, Farghadan et al. demonstrated that under heavy breathing, even submicron particles showed altered distribution due to higher convective forces and more complex flow structures in bifurcations [64].

Studies comparing sinusoidal, ramped, and real-world inhalation profiles show that the rate of acceleration and deceleration affects vortex formation and secondary flows, which in turn modulate particle pathlines. Kakade et al. (2002) reported that phase-specific flow transitions could shift deposition regions by several generations of airways, especially for particles between 1 and 5 micrometers [59].

Airflow changes also impact the lobe-wise distribution of aerosol. In a multicycle CFD study, Journal of Pharmaceutical Sciences (2022) found that during light breathing, small particles followed streamlines into the lower lobes, while under heavy breathing, deposition became concentrated in upper generations and shifted toward the right upper lobe due to enhanced inertia [65].

Increased airflow leads to turbulence in upper airways, especially near the larynx and trachea. This introduces random fluctuations that can increase particle-wall collisions and deposition. Spasov et al. (2024) highlighted that neglecting turbulent fluctuations led to underprediction of local hot-spot deposition in upper bronchial bifurcations [66].

2.6.4 Comparative Studies of Aerosol Deposition Under Different Inhalation Waveforms

Several computational and experimental studies have investigated how varying inhalation waveforms influence the transport and deposition of aerosol particles in the lung. These waveforms typically include constant flow (square-wave), ramped flow, sinusoidal breathing, and more complex realistic or patient-specific profiles. The outcomes of such comparative studies reveal that deposition predictions can vary significantly depending on the inhalation pattern assumed.

In a comprehensive validation study, Longest et al. (2016) developed a whole-airway CFD model for a dry powder inhaler and compared three distinct inhalation waveforms—constant, ramp, and realistic patient-breathing profiles—against gamma scintigraphy imaging data. Their findings demonstrated that models using realistic waveforms provided the most accurate predictions of regional deposition, with relative errors below 10 percent in both the tracheobronchial and peripheral airway regions. In contrast, constant and ramp profiles showed larger discrepancies, particularly in estimating alveolar deposition, due to their inability to capture peak inspiratory acceleration and deceleration phases [67].

Augusto et al. (2016) performed a simulation using a triple bifurcation airway model to compare particle deposition under inhalation, exhalation, and breath-hold conditions. Using 5-micrometer particles, they observed that breath-holding after inhalation significantly increased deposition efficiency, particularly in distal airway branches. This was attributed to prolonged particle residence time, which allowed gravitational sedimentation and Brownian diffusion to take effect. Their study provides computational support for the medical recommendation to hold one’s breath after inhaling aerosolized medication [68].

Tian et al. (2015) also conducted a comparative analysis using CFD models validated against in vivo data from monodisperse aerosol exposures. Their investigation revealed that fast, forceful inhalation waveforms enhanced deposition in the upper airway due to increased

inertial impaction, while slower inhalation profiles promoted deeper penetration of particles into the central and peripheral lung regions. These findings are particularly relevant for optimizing inhaler techniques, where the velocity and duration of inhalation can be controlled for targeted drug delivery [23].

Collectively, these studies emphasize that the inhalation waveform is not a trivial modeling parameter but a critical determinant of deposition outcomes. Realistic and patient-specific profiles are consistently shown to enhance predictive accuracy, both in regional targeting and total lung deposition estimation. They are especially essential in therapeutic scenarios requiring precision, such as in treating obstructive airway diseases or delivering inhaled vaccines.

2.7 Role of Body Orientation and Gravity

The influence of gravity on particle behavior becomes particularly significant in the lungs, where body posture and orientation relative to the gravitational vector can alter airflow patterns, regional ventilation, and deposition sites. The following subsections explore how gravitational direction, posture, and experimental observations contribute to understanding posture-dependent aerosol transport and highlight the limitations in current modeling approaches.

2.7.1 Gravity Vector Effects on Aerosol Transport

Gravitational sedimentation is one of the dominant mechanisms for aerosol deposition in the lung, especially for particles ranging from 0.5 to 5 micrometers under resting breathing conditions. The direction of gravity relative to lung geometry significantly influences airflow distribution, particle trajectories, and ultimately, the regional and lobar deposition patterns.

In a modeling study by Asgharian, Price, and Oberdörster (2006), the authors demonstrated that gravity affects lung ventilation by altering lobar expansion and contraction dynamics. Increased gravitational force resulted in enhanced upper lobe expansion and decreased lower lobe inflation in upright posture, influencing both airflow pathways and particle sedimentation sites. The study also showed that under reduced gravity, such as microgravity conditions, deposition of coarse particles (greater than 2.5 μm) shifted toward a more uniform distribution, while fine particle behavior was less affected [69].

In a more recent study, Koullapis et al. (2020) used a deep lung model (DLM) to investigate the effect of gravitational orientation on deposition in distal airways. By rotating the lung model in seven different directions relative to gravity, the authors found that subtle orientation changes can result in meaningful shifts in local deposition patterns, even under the same breathing profile. Their findings suggest that posture plays a critical role in particle targeting, especially for small to intermediate-sized particles [70].

Experimental results from Darquenne (2014) also validate this principle. During parabolic flights mimicking microgravity and hypergravity conditions, she observed that while overall deposition increased with gravity, the peripheral deposition (below 200 mL penetration depth) was most sensitive to gravitational influence. This supports the idea that gravity critically governs sedimentation in the distal acinar and alveolar regions [45].

These findings collectively show that gravity is not merely a constant parameter but a spatially dependent vector that influences not only how much but also where particles deposit in the lung. Accurate CFD simulations must therefore incorporate gravitational directionality, especially when modeling posture-dependent deposition, sleep-related therapies, or microgravity conditions such as spaceflight.

2.7.2 Effect of Body Posture on Aerosol Deposition

The orientation of the body relative to gravity alters lung shape, airway geometry, and regional ventilation, which in turn affects aerosol particle distribution. Multiple experimental and clinical studies have demonstrated posture-dependent differences in deposition patterns, highlighting the need to consider body position in both inhalation therapy and aerosol exposure risk assessments.

In an imaging-based study, Darquenne et al. (2016) measured regional deposition in supine healthy subjects and patients with mild-to-moderate COPD. Using aerosol bolus inhalation and gamma scintigraphy, they found that although total deposition did not differ significantly between upright and supine postures, the distribution pattern shifted, with increased aerosol dispersion and altered flow sequencing in the supine condition. The effect was more pronounced in COPD patients, suggesting that posture amplifies underlying ventilation inhomogeneity [71].

Mills et al. (2002) studied the effect of posture shift from upright to supine on aerosol bolus mode shift in healthy subjects. Their results revealed more mouthward particle displacement (indicating shallower penetration) in the supine position, which was attributed to increased flow heterogeneity. Interestingly, deposition did not significantly change, but particle distribution was strongly influenced by convective inhomogeneity arising from postural shifts [72].

In a study evaluating lateral decubitus positions, Alcoforado et al. (2011) used pulmonary scintigraphy to analyze deposition while subjects lay on their left or right side. They found significantly higher deposition in the dependent lung (i.e., the side facing downward), consistent with posture-induced shifts in regional ventilation and gravitational sedimentation.

This position-dependent redistribution supports the use of lateral positioning in therapeutic strategies to enhance delivery to specific lung zones [73].

Sa et al. (2017) further investigated the supine posture and showed, using co-registered MRI and gamma scintigraphy, that alveolar deposition of coarse particles was predominantly determined by the regional ventilation pattern, which shifts posteriorly when lying down. These results underscore how posture modifies the ventilation-perfusion relationship and deposition efficiency [74].

In summary, posture substantially impacts aerosol deposition. Supine and lateral positions alter gravitational gradients and ventilation distributions, while prone positioning (though less studied) is hypothesized to enhance posterior lung ventilation, potentially improving deposition in dorsal regions. Such insights are essential when designing aerosol therapy protocols for bedridden patients or understanding risk under different environmental exposure settings.

2.7.3 Experimental Studies on Gravity and Posture Effects

Experimental studies using imaging techniques and animal models have provided compelling insights into how body orientation and gravity shape aerosol deposition patterns in the lungs. These studies serve as critical validation references for computational fluid dynamics (CFD) models and also inform clinical strategies for posture-based therapy optimization.

In a classic animal study, Sneddon and Brain (1981) examined aerosol deposition in rats placed in upright, prone, and inverted postures. After exposing the animals to 0.7–0.8 μm radioactive aerosols, they observed a consistent apex-to-base deposition gradient, with more particles deposited in apical lung regions across all postures. Interestingly, these gradients persisted regardless of body orientation, suggesting that gravitational effects interact with airway anatomy and ventilation distribution in complex ways [75].

Chantal Darquenne et al. (2014) conducted microgravity experiments aboard NASA aircraft to isolate the role of gravity in particle transport. Using MRI-based measurements in rats, they found that in the absence of gravity, fine particles (~0.95 μm) deposited deeper in the lungs, particularly in peripheral regions. This shift in spatial distribution underlined the importance of gravitational sedimentation in normal gravity environments and its reduction in microgravity, which alters residence time and particle dynamics [76].

In vitro experiments have also contributed significant data. Theunissen et al. (2006) constructed a physical model mimicking the 21st generation of the Weibel lung model using cylindrical alveolar cavities. By tracking iron particles in a silicone oil flow, they quantified how aerosol trajectories were altered by curved airway geometry and gravity. Their results revealed that despite low Reynolds numbers (~0.07), gravitational sedimentation was the dominant

mechanism, and no particles followed streamlines perfectly, highlighting the challenge of modeling these flows numerically [77].

Moreover, MRI and gamma scintigraphy have increasingly been used in human and animal studies to quantify posture-induced changes in deposition. A study by Sa et al. (2017) using coarse 5 μm particles confirmed that supine posture significantly altered regional lung deformation and shifted deposition posteriorly compared to seated posture.

These experimental approaches provide robust data on the interplay between gravity, posture, and aerosol physics. Their results confirm that even subtle orientation changes can lead to non-trivial variations in both total and regional deposition, particularly for particles in the sedimentation-dominant size range. They also highlight that validation of CFD models requires careful consideration of posture-specific gravitational influences.

2.7.4 Limitations of Past CFD Studies on Body Orientation

Although computational fluid dynamics (CFD) has proven instrumental in advancing our understanding of aerosol behavior in the respiratory system, a critical gap persists in how body orientation is integrated into these simulations. Most existing CFD models either ignore postural variation altogether or assume a fixed, upright gravitational vector, irrespective of the actual body posture under study.

A key limitation lies in the widespread use of steady-state or idealized breathing profiles. Studies such as those by Koullapis et al. have simulated aerosol deposition across various anatomical models and flow conditions, but typically retain a vertical gravity direction, even when evaluating non-upright positions. As a result, these models may inaccurately estimate gravitational sedimentation in supine or lateral orientations.

Furthermore, body orientation has often been treated as a peripheral parameter, rather than a primary variable influencing deposition. Several studies introduce orientation-based simulations without updating flow partitioning or lobar deformation patterns that naturally arise from changes in thoracic geometry during postural shifts. This simplification overlooks the dynamic interplay between lung deformation, regional ventilation, and gravity-dependent particle motion.

Miyawaki et al. (2017) highlighted some of these challenges in their multi-patient airway modeling study. While their work used anatomically realistic CT-based lung models, all simulations were conducted under upright posture assumptions. No gravitational reorientation or posture-specific deformation was incorporated, limiting the translatability of results to real-life clinical scenarios involving recumbent or side-lying patients [78].

Another overlooked aspect is the impact of posture on local flow fields and turbulence, particularly in branching regions where airflow direction shifts in response to gravity. Most CFD studies to date use simplified geometries or omit phase-specific deformation (such as lung shape changes between upright and supine positions), which can substantially alter airflow velocities and particle residence times.

These limitations suggest that, despite growing interest, the incorporation of body orientation into aerosol transport modeling remains incomplete. To fully understand how posture influences deposition outcomes, future CFD studies must integrate gravitational reorientation with dynamic lung geometry, individualized flow rates, and realistic boundary conditions.

2.8 Drug Delivery and Clinical Relevance

In the following sections, we explore the clinical applications of aerosol delivery in respiratory diseases, the challenges of targeting specific lung regions, the role of device-based studies, and the emerging paradigm of personalized aerosol therapy.

2.8.1 Applications in Asthma, COPD, and Cystic Fibrosis

Aerosol drug delivery is a mainstay in the treatment of obstructive lung diseases such as asthma, chronic obstructive pulmonary disease (COPD), and cystic fibrosis (CF). These diseases, despite their distinct etiologies, share a common therapeutic approach: targeted pulmonary delivery that bypasses systemic circulation, minimizes side effects, and allows for rapid onset of action.

In asthma and COPD, the inhalation route is used for bronchodilators, corticosteroids, and combination therapies. Inhalers, whether pressurized metered dose inhalers (pMDIs), dry powder inhalers (DPIs), or nebulizers, are optimized for deposition in central or peripheral airways depending on the particle characteristics and breathing patterns. A comprehensive review by Hindle (2010) outlined how DPI and MDI technologies were tailored to different disease needs, with DPIs generally favored in COPD due to their breath-actuated design [79].

In CF, aerosol therapy is particularly crucial for delivering antibiotics (e.g., tobramycin), mucolytics (e.g., recombinant human DNase), and anti-inflammatory agents directly to the airways where mucus obstruction and bacterial colonization are prevalent. Diot et al. (1998) highlighted that nebulized delivery of DNAse in CF improved mucus clearance and lung function, an approach now widely used in clinical protocols [80].

Furthermore, Cheng (2003) emphasized the growing interest in systemic drug delivery via inhalation for conditions beyond the lung. The large surface area and vascularization of alveoli have made inhalation a candidate for delivering insulin, vaccines, and even chemotherapeutics in experimental contexts [81].

Recent trials like the TELOS study (Ferguson et al., 2018) have investigated co-suspension delivery in MDIs for better particle uniformity and lung deposition in COPD patients, showing improvement in FEV_1 and symptom scores [82].

These studies collectively underscore how computational and experimental advancements in inhaler design and particle characterization directly inform personalized treatment for respiratory diseases. They also provide critical validation cases for CFD models used to optimize drug targeting across different airway generations.

2.8.2 Challenges in Targeting Specific Lung Regions

Despite the advances in inhalation therapy, precisely targeting aerosolized drugs to specific lung regions such as lobes, segments, or pathological zones remains a fundamental challenge in both clinical and computational domains. A major reason for this limitation is the complex interplay between lung anatomy, airflow heterogeneity, particle properties, and patient-specific physiology.

One of the key challenges is controlling particle deposition depth. The ideal scenario in treating diseases such as bronchiectasis or localized infections is to deposit therapeutic agents deep into the lower lobes or affected airways while avoiding unnecessary deposition in the mouth-throat or central bronchi. However, this is complicated by factors like airway curvature, turbulence, and impaction, which cause large particles to deposit prematurely and small particles to be exhaled without deposition.

Yan Ostrovski et al. (2019) proposed a novel inhalation framework using pulsed aerosol boluses followed by controlled inhalation volumes and breath-hold maneuvers. Using CFD simulations, they showed that this approach can confine deposition to targeted upper-airway regions by manipulating particle entry timing and flow rate. While promising for targeting specific airway generations, such techniques are yet to be widely translated into clinical inhaler design [83].

Ghanem et al. (2025) reviewed the practical barriers to regional drug delivery, highlighting key physiological defenses such as mucociliary clearance, airway humidity, and surface liquid dynamics. These mechanisms, while protective, limit drug residence time and bioavailability. They also emphasized the challenge of immune system interference and inconsistent lung inflation, particularly in conditions like asthma or fibrosis, where disease morphology varies dramatically between patients [84].

Xu et al. (2023) further highlighted the computational challenges in achieving targeted delivery using patient-specific lung models. Even when using transient RANS or LES simulations, variations in local deposition caused by subtle differences in airway bifurcation angles or

localized turbulence were difficult to predict accurately. Their findings suggest that small deviations in particle injection angle or breathing profile can shift the deposition site from one lobe to another [85].

Another limitation lies in the lack of dynamic lobe-based targeting in current commercial inhalers. Most devices deliver aerosols uniformly across the lung, despite disease often being region-specific. Computational models and experimental data suggest that strategic control of flow rate, particle diameter, and posture during inhalation could optimize lobar targeting, but such strategies remain largely unimplemented in clinical practice.

In summary, while numerical and experimental studies have introduced innovative methods for enhancing regional delivery, real-world application remains constrained by anatomical variability, breathing dynamics, and limited control over inhaler actuation. Overcoming these barriers will require further integration of CFD models with personalized treatment planning and smart inhaler technologies.

2.8.3 Device-Based Studies

The efficiency of aerosol drug delivery is closely tied to the design and functionality of the delivery device. Among the most widely used devices are Dry Powder Inhalers (DPIs)**,** Metered Dose Inhalers (MDIs), and nebulizers, each with distinct aerosolization mechanisms, flow dependencies, and delivery profiles. Computational and experimental studies have played a key role in quantifying their deposition efficiencies and optimizing their design for therapeutic use.

A seminal study by Longest et al. (2012) compared MDI and DPI deposition using both in vitro experiments and a validated CFD model based on a stochastic individual path (SIP) approach. They showed that for the same drug and airway geometry, MDIs delivered approximately twice as much drug to the tracheobronchial region compared to DPIs, especially under low-flow conditions. The DPI showed greater oropharyngeal deposition (~70%), while MDI had better distal reach (~50% alveolar deposition). Both devices exhibited decreased efficiency with improper inhalation, dropping by up to 30% [86].

Traditional jet and ultrasonic nebulizers are valued for their ability to deliver high drug loads and are often used in pediatric and geriatric populations. However, their lack of synchrony with inhalation results in drug waste and environmental exposure. Recent technologies such as surface acoustic wave (SAW) nebulizers have addressed these inefficiencies. In a study by Yousefi et al. (2017), CFD simulations demonstrated that SAW-generated aerosols had finer particle sizes and better penetration into the lower lung when introduced near the spacer

centerline. The study also highlighted that right lung deposition dominated regardless of device or posture, emphasizing the importance of device positioning and flow symmetry [87].

Using Functional Respiratory Imaging (FRI), Suggett et al. (2022) compared deposition from MDIs with spacers and DPIs in a COPD patient-specific model. At both low and high flow rates, the MDI with AeroChamber Plus Flow-Vu spacer delivered a significantly higher lung dose than either DPI tested. DPI usage, even at optimal flow, resulted in higher oropharyngeal deposition and less lung penetration. This reinforces the role of spacers in enhancing deposition for patients with coordination issues [88].

Several studies, including Kim & Chen (2008), have shown that the internal geometry of inhalers and patient-specific inhalation profiles dramatically alter aerosol trajectory. Their CFD analysis in a realistic oral–tracheal geometry found that turbulent regions caused substantial inertial impaction, especially for MDIs actuated during early inhalation phases [89].

These findings collectively suggest that no inhaler type is universally superior; each must be tailored to the patient's anatomy, breathing capacity, and disease localization. CFD and in vitro studies continue to play a central role in guiding device innovation and dosage optimization.

2.8.4 Personalized Aerosol Therapy Approaches

The paradigm of personalized aerosol therapy has emerged in response to the limitations of conventional, one-size-fits-all inhalation strategies. Differences in airway geometry, lung compliance, breathing effort, and disease morphology across patients can lead to substantial variability in drug delivery outcomes, even when using the same device and medication. As such, integrating patient-specific data into the design and delivery of aerosol therapy is increasingly recognized as essential to improving efficacy and minimizing off-target deposition.

A recent study by Bartlett et al. (2021) developed a computational model that incorporated the lung’s mucus layer properties to simulate the diffusion and clearance of inhaled particles. By accounting for disease-specific mucus viscosity and transport rates, the model predicted how different aerosolized particles behaved in pathological environments such as cystic fibrosis and chronic bronchitis. This framework enables the tailoring of drug particle size and dosage based on disease state and patient physiology [90].

Peterman et al. (2020) demonstrated the utility of 3D-printed lung replicas derived from patient imaging data to experimentally validate CFD predictions. Their setup allowed differential control of flow into each lobe and enabled high-throughput assessment of deposition patterns using fluorescent aerosols. This in vitro platform supports rapid prototyping of personalized

treatments and has been applied to optimize ventilation-perfusion matching in patients with heterogeneous lung disease [91].

Feng (2018) proposed the concept of a "digital twin" for pulmonary healthcare. This approach combines CFD simulations, spirometry data, and anthropometric measurements to create a virtual copy of a patient's lung for predictive modeling. With such tools, clinicians can simulate various inhaler-device combinations and inhalation profiles to identify the optimal treatment regimen. This has been especially useful in targeting localized lesions such as lung tumors or infected zones in tuberculosis and COVID-19 [92].

Personalized aerosol delivery is also being explored in acute care settings. Wang et al. (2022) used a patient-specific model of moderate COVID-19 and tested a point-source aerosol release method using a customized tracheobronchial geometry. They showed that particle targeting to infected segments (pneumonia alba) could be improved by more than 3× compared to conventional random delivery [93].

These advances highlight a growing convergence of imaging, CFD, and experimental design in pursuit of personalized respiratory care. Personalized therapy platforms not only promise higher deposition efficiency and better therapeutic targeting but also offer a pathway to reduce dosing frequency, lower drug toxicity, and enhance patient adherence.

2.9 Summary of Gaps in the Literature

2.9.1 Posture-Insensitive Use of Realistic Lung Geometry in Aerosol CFD Studies

The emergence of CT-based and MRI-derived airway geometries has significantly improved the anatomical fidelity of CFD simulations in pulmonary medicine. Many contemporary models incorporate subject-specific branching patterns, lobe segmentation, and detailed tracheobronchial structures. However, a major limitation remains: these geometries are typically simulated under a fixed upright posture, with a gravitational vector that does not reflect the body's orientation during clinical conditions such as sleep, supine ventilation, or lateral positioning.

For example, Miyawaki et al. (2017) introduced an automated mesh generation method for CT-derived airway models, successfully combining high anatomical detail with computational efficiency. Their study improved realism in geometry and airflow simulation but maintained a vertical gravitational vector across all simulations, regardless of posture [78].

In a similar vein, von Wedel et al. (2022) compared deposition patterns in three distinct subject-specific lung geometries using unsteady Reynolds-averaged Navier-Stokes (URANS) simulations. While the study revealed that anatomical variation significantly alters aerosol

behavior—particularly in the laryngeal region—it did not incorporate body orientation or reorientation of the gravity vector [94].

Earlier, Ma and Lutchen (2009**)** had demonstrated that the use of realistic large-to-medium airway structures altered deposition predictions compared to idealized geometries. However, this study also retained an upright gravitational reference frame throughout [24].

These examples underscore a consistent trend: while anatomical accuracy has improved**,** the simulations remain posture-insensitive, effectively decoupling the geometry from its orientation-dependent physiological function. In doing so, these models may misrepresent gravity-driven phenomena such as sedimentation, especially in the peripheral lung regions and lower lobes.

This gap is particularly relevant for aerosol therapies administered in non-upright patients such as those in intensive care, undergoing surgery, or sleeping, where gravity-altered flow redistribution can significantly affect regional drug deposition. The lack of posture variation in geometrically realistic CFD studies limits their ability to provide precise, clinically actionable predictions for such scenarios.

2.9.2 Lack of Posture-Integrated Studies with Realistic Aerosol Breathing Profiles

Accurate simulation of aerosol dynamics in the respiratory tract requires not only realistic anatomical models and accurate physical forces but also a faithful representation of human breathing profiles. Over the years, computational models have moved from simple sinusoidal waveforms to more physiologically representative time-varying profiles derived from spirometry. However, despite these advancements, the impact of body orientation on simulations using realistic breathing waveforms has not been adequately explored.

A major contribution in this domain was made by Mirzaaghaian et al. (2024)**,** who developed measured aerosol breathing profiles based on spirometric data. Their model captured real inhalation dynamics, showing peak inspiratory flow rates of 263 L/min for males and 161.6 L/min for females, and incorporated these profiles into simulations using anatomically reconstructed lung geometries. Although this study represents a significant step toward physiologically relevant simulations, it assumed a fixed upright gravitational vector, leaving the effects of posture on deposition under realistic breathing conditions unexplored [63].

Other studies have also modeled transient respiratory cycles in anatomically realistic airway structures. For example, Kizuka et al. (2023) reproduced two unsteady breathing cycles to simulate deposition of particles ranging from 2 nm to 10 μm. Their results revealed significant variation in particle transport and deposition under different breathing profiles. Yet, like many similar studies, posture-related gravity effects were omitted.

This lack of orientation-aware modeling during realistic, time-resolved breathing conditions represents a significant shortcoming in the field. Posture not only changes gravitational sedimentation paths but also alters regional lung compliance and airflow partitioning, especially during peak inhalation. As such, using realistic breathing profiles without incorporating posture restricts the applicability of these models to clinical scenarios such as drug delivery during sleep, rehabilitation, or intensive care.

Therefore, while substantial efforts have been made to replicate the dynamic nature of breathing, their clinical relevance remains limited unless the effect of posture is concurrently modeled. This calls for an integrative modeling framework that combines real-time breathing dynamics with body orientation, enabling more predictive simulations of aerosol transport and deposition.

2.9.3 Lack of Integrated Models Combining Anatomy, Breathing Pattern, and Body Orientation

A major gap in the current computational literature lies in the absence of studies that simultaneously consider realistic lung geometry, physiologically measured breathing profiles, and posture-specific gravitational orientation. While the individual significance of each of these components has been demonstrated, they have never been modeled together in a single simulation framework.

As discussed in the previous subsections, several studies have utilized anatomically accurate airway models reconstructed from imaging data. Others have focused on reproducing time-varying aerosol breathing patterns based on spirometric measurements. Some works have addressed the influence of gravity by simulating different body orientations. However, these elements have typically been examined in isolation.

None of the earlier studies incorporated all three critical factors together. Most assumed a fixed upright posture when evaluating deposition in realistic airway geometries. Similarly, studies that adopted transient inhalation waveforms did not examine how posture might alter airflow partitioning and particle sedimentation. Even in works where posture was varied, breathing was simplified and anatomical representation was either idealized or limited in extent.

This fragmentation in methodology restricts the predictive accuracy of models, particularly in clinical conditions where posture plays a central role. Examples include aerosol therapy during sleep, drug delivery in intensive care settings, and posture-dependent lung disorders. Without an integrated approach, such applications cannot be fully simulated or optimized.

The present study fills this critical gap by combining a realistic human airway geometry, dynamic aerosol breathing profiles derived from actual measurements, and posture-specific

gravitational conditions. By doing so, it enables the first comprehensive assessment of how body orientation affects regional aerosol deposition across lobar and segmental structures under physiologically relevant conditions. This integrative model offers new insights that are essential for the development of posture-aware therapeutic strategies and personalized pulmonary drug delivery.

Chapter 03

Methodology

3.1 Reconstruction of the Realistic Lung Model

The three-dimensional anatomical model of the human respiratory system used in this study was developed through a rigorous image-based reconstruction process using high-resolution Computed Tomography (CT) scan images. These images were acquired from a healthy 45 years old adult female subject and served as the foundational dataset for generating a geometrically accurate lung model. The reconstruction was carried out using MIMICS (Materialise, Belgium), a specialized medical image processing software widely used for creating patient-specific anatomical models from radiographic imaging data.

MIMICS allows for advanced segmentation, surface generation, and smoothing capabilities, enabling the transformation of raw grayscale CT slices into a digital 3D model that accurately represents the internal airway structure. In the segmentation phase, thresholding and region-growing techniques were used to isolate the airway lumen from surrounding tissues. Careful manual editing was also applied where necessary to enhance segmentation accuracy, particularly in regions with low contrast or partial volume effects. The result was a high-fidelity STL (stereolithography) surface mesh representing the inner airway walls, which could be further processed for computational simulation.

The reconstructed geometry includes the trachea, carina, and major conducting airway branches extending to the lobar bronchi of both lungs. Specifically, the model captures the three lobes of the right lung—namely, the right upper lobe (RUL), right middle lobe (RML), and right lower lobe (RLL)—as well as the two lobes of the left lung—the left upper lobe (LUL) and left lower lobe (LLL). These anatomical features were segmented with high resolution, preserving key structural aspects such as bifurcation points, curvature of bronchial tubes, and inter-lobar branching patterns.

An important aspect of the reconstruction process was the preservation of the natural asymmetry between the left and right lungs. Unlike symmetric simplified models often used in respiratory studies, the current model retains the true anatomical configuration, including the larger volume of the right lung and the distinctive branching angles found on each side. This asymmetry plays a significant role in influencing airflow dynamics and particle transport, especially under varying gravitational orientations.

In addition to the main airways, the model also captured cross-sectional changes along the bronchial tree, which can affect the development of secondary flows and turbulence within the respiratory passages. By resolving these subtle geometric variations, the reconstructed model provides a physiologically realistic basis for simulating transient airflow during breathing and analyzing particle deposition behavior in different lobes.

The resulting geometry serves as the computational domain for the CFD simulations performed in this study. Its anatomical accuracy ensures that simulation results can reflect physiologically meaningful flow and deposition patterns, providing a robust platform for exploring the influence of body orientation, particle size, and breathing dynamics on targeted aerosol delivery. Overall, this image-based reconstruction process bridges the gap between medical imaging and computational modeling, enabling high-precision studies of respiratory fluid mechanics.

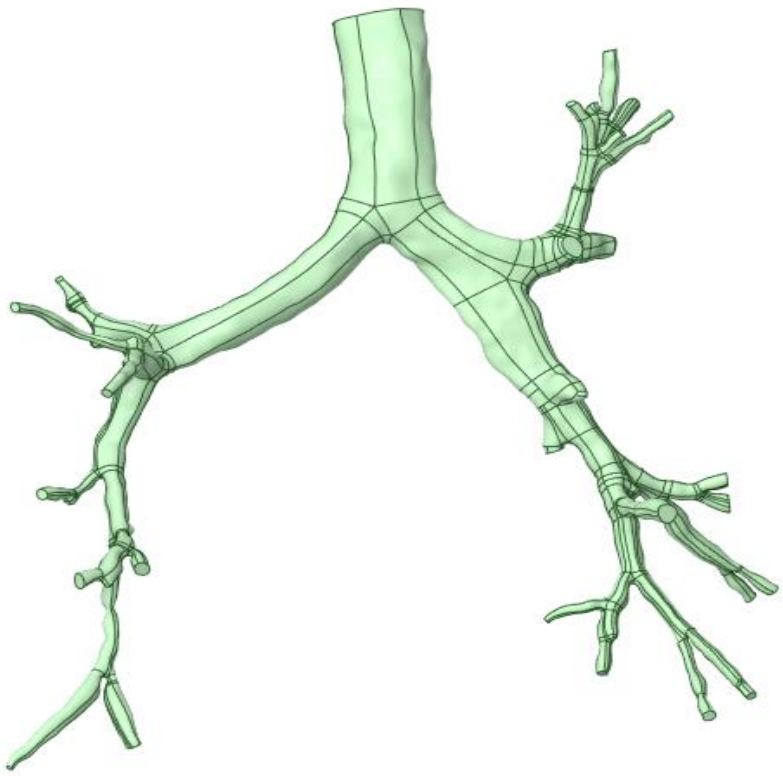
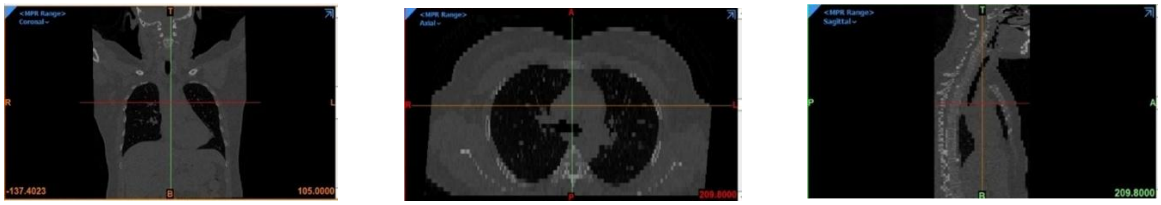


Figure 3.1: *Reconstructed model of human lung using CT scan images*



(a): Coronal view (b): Axial view (c): Sagittal view

***Figure 3.2**: Sample CT image slices in MIMICS during lung model reconstruction (a) Coronal view, (b) Axial view, and (c) Sagittal view.*

3.2 Governing Equations and Physical Models

To model airflow and particle transport within the lung, this study employs governing equations for both the continuous and discrete phases under a one-way coupling framework. The airflow field is first computed and then used to track aerosol motion. The following subsection presents the mathematical formulation for the continuous-phase airflow.

3.2.1 Mathematical Formulation of Continuous-Phase Airflow

In this study, the airflow through the reconstructed human lung model was simulated using the incompressible, unsteady Navier–Stokes equations, which govern the motion of Newtonian fluids. These equations were solved numerically using ANSYS Fluent to capture the time-dependent behavior of inhaled air under realistic reathing conditions.

The governing equations for the continuous phase are given by:

Continuity Equation (3.1):

$$\nabla \cdot u = 0$$

Momentum Equation (3.2):

$$\frac{\partial u}{\partial t} + (u \cdot \nabla)u = -(1/\rho)\,\nabla p + \nu\,\nabla^2 u$$

where:

- u is the velocity vector
- p is the static pressure
- ρ is the fluid density
- ν is the kinematic viscosity ($\nu = \mu/\rho$)
- t is the time variable

The continuity equation ensures that the net volume flow rate into any control volume is zero, which is a fundamental requirement for mass conservation in incompressible flows. The

momentum equation represents the conservation of linear momentum and accounts for the effects of pressure gradients, viscous diffusion and inertial forces due to the unsteadiness and acceleration of flow.

To provide greater physical insight into the transport processes along each spatial direction, the momentum and continuity equations can be written in their Cartesian scalar form as follows:

Scalar Continuity Equation:

$$\frac{\delta \mathrm{u}}{\delta x} + \frac{\delta v}{\delta y} + \frac{\delta w}{\delta z} = 0$$

Momentum Equation at X-direction:

$$\frac{\delta \mathrm{u}}{\delta t} + \mathrm{u}\,\frac{\delta \mathrm{u}}{\delta x} + v\frac{\delta \mathrm{u}}{\delta y} + w\,\frac{\delta \mathrm{u}}{\delta z} = -\frac{1}{\rho}\,\frac{\delta p}{\delta x} + \nu\left(\frac{\delta^2 \mathrm{u}}{\delta x^2} + \frac{\delta^2 \mathrm{u}}{\delta y^2} + \frac{\delta^2 \mathrm{u}}{\delta z^2}\right)$$

Momentum Equation at Y-direction:

$$\frac{\delta v}{\delta t} + \mathrm{u}\,\frac{\delta v}{\delta x} + v\frac{\delta v}{\delta y} + w\,\frac{\delta v}{\delta z} = -\frac{1}{\rho}\,\frac{\delta p}{\delta y} + \nu\left(\frac{\delta^2 v}{\delta x^2} + \frac{\delta^2 v}{\delta y^2} + \frac{\delta^2 v}{\delta z^2}\right)$$

Momentum Equation at Z-direction:

$$\frac{\delta w}{\delta t} + \mathrm{u}\,\frac{\delta w}{\delta x} + v\frac{\delta w}{\delta y} + w\,\frac{\delta w}{\delta z} = -\frac{1}{\rho}\,\frac{\delta p}{\delta y} + \nu\left(\frac{\delta^2 w}{\delta x^2} + \frac{\delta^2 w}{\delta y^2} + \frac{\delta^2 w}{\delta z^2}\right)$$

These scalar equations explicitly represent the transport of momentum and conservation of mass in each coordinate direction, and serve as the mathematical basis for the numerical solution of the fluid field. While the equations are originally formulated as partial differential equations defined over a continuous space-time domain, they must be converted into algebraic form to be solved computationally.

This conversion is achieved through a process known as discretization, in which the spatial domain is divided into small control volumes and the governing equations are approximated in integral form. The resulting algebraic equations are then solved iteratively across the entire computational domain. In this study, the finite volume method (FVM) is used for this transformation. It is implemented in ANSYS Fluent. This method ensures that mass and momentum are conserved within each control volume and is well-suited for complex shapes like the human airway tree.

The complete discretization and numerical implementation strategy using FVM in ANSYS Fluent is described in the following subsection.

3.2.2 Finite Volume Discretization and Numerical Implementation in ANSYS Fluent

To solve the incompressible Navier–Stokes and continuity equations in the complex geometry of the human lung, the finite volume method (FVM) was employed. This method is widely used in CFD due to its inherent conservation properties and its ability to handle irregular and anatomically realistic domains. All simulations in this study were performed using ANSYS Fluent, which utilizes FVM as the core numerical technique for solving governing flow equations over a discretized domain.

In the FVM approach, the computational domain is divided into a finite number of small, non-overlapping control volumes (cells)**.** These control volumes were generated from the pre-processed lung geometry using a high-quality polyhedral mesh with local refinement near bifurcations and curved surfaces to capture critical flow features. The fundamental idea is that the governing equations are applied to each control volume in integral form, rather than their differential form, which is more suitable for complex, non-uniform geometries.

The integral form of the conservation laws ensures that fluxes of mass, momentum, and energy are conserved within each control volume. For instance, the integral form of the continuity equation over a control volume V with surface S is given by:

$\int_S \rho u.\,\mathrm{n}\, dS = 0$

where n is the outward-pointing normal vector on the surface S. This equation implies that the net mass flux through the surface of the control volume is zero, thereby enforcing mass conservation.

By applying the divergence theorem and appropriate numerical interpolation schemes to the integrated equations, the surface integrals are transformed into algebraic equations involving values of velocity, pressure, and other variables at discrete cell centers and face centers. These equations are then assembled for all control volumes to form a large system of coupled algebraic equations. These take the general matrix form:

$$Ax=b$$

where A is the coefficient matrix derived from the discretized terms, x is the vector of unknown flow variables (e.g., velocity components, pressure), and b is the source term vector arising from boundary conditions and body forces.

Since the governing equations are nonlinear, particularly due to the convective term $u\cdot\nabla u$, the algebraic system must be linearized before being solved. ANSYS Fluent uses iterative algorithms to solve these linearized systems at each step of the solution process.

To solve the coupled momentum and continuity equations, a pressure–velocity coupling algorithm is required. In this study, the SIMPLE (Semi-Implicit Method for Pressure-Linked Equations) algorithm was employed, which is widely used for incompressible flow problems. SIMPLE iteratively updates pressure and velocity fields to ensure that the continuity and momentum equations are simultaneously satisfied.

The algorithm involves:

- Predicting the velocity field from an initial pressure guess,
- Computing the pressure correction to reduce the continuity error,
- Updating the pressure and velocity fields,
- Repeating this cycle until convergence.

Because the airflow simulation in this study is transient, the governing equations were also discretized in time using a second-order implicit scheme. This scheme provides good accuracy for time-dependent flows and allows for relatively larger time steps without sacrificing numerical stability.

At each time step:

- The solver marches forward by solving the discretized equations using the previously computed flow field as the initial condition.
- Convergence within each time step is monitored through residuals and continuity criteria.
- A complete breathing cycle is simulated over multiple time steps to capture the unsteady evolution of the airflow field.

The solution process was considered converged at each time step when the scaled residuals of continuity and momentum equations fell below 10^{-4}. The use of the finite volume method combined with a robust solver architecture in ANSYS Fluent enabled accurate and stable simulation of airflow dynamics in the anatomically realistic lung model under transient inhalation conditions. The resulting velocity and pressure fields were later used to calculate wall shear stress and to drive particle motion in the discrete phase simulation.

3.2.3 Turbulence Modeling

To capture the turbulent characteristics of airflow within the complex and branching lung geometry, the Shear Stress Transport (SST) k–ω model was employed in this study. This two-equation Reynolds-Averaged Navier–Stokes (RANS) model is particularly well-suited for internal flows involving separation, curvature, and adverse pressure gradients—conditions that are commonly present in pulmonary airways, especially near bifurcations and turning regions.

The SST model combines the strengths of the standard k–ω near the wall with the k–ε model in the free stream. A blending function smoothly transitions between the two models based on the distance to the wall and the local turbulence properties. This hybrid approach allows the model to deliver accurate predictions of flow separation while maintaining robustness and mesh independence.

The model solves two additional transport equations:

Turbulent Kinetic Energy Equation:

$$\frac{\delta k}{\delta t} + u \cdot \nabla k = P_k - \beta^* \cdot k \cdot \omega + \nabla \cdot [(\nu + \sigma_k \cdot \nu_t) \cdot \nabla k]$$

Specific Dissipation Rate Equation:

$$\frac{\delta \omega}{\delta t} + u \cdot \nabla \omega = \gamma \cdot \left(\frac{\omega}{k} \right) \cdot P_k - \beta \cdot \omega^2 + \nabla \cdot [(\nu + \sigma\omega \cdot \nu_t) \cdot \nabla \omega] + 2(1 - F_1) \cdot \sigma\omega_2 \cdot \left(\frac{1}{\omega} \right) \cdot \nabla k \cdot \nabla \omega$$

where:

- k: turbulent kinetic energy
- ω: specific dissipation rate
- ν: kinematic viscosity
- ν_t: turbulent (eddy) viscosity, given by $\nu_t = \frac{a_1 \cdot k}{\max(a_1 \cdot \omega, S \cdot F_2)}$
- Pk: production of turbulent kinetic energy
- S: invariant measure of the strain rate
- F_1, F_2: blending functions
- α, β, β^*, σ_k, σ_ω, $\sigma_{\omega 2}$: empirical constants

This formulation enhances near-wall accuracy while suppressing turbulent viscosity in stagnation zones or regions with high strain, thus preventing excessive eddy viscosity that may otherwise dampen important flow features.

In ANSYS Fluent, the SST model automatically applies low-Reynolds number corrections and resolves the viscous sublayer without wall functions, making it suitable for resolving wall shear stress distributions in small airway branches. This is particularly beneficial for simulations of aerosol deposition, where near-wall accuracy directly influences particle capture.

Default model constants and wall treatment parameters provided by Fluent were used. Turbulence intensity and length scale were set at the tracheal inlet based on physiological estimates, assuming fully developed flow at entry. The SST model's enhanced predictive capabilities make it a robust choice for respiratory flow simulations, and its use in this study provides high-fidelity resolution of both global flow patterns and localized shear effects across different body orientations.

3.2.4 Discrete Phase Model (DPM): Particle Tracking

A Discrete Phase Model (DPM) was utilized to simulate the behavior of aerosol particles within the respiratory tract, accounting for drag and gravitational forces. The motion of aerosol particles is governed by:

$$\frac{du_p}{dt} = F_D(u - u_{p)} + \frac{g_{(\rho_{p-\rho})}}{\rho_p} + F$$

where F is an additional acceleration term, $F_D(u - u_{p)}$ is the drag force per unit particle mass, u is the fluid phase velocity, u_p is the particle velocity, ρ_p is the density of the particle, ρ is the density of the fluid and g is the gravitational acceleration component in the direction of flow. $\boldsymbol{F_D}$ can be calculated as the following:

$$F_D = \frac{18u}{\rho_p d_p^2} C_D \frac{Re_p}{24}$$

where C_D is the drag coefficient, d_p is the diameter and Re_p is the particle's Reynolds number which is defined as:

$$Re_p = \frac{\rho d_p |u_p - u|}{\mu}$$

Here, μ is the dynamic viscosity of air (μ=1.79×10−5 kg/m·s)

Virtual mass forces were neglected due to their negligible effect on the dynamics of high-density particles. Similarly, Saffman's lift force and Brownian motion were excluded, as they primarily influence submicron particles, whereas this study focuses on particles with diameters larger than 1 μm.

3.2.5 Coupling Between Phases

A one-way coupling approach was used in this study, where the continuous phase (airflow) influences particle motion, but the particles do not affect the airflow dynamics. This assumption is valid for dilute aerosol concentrations, where the volume fraction of particles is sufficiently low. Specifically, according to commonly accepted CFD modeling guidelines, one-way coupling can be reasonably applied when the particle volume concentration remains below 15% [35,36]. In typical inhalation therapies and medical aerosol applications, particle concentrations are generally much lower than this threshold, making one-way coupling an appropriate assumption for the present study.

3.3 Mesh Generation and Grid Independence Study

To ensure the accuracy and reliability of the simulation results, a comprehensive grid independence study was conducted. Five different computational grids with varying element counts, ranging from approximately 1.37 million to 6.33 million elements, were generated and

tested. The evaluation was based on the sensitivity of key flow parameters—namely, average velocity and static pressure—monitored at selected cross-sections within the airway model.

The computational mesh was generated using ANSYS Meshing. An unstructured tetrahedral mesh was employed to accurately capture the complex branching geometry of the reconstructed lung model. Local refinement was applied at bifurcations and curved regions to improve resolution of secondary flows and aerosol trajectories. Additionally, five layers of boundary layer inflation were applied near the airway walls to better resolve near-wall airflow and particle interactions critical to deposition processes.

Mesh quality was carefully assessed through parameters such as element aspect ratio and element quality (skewness-based). As shown in Table 3.2, the minimum aspect ratio across all grids remained close to 1.0, indicating highly regular element shapes. For Grid 3 (the selected optimal grid), the maximum aspect ratio was 4.232, while the minimum element quality reached 0.31. These values reflect a high-quality mesh suitable for complex airflow and particle tracking simulations.

The results of the grid independence study are presented in Table 3.1. It was observed that beyond Grid 3, further mesh refinement yielded negligible changes in the monitored quantities. Specifically, the difference in average velocity between Grid 1 and Grid 3 was less than 0.2%, while the static pressure variation was below 1%. Similar stability was observed between Grid 3 and the finer meshes (Grid 4 and Grid 5), confirming mesh convergence. Based on these findings, Grid 3, with approximately 4 million elements, was selected as the optimal mesh for all subsequent simulations, offering a balance between numerical accuracy and computational efficiency.

Table 3.1: Grid independence study results and mesh quality parameters

Grid	Number of Cells	Avg. Velocity (m/s)	Static Pressure (Pa)	Min Aspect Ratio	Max Aspect Ratio	Min Element Quality	Max Element Quality
Grid 1	1,372,472	0.3498	1.96325	1.603	31.133	0.053	0.999
Grid 2	2,675,721	0.3488	1.95478	1.167	19.423	0.098	0.980
Grid 3	3,999,040	0.3492	1.94400	1.0007	4.232	0.310	0.920
Grid 4	4,769,300	0.3485	1.96140	1.0005	4.4051	0.3147	1.000
Grid 5	6,328,543	0.3492	1.94400	1.1602	20.971	0.089	0.999

The final mesh is illustrated in ***Figure 3.3***, providing a representative view of the mesh resolution applied to the airway geometry.

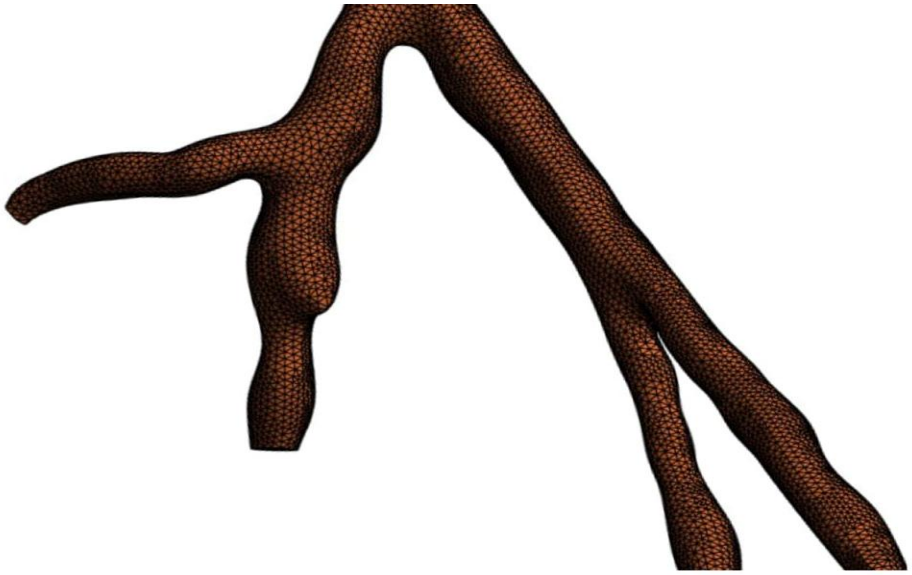


Figure 3.3*: Computational mesh of the reconstructed lung model*

To further support the conclusion of mesh convergence, a grid independence plot based on average velocity is presented in ***Figure 3.4***. The plot demonstrates that the changes in average velocity across different grid resolutions are minimal, with the curve nearly flattening beyond Grid 3. This graphical evidence complements the tabulated data and reinforces the decision to adopt Grid 3 as the computational baseline for the study.

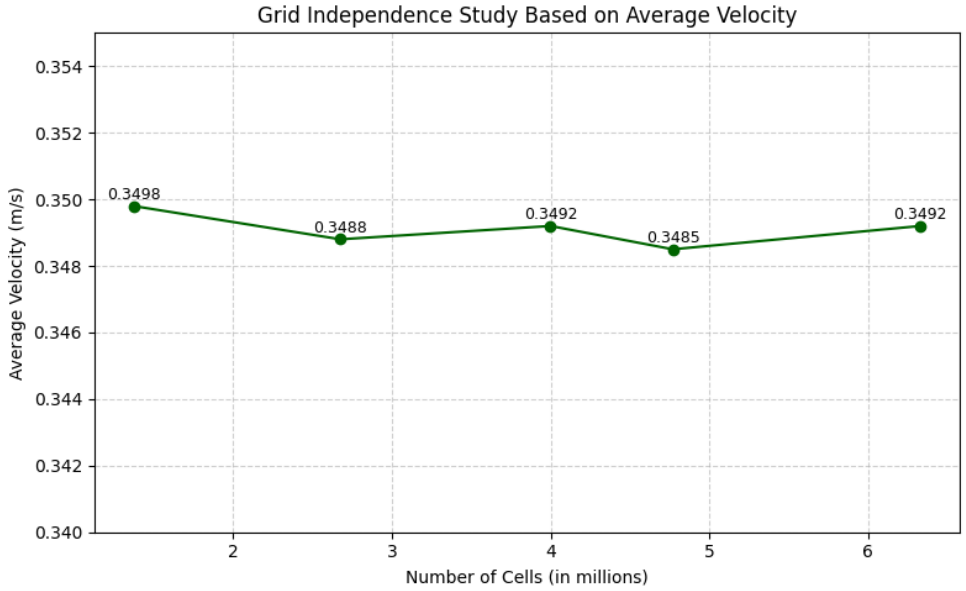


Figure 3.4*: Variation of average velocity with number of cells*

3.4 Numerical Setup and Boundary Conditions

Accurate simulation of airflow and aerosol transport requires careful selection of solver settings and boundary conditions. The following sections detail the numerical framework adopted to ensure physiological relevance and computational stability.

3.4.1 Solver Settings

The numerical solution was carried out using ANSYS Fluent. The governing equations described in Section 2.3 were solved using a pressure-based solver under the absolute velocity formulation. The transient simulation was performed with a time step size of 0.01 seconds, and a total of 92 time steps were computed for each breathing cycle.

The Discrete Phase Model (DPM) was activated to model aerosol particle transport through the Lagrangian tracking framework. A one-way coupling approach was applied, consistent with dilute particle concentrations encountered in inhalation therapies.

For time discretization, the second-order implicit scheme was applied to improve temporal accuracy. Spatial discretization of momentum, pressure, and turbulence equations employed second-order upwind schemes, providing a good balance between solution accuracy and

numerical stability for internal flows. The pressure-velocity coupling was handled using the Coupled algorithm, which is well-suited for transient simulations in complex geometries with strong pressure-velocity interactions.

Convergence was monitored at every time step, and residuals for all governing equations were required to drop below 10^{-4} to ensure solution stability and accuracy.

3.4.2 Continuous Phase Boundary Conditions

Boundary conditions for the continuous phase were applied to accurately represent airflow through the reconstructed lung model under realistic breathing conditions. The inlet boundary was defined at the tracheal opening, representing the entry point for inhaled air into the respiratory system. At this location, a transient velocity inlet condition was prescribed based on a realistic breathing profile, as described in Section 3.4.3. This time-dependent velocity profile captures the natural variation of inhalation airflow during the breathing cycle.

The outlet boundary condition was applied at the distal ends of the lobar bronchi, where airflow exits the modeled domain. A pressure outlet condition with zero gauge pressure was assigned to these outlets, reflecting the physiological assumption that airflow exits into atmospheric conditions without additional pressure gradients at the boundaries of the computational domain.

All airway walls were treated as rigid, stationary walls with a no-slip condition applied. Heat transfer and temperature variations were neglected, assuming isothermal conditions throughout the simulations.

3.4.3 Realistic Breathing Profile

Before the airflow reverses, the particles remaining in the fluid after inhalation are found to be zero; therefore, the exhalation period is not simulated. To simulate realistic aerosol inhalation for a dry powder inhaler, a transient velocity profile, as proposed by Mirzaaghaian et al., was applied at the tracheal inlet. In this study, only the inhalation phase was simulated, with a total inhalation duration of 0.92 seconds, corresponding to the inhalation portion of the breathing cycle. The exhalation phase was excluded, as all particles were either deposited or exited the model before airflow reversal. The airflow rate is modeled as:

$$\frac{Q}{Q_{max}} = Q_0 + \sum_{k=1}^{k} Q_k sin\,(2\pi k \frac{t}{T} + \theta_k)$$

where:

T = Breathing period (3.29 s for males, 3.19 s for females)

Q = Airflow rate at the mouth inlet

Q_{max} = Maximum airflow rate during a breathing period (263.1 L/min for males, 161.6 L/min for females)

Q_0 = Average airflow rate over time

Q_k and θ_k [rad] = Amplitude and phase of the k-th harmonic

The transient airflow profile used in this study is characterized by the first 10 harmonics for fitting the measured flow rate profiles, as detailed in Table 3.2. These parameters provide an accurate representation of the female breathing pattern applied at the tracheal inlet.

Table 3. 2: Parameters of the First 10 Harmonics for Female Realistic Breathing

k	**Q_k**	**θ_k**
0	-0.0042	–
1	0.50378	0.784149
2	0.273449	-0.09948
3	0.153554	-0.64609
4	0.072959	-1.14653
5	0.040757	-0.89197
6	0.035664	-1.03963
7	0.028894	-1.29181
8	0.021874	-1.69532
9	0.009872	-1.7888
10	0.007308	-1.57803

The volume flow rate and velocity profiles representing the realistic breathing pattern during aerosol inhalation are shown in ***Figure 3.5*** and ***Figure 3.6***, respectively. The volume flow rate profile was derived from the transient airflow model at the tracheal inlet. To obtain the corresponding velocity profile, the volume flow rate was divided by the cross-sectional area of the inlet (202.9673 mm²). The cross-sectional area of the tracheal inlet was measured directly from the reconstructed lung geometry.

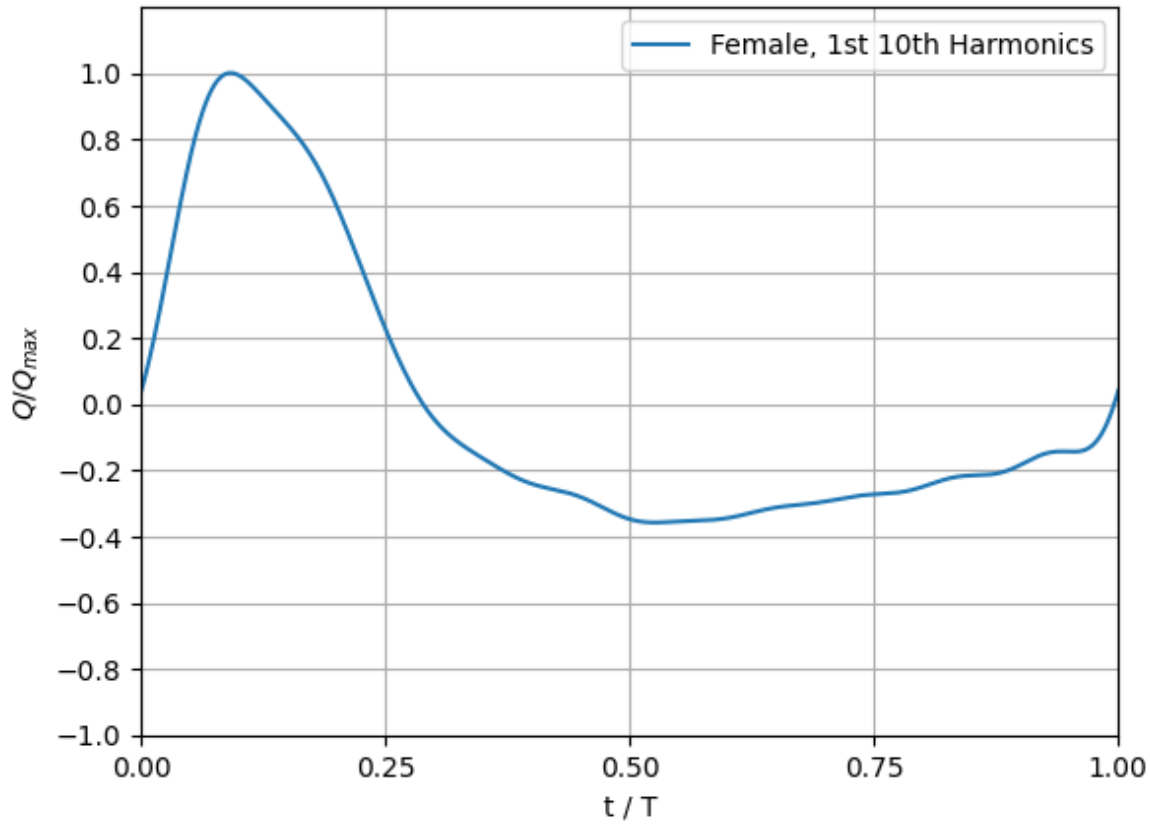


***Figure 3.5**: Realistic Aerosol Breathing Pattern for Female (Volume Flow Rate vs. Normalized Time, t/T)*

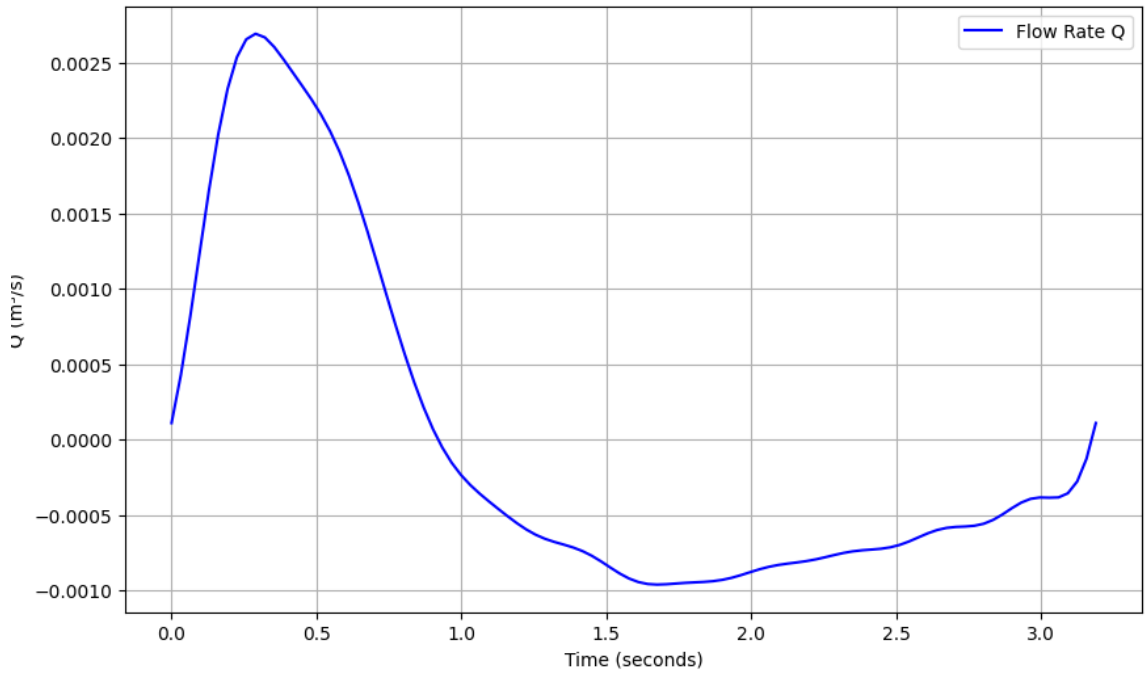


***Figure 3. 6**: Velocity Profile vs. Time for Realistic Aerosol Breathing*

3.4.4 Particle Properties and Injection Settings

In this study, aerosol particles were injected at the tracheal inlet surface using Fluent's surface injection method. For each simulation, a monodisperse aerosol distribution was used, with one particle size selected per simulation run. The particle sizes investigated were 3 µm, 5 µm, 7 µm, 9 µm, and 10 µm. Each simulation was performed separately for each particle size.

The physical properties of the aerosol particles were defined as spherical particles with a density of 1000 kg/m³, representing typical pharmaceutical dry powder aerosols. A total of 17,000 particles were injected for each simulation.

An instantaneous injection approach was adopted, where all particles were released at the beginning of the inhalation phase (start time = 0 s, stop time = 0 s). Although Fluent's DPM interface allows specification of a constant diameter (which was set at its default value of 10 µm), this setting was only used internally for mass flow rate calculation. The actual particle size was defined directly in the injection settings for each simulation case.

The total injected mass was calculated based on the default constant diameter using the volume of a perfect sphere:

Particle volume= $\frac{1}{6}\pi d^3$

Mass of one particle= $\frac{1}{6}\pi(10\times10^{-6}\ \text{m})^3 \times 1000\ \text{kg/m}^3$

Total mass=17,000× $\frac{1}{6}\pi(10\times10^{-6}\ \text{m})^3 \times 1000\ \text{kg/m}^3 = 8.901179\times10^{-9}\ \text{kg}$

Since the injection was performed over a single time step of 0.01 s, the corresponding mass flow rate applied in Fluent was calculated as:

Mass flow rate= $\frac{Total\ mass}{\Delta t} = \frac{8.901179\times10-9}{0.01s}$ kg/s

This mass flow rate was specified to ensure that 17,000 particles were released instantaneously at the start of the simulation.

Gravity and drag forces were included in the particle tracking calculations to capture inertial and gravitational effects on particle motion. Brownian motion, Saffman lift, and virtual mass forces were neglected, as these effects are typically insignificant for particles within the studied size range (3–10 µm).

3.4.5 Discrete Phase Boundary Conditions

For the discrete phase, specific boundary conditions were assigned to accurately model particle-wall interactions and track deposition in different lung regions.

The airway walls were divided into multiple zones corresponding to the lobes and trachea. A trap boundary condition was applied to all wall surfaces, assuming that any particle coming

into contact with the airway walls would adhere and deposit. This assumption is justified for aerosol particles in the respiratory system, where wall impaction often leads to deposition due to the presence of mucus layers lining the airways, which facilitate particle capture and prevent rebound or resuspension. Applying the trap condition allowed direct quantification of deposition by monitoring the number of particles trapped on each lobe-specific wall region.

At the outlet boundaries, located at the distal ends of the lobar bronchi, an escape boundary condition was assigned. This condition assumes that any particle exiting the domain at these outlets leaves the respiratory system and does not return for subsequent deposition. This is consistent with physiological airflow, where particles not deposited in the conducting airways may pass into deeper lung regions not included in the current model or may be exhaled during the breathing cycle.

At the inlet (tracheal inlet), a reinjection condition was applied automatically by ANSYS Fluent to allow proper particle tracking in transient simulations. Since the injection was performed instantaneously at the beginning of inhalation, no additional particles entered after the initial release; however, the reinjection setting ensured that any particles crossing the inlet plane during the transient solution were correctly handled.

This boundary condition configuration allowed for accurate determination of regional deposition by directly counting the number of particles trapped in each lung lobe and identifying particles that exited the system through the outlets.

3.4.6 Modeling Body Orientations

To investigate the influence of body posture on aerosol deposition, simulations were conducted for three different body orientations: upright**,** dorsal, and lateral. The anatomical geometry of the lung remained unchanged across all cases. Instead, posture was represented by altering the direction of gravitational acceleration within ANSYS Fluent, while keeping the geometry and boundary conditions fixed.

For the upright orientation, gravity was applied along the negative Z-direction (–Z), corresponding to a standing or seated posture (***Figure 3.7***). In this configuration, gravitational settling occurs vertically downward, aligning with natural anatomical orientation.

In the dorsal orientation, representing a supine posture (lying on the back), gravity was reassigned to the positive Y-direction (+Y)**,** simulating a shift in the gravitational vector perpendicular to the upright posture (***Figure 3.8***). This change reorients the influence of gravity such that particles experience settling toward the posterior lung surface.

The lateral orientation simulates a person lying on one side, with gravity directed along the positive X-direction (+X) (***Figure 3.9***). In this posture, gravitational forces act laterally across the lungs, modifying the deposition distribution due to sideways sedimentation.

In all orientations, the magnitude of gravitational acceleration was maintained at 9.8 m/s^2**.** By modifying only the direction of gravity and not the geometry or flow conditions, the effects of posture-induced gravitational variation on particle behavior were isolated. This approach allowed a systematic analysis of how body position influences regional aerosol deposition within the lungs.

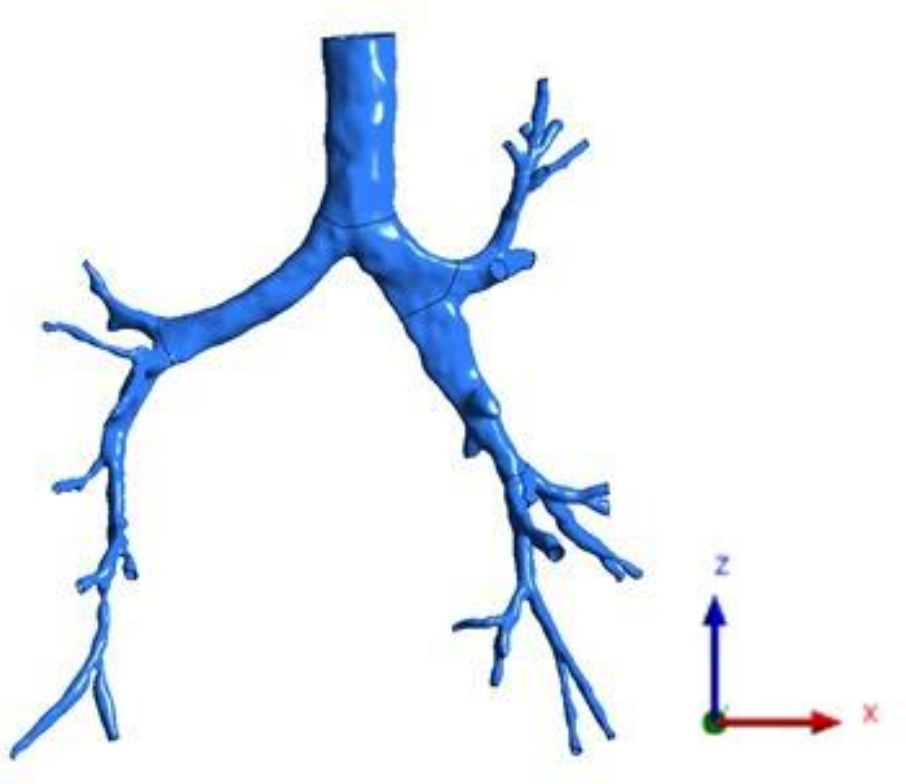


Figure 3.7*: Upright orientation (gravity applied along -Z direction)*

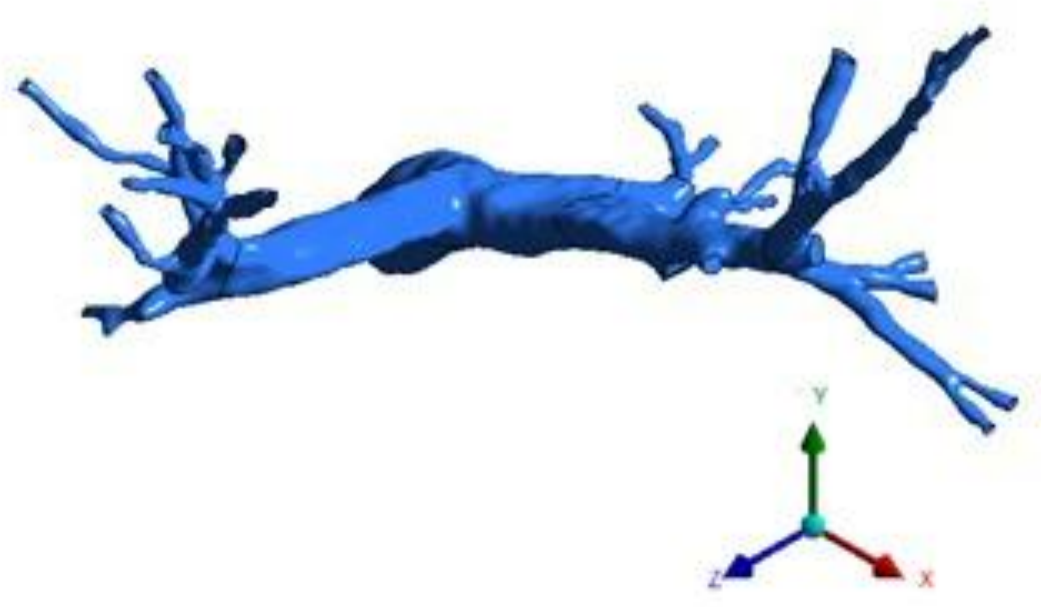


Figure 3. 8*: Dorsal orientation (gravity applied along +Y direction)*

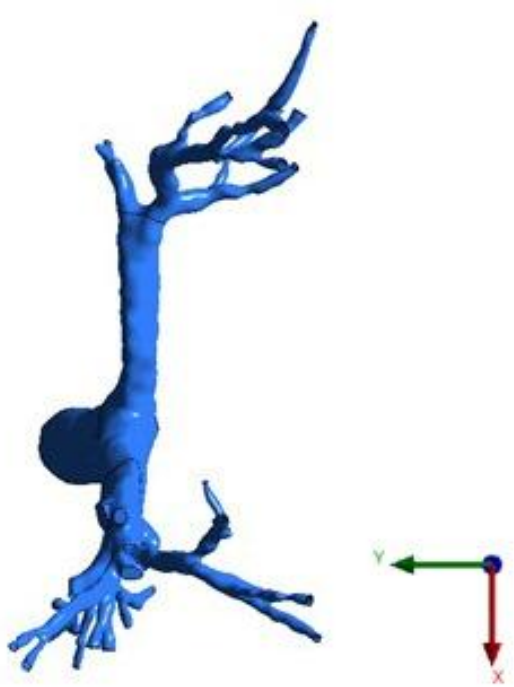


Figure 3.9*: Lateral orientation (gravity applied along +X direction)*

3.5 Post-Processing and Deposition Analysis

Following the completion of each simulation, the deposition results were analyzed based on the output provided in the ANSYS Fluent console and reports. Fluent's discrete phase tracking automatically recorded the number of particles that were trapped**,** escaped, or remained in the domain at the end of the transient simulation. In all cases, particles were either trapped or escaped by the end of inhalation.

The Fluent console summary provided the total number of particles trapped on wall surfaces and the number of particles that escaped through the outlet boundaries. As the number of particles injected was constant at 17,000 in all cases, the deposition efficiency was calculated using the following expression:

$$\text{Deposition efficiency, } \eta\ (\%) = \frac{\text{Number of deposited aerosols}}{\text{Total number of injected aerosols at the inlet}} \times 100$$

For regional analysis, the airway walls were predefined as distinct zones corresponding to individual lung lobes and the trachea. Fluent's DPM summary and surface reports were used to extract the number of trapped particles in each zone, allowing for direct calculation of lobe-specific deposition efficiencies using the same formula.

Particles that escaped through the outlets were considered to have exited the domain and were not included in the deposition efficiency calculations.

Chapter 04

Results and Discussion

4.1 Overview of Regional Deposition Data

Various lung lobes have different deposition efficiencies for aerosol particles based on the body orientation of the inhaler user. However, in the case of the entire lung's efficiency, posture-related changes seem to have little effect. In regard to behavior, it is clear that there are dependencies in the size of the particle, since smaller ones would have lower efficiencies compared to larger ones. For this study, three body positions were paired with five different particle sizes (3 – 10 μm), and in all cases, deposition increased alongside particle size.

There is evidence suggesting that changing the orientation of the body may assist with the targeted delivery of certain drugs based on the pose. For inhaled drugs, optimization of regional deposition has been associated with a reasonable body position for inhalation, thereby facilitating enhanced delivery. These findings can be efficiently applied toward the advancement of precision aerosol-based therapy treatment.

Tables 4.1–4.3 summarize the regional deposition data obtained for upright, dorsal, and lateral positions. The subsequent sections analyze these data to explore particle size dependency, regional distribution patterns, and the effects of postural transitions on aerosol deposition.

Table 4.1: Deposition Efficiency in Upright Position

Region	3 μm	5 μm	7 μm	9 μm	10 μm
Right Upper Lobe	1.21%	7.12%	15.34%	22.064%	23.44%
Right Middle Lobe	0.64%	4.55%	10.41%	18.88%	22.58%
Right Lower Lobe	0.14%	6.52%	12.74%	13.23%	11.53%
Total Right Lung	1.99%	18.19%	38.48%	54.174%	57.55%
Left Upper Lobe	1.63%	9.55%	19.2%	23.04%	23.7%
Left Lower Lobe	0.717%	2.87%	3.57%	1.91%	1.28%
Total Left Lung	2.347%	12.42%	22.77%	24.95%	24.98%
Total Deposition	4.337%	30.61%	61.25%	79.124%	82.53%

Table 4.2: Deposition Efficiency in Dorsal Position

Region	3 µm	5 µm	7 µm	9 µm	10 µm
Right Upper Lobe	1.08%	7.094%	15.15%	22.1%	23.63%
Right Middle Lobe	0.74%	4.435%	10.68%	19.2%	22.27%
Right Lower Lobe	0.088%	7.094%	12.3%	13.34%	12.31%
Total Right Lung	1.908%	18.058%	38.13%	54.64%	57.21%
Left Upper Lobe	1.923%	9.817%	19.5%	23.43%	24.19%
Left Lower Lobe	0.823%	3.088%	3.47%	1.88%	1.15%
Total Left Lung	2.746%	12.905%	22.97%	25.31%	25.34%
Total Deposition	4.654%	30.963%	61.1%	79.95%	82.55%

Table 4.3: Deposition Efficiency in Lateral Position

Region	3 µm	5 µm	7 µm	9 µm	10 µm
Right Upper Lobe	1.058%	7.223%	15.78%	22%	23.72%
Right Middle Lobe	0.864%	4.68%	10.65%	18.93%	22.43%
Right Lower Lobe	0.053%	6.37%	11.87%	13.21%	11.91%
Total Right Lung	1.975%	18.273%	38.3%	54.14%	58.06%
Left Upper Lobe	1.776%	9.63%	18.68%	22.86%	23.37%
Left Lower Lobe	0.817%	2.911%	3.8%	1.78%	1.15%
Total Left Lung	2.593%	12.54%	22.48%	24.64%	24.52%
Total Deposition	4.568%	30.814%	60.78%	78.78%	82.58%

4.2 Influence of Particle Size on Deposition Behavior

In the upright posture, aerosol deposition efficiency exhibits a strong, non-linear dependence on particle size across all lung regions. As particle diameter increases from 3 µm to 10 µm, total deposition efficiency rises markedly from 4.34% to 82.53%. This pronounced increase can be attributed to the growing inertial effects of larger particles, which enhance their tendency

to deviate from airflow streamlines and impact airway surfaces. The deposition trend accelerates most notably between 3 μm and 7 μm, where total deposition efficiency escalates from 4.34% to 61.25%, highlighting a regime of rapid transition dominated by inertial impaction. Beyond 7 μm, deposition continues to increase but at a diminishing rate, approaching a plateau as size-dependent enhancement in deposition becomes less significant. This trend is clearly illustrated in Figure 4.1, which depicts the variation of deposition efficiency with particle size across all lung lobes in the upright position.

Regionally, the right lung generally demonstrates higher deposition efficiency than the left for particle sizes larger than 3 μm. At 10 μm, the total deposition in the right lung reaches 57.55%, in contrast to 24.98% in the left lung. Among the right lung lobes, the Right Upper Lobe (RUL) and Right Middle Lobe (RML) exhibit substantial deposition growth with increasing particle size, reaching 23.44% and 22.58%, respectively, at 10 μm. The Right Lower Lobe (RLL), however, peaks at 13.23% for 9 μm particles and exhibits a slight decline to 11.53% at 10 μm, potentially due to gravitational effects and flow redistribution. On the left side, the Left Upper Lobe (LUL) contributes most significantly to deposition, with efficiency rising from 1.63% to 23.7% across the particle size range. Conversely, the Left Lower Lobe (LLL) shows minimal deposition and even a decrease beyond 7 μm, reducing from 3.57% to 1.28%. This asymmetry between lobes and lungs is likely influenced by anatomical geometry, branching angles, and variations in airflow distribution. Collectively, the data presented in ***Figure 4.1*** underscore the critical role of particle size in determining regional and total deposition patterns under upright conditions.

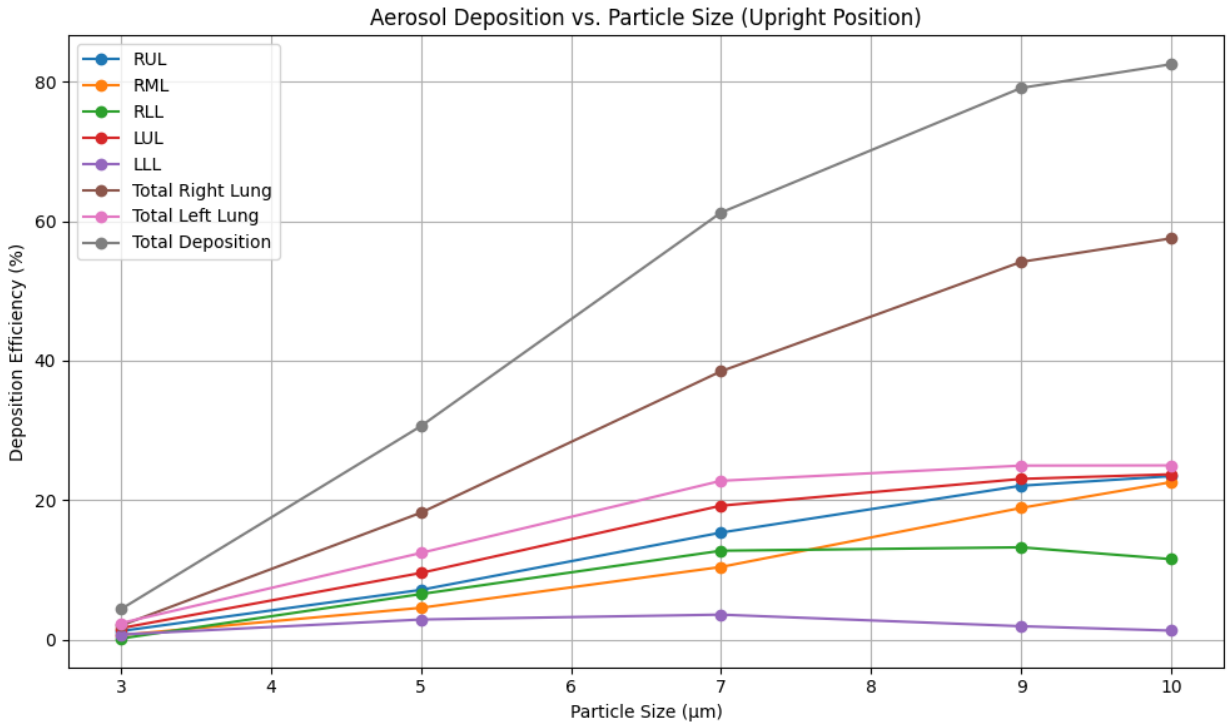


***Figure 4.1**:Deposition efficiency variation with particle size (upright position)*

A similar pattern is observed in the dorsal position, as illustrated in ***Figure 4.2***, where deposition efficiency increases with particle size across all lung lobes. While the overall trend aligns with a gradual plateau, some regional variations are noteworthy. The right lung continues to exhibit higher deposition than the left, with the right upper and middle lobes showing firm increases. Specifically, the total right lung deposition increases from 1.91% at 3 µm to 57.21% at 10 µm, while the left lung increases from 2.75% to 25.34% over the same particle size range. Among individual lobes, the right upper lobe reaches 23.63% at 10 µm, comparable to the left upper lobe's 24.19%. The right lower lobe displays a mild peak at 9 µm (13.34%) followed by a slight decline, and the left lower lobe continues to record the lowest deposition, dropping beyond 7 µm. Total deposition across both lungs reaches 82.55% at 10 µm, nearly identical to the upright case. These findings further highlight the inertial influence of larger particles, with positional changes producing only minor variations in deposition distribution patterns.

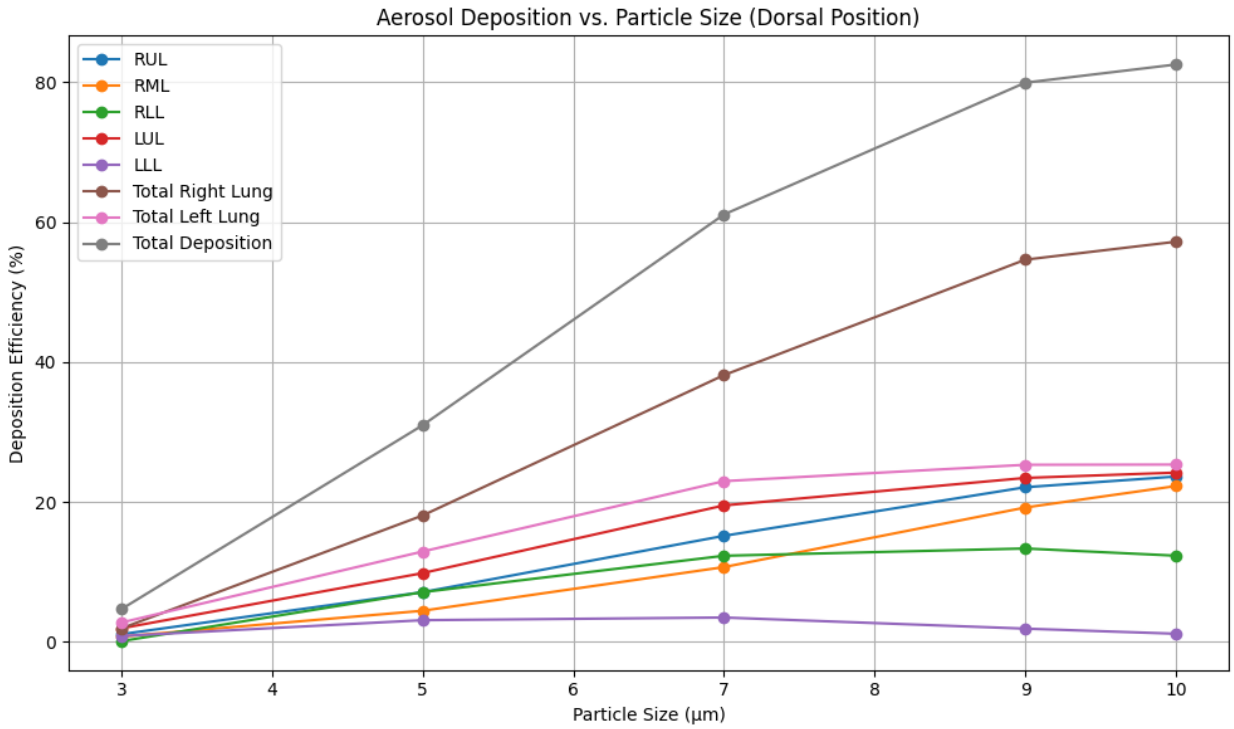


***Figure 4.2**: Deposition efficiency variation with particle size (Dorsal position)*

In the lateral position, the deposition trend similarly reflects a particle size-dependent increase, as demonstrated in ***Figure 4.3***. The total deposition rises sharply from 4.57% at 3 µm to 82.58% at 10 µm, showing remarkable consistency with the dorsal and upright cases. Regionally, the right lung continues to dominate deposition, with its total rising from 1.98% at 3 µm to 58.06% at 10 µm. The right upper lobe again shows a strong response to particle size, peaking at 23.72%, while the right lower lobe slightly decreases beyond 9 µm. The left lung, though recording lower overall deposition, demonstrates a comparable trend with increasing particle size—reaching 24.52% at 10 µm. However, the left lower lobe remains the least efficient, dropping below 2% for larger particles. These findings confirm that while body orientation influences the magnitude and regional distribution of aerosol deposition to some extent, the dominant role of particle inertia remains consistent across postures.

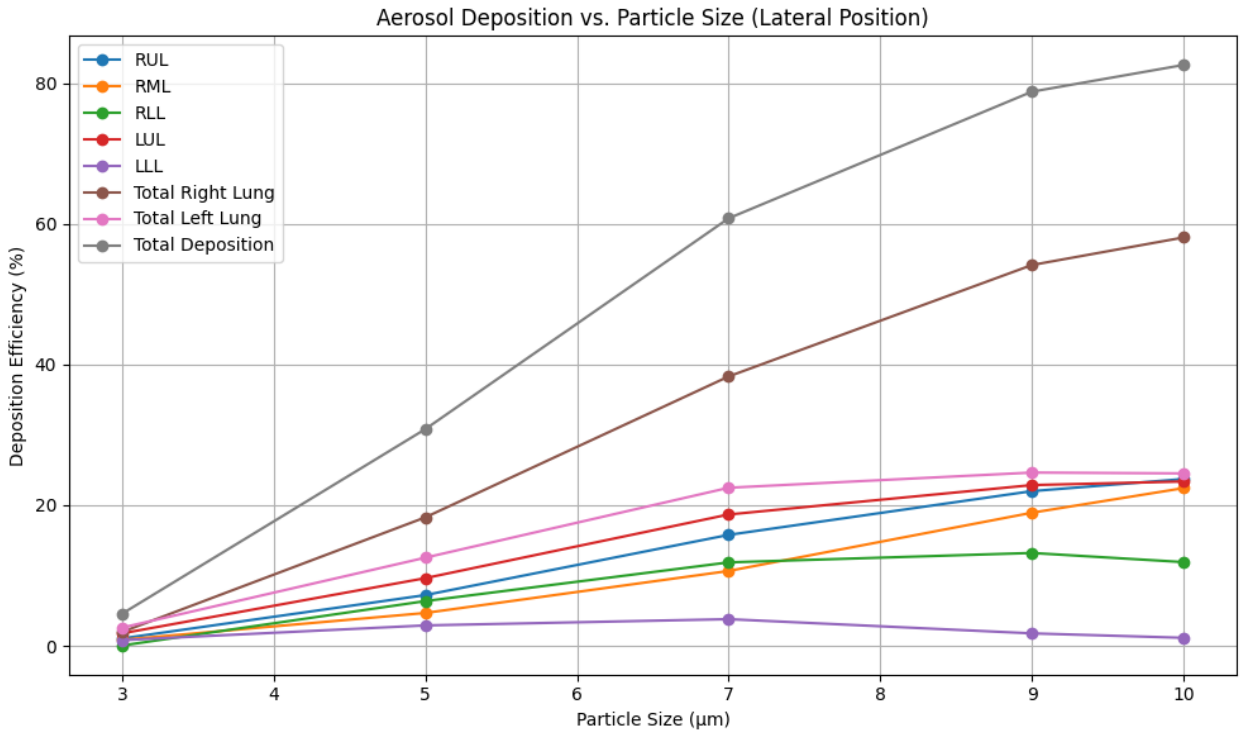


***Figure 4.3**: Deposition efficiency variation with particle size (Lateral Position)*

4.3 Regional Distribution Patterns under Different Body Orientations

Understanding how aerosol deposition distributes among different lung regions under varying body orientations offers crucial insights into optimizing therapeutic delivery and assessing exposure risks. Unlike total deposition efficiency, which is primarily governed by particle size and inertia, regional deposition patterns are strongly influenced by the flow path geometry, gravitational alignment, and airway branching asymmetry. In this section, we analyze the spatial distribution of aerosol deposition across the five lung lobes for multiple particle sizes, comparing how upright, dorsal, and lateral orientations influence deposition behavior. The analysis begins with the 3 μm case, which, due to its small size and relatively low inertia, is expected to highlight the influence of airflow and anatomical path length more than gravitational sedimentation.

As shown in ***Figure 4.4***, for 3 μm particles, the left upper lobe (LUL) consistently receives the highest deposition across all three orientations—1.63% in upright, 1.92% in dorsal, and 1.77% in lateral. In contrast, the right lower lobe (RLL) shows minimal deposition, especially in the lateral (0.053%) and dorsal (0.088%) positions.

Interestingly, while RUL shows relatively uniform deposition (1.06–1.22%) across positions, the right middle lobe (RML) deposition gradually increases from upright (0.64%) to lateral (0.86%), likely due to slight gravitational shifts in flow partitioning. The left lower lobe (LLL)

also shows consistent values across all positions (approximately 0.74–0.82%), indicating limited orientation sensitivity at this particle size.

These results suggest that for smaller particles, deposition is influenced more by geometric and flow dynamics rather than body posture, although subtle redistribution due to orientation changes is evident.

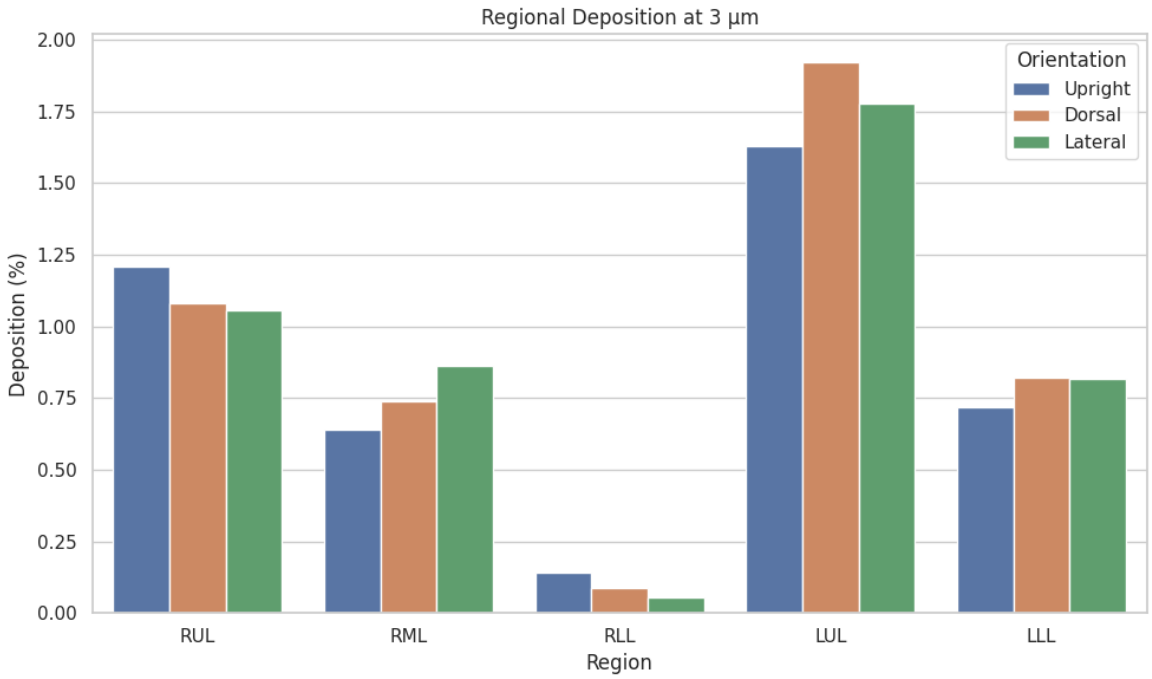


Figure 4.4: *Regional Aerosol Deposition at Different Body Orientations for Particle Size 3 µm*

With an increase in particle size to 5 µm, deposition patterns shift noticeably, reflecting the growing influence of gravitational sedimentation and inertial impaction. As illustrated in ***Figure 4.5***, the overall deposition efficiency increases across all lobes compared to the 3 µm case, and the effect of body orientation becomes more prominent.

The left upper lobe (LUL) again receives the highest regional deposition in all three orientations, rising to 9.81% in the dorsal, 9.63% in lateral, and 9.55% in upright. The enhancement under dorsal and lateral conditions can be attributed to gravitational settling along the dominant airflow paths when the body is reoriented, especially favoring upper lobes.

The right upper lobe (RUL) shows deposition values of 7.12% (upright), 7.094% (dorsal), and 7.22% (lateral). Interestingly, the right middle lobe (RML) also shows increasing deposition in lateral position (4.68%) compared to upright (4.55%) and dorsal (4.43%), suggesting a shift in flow toward the middle lobe under lateral tilt, potentially due to airway curvature and gravitational redistribution.

The right lower lobe (RLL**)** exhibits a significant deposition rise in the dorsal (7.09%) and upright (6.52%) positions, while the lateral position leads to a higher deposition (6.37%) than seen with 3 µm but still lower than upper lobes, likely due to longer path length and gravity opposing flow access in the lateral orientation.

Left lower lobe (LLL) deposition remains modest, increasing to 2.87% (upright) and 2.91% (lateral), while dorsal positioning slightly enhances it to 3.08%, suggesting minor sensitivity to posture at this size in lower lobe pathways.

Overall, the 5 µm particle data reveal that gravitational effects begin to distinctly influence deposition patterns.

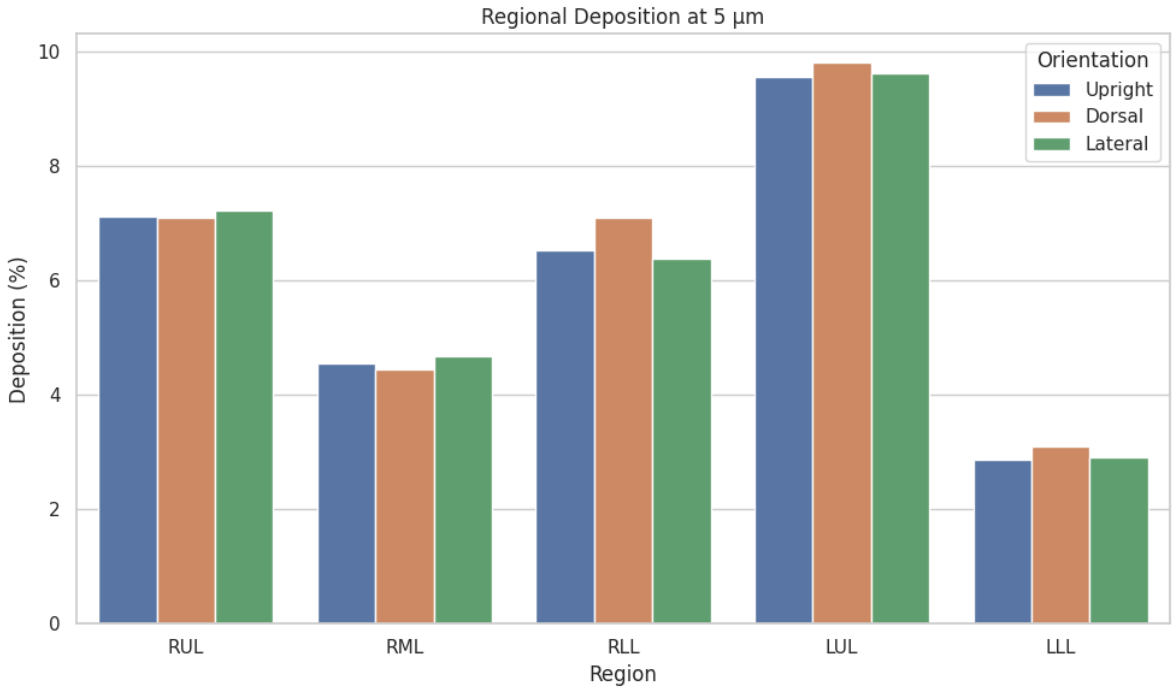


Figure 4.5*: Regional Aerosol Deposition at Different Body Orientations for Particle Size 5 µm*

As particle size increased to 7 µm, the deposition efficiency rose markedly across all lung lobes and body orientations. This size threshold appeared to significantly amplify gravitational sedimentation effects, further influencing the distribution of aerosols.

In the lateral position, the right upper lobe (RUL) showed a substantial increase in deposition to 15.78%, while the right middle lobe (RML) and right lower lobe (RLL) reached 10.65% and 11.87%, respectively. Notably, the left upper lobe (LUL) demonstrated the highest single-lobe deposition at 18.68%, reinforcing its sensitivity to orientation. Conversely, the left lower lobe (LLL) remained low at just 3.8%, suggesting persistent underexposure due to gravitational displacement of flow.

For the dorsal position, similar tendencies were observed, with RUL and LUL both showing elevated deposition, while LLL again had minimal efficiency. In the upright orientation, deposition values were more evenly spread across lobes but generally lower than in the other two orientations—highlighting how horizontal body positions enhance particle settling.

Total deposition efficiency at 7 µm reached 60.78% in the lateral position, a significant rise from the 30.81% observed at 5 µm, suggesting this size falls within an optimal range for maximizing overall lung deposition. Total right lung contribution dominated over the left in all orientations, especially in the lateral position, where the right side alone accounted for 38.3% of the total. The regional deposition behavior at 7 µm is clearly illustrated in ***Figure 4.6***, which presents the spatial distribution of aerosol across lung lobes at different body orientations.

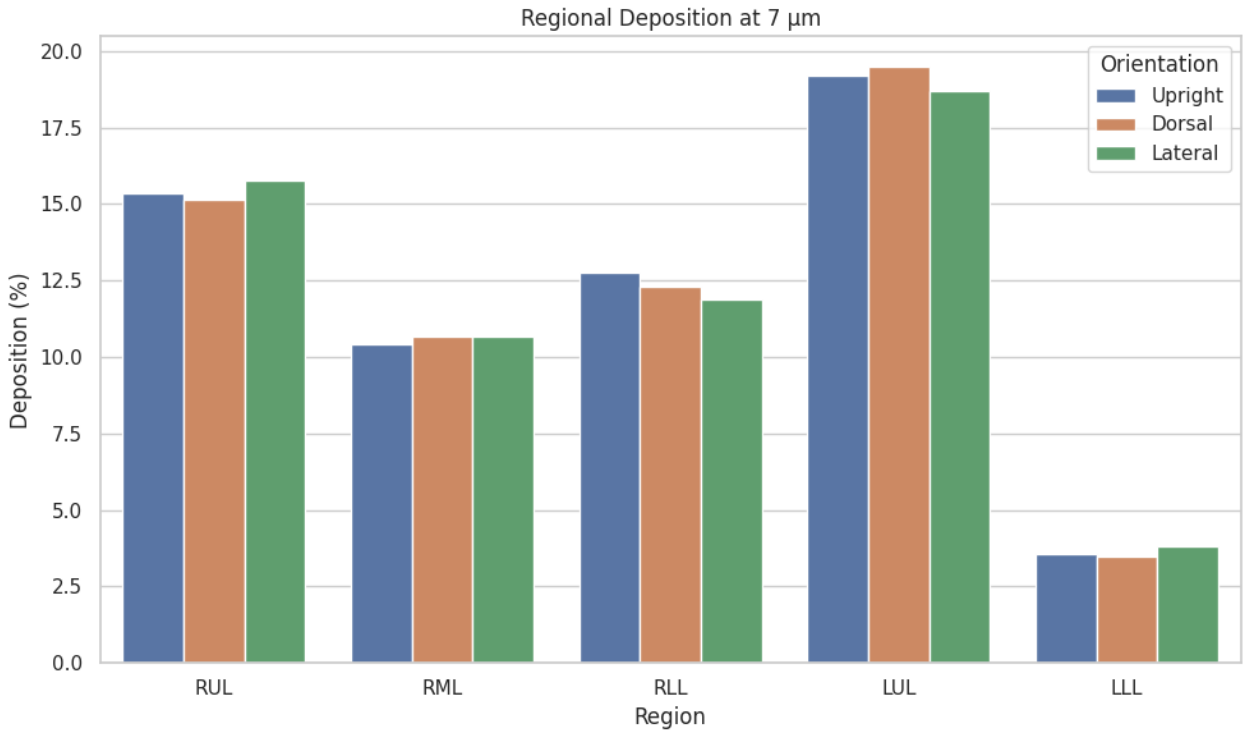


***Figure 4.6**: Regional Aerosol Deposition at Different Body Orientations for Particle Size 7 µm*

At a particle size of 9 µm, deposition efficiency further intensified, continuing the trend of sharp increases observed between 5 µm and 7 µm. The influence of inertial impaction became more pronounced, with particles increasingly deviating from airflow streamlines and depositing along airway walls.

In the lateral position, the right upper, middle, and lower lobes registered depositions of 22.00%, 18.93%, and 13.21%, respectively, collectively comprising 54.14% for the right lung alone. The left lung contributed notably less, with the upper lobe reaching 22.86%, while the

lower lobe dropped to 1.78%. This stark asymmetry emphasizes how particle inertia, combined with lateral gravitational effects, favors the right-sided airways.

In the dorsal orientation, the pattern remained similar, with the right lung again showing dominant deposition. RUL reached 22.1%, and RML and RLL also maintained elevated levels. The left upper lobe (23.43%) nearly equaled the RUL, suggesting dorsal positioning may partially redistribute airflow to upper lobes. However, the left lower lobe maintained minimal deposition (1.88%), indicating a consistent anatomical disadvantage for large particle access.

In the upright posture, while the overall deposition rose to 79.12%, distribution became more balanced across lobes. Nevertheless, the right lung (54.17%) again surpassed the left in deposition share. The trend illustrates how vertical posture, while moderating gravitational extremes, still allows particle inertia to shape regional outcomes.

Overall, 9 μm particles demonstrated strong lobe-dependent and orientation-sensitive deposition behavior. The total deposition remained high and consistent across all orientations (78–80%), underscoring the dominant role of inertial and gravitational forces at this size.

At a particle size of 9 μm, deposition efficiency further intensified, continuing the trend of sharp increases observed between 5 μm and 7 μm. The influence of inertial impaction became more pronounced, with particles increasingly deviating from airflow streamlines and depositing along airway walls.

In the lateral position, the right upper, middle, and lower lobes registered depositions of 22.00%, 18.88%, and 13.23%, respectively, collectively comprising 54.17% for the right lung alone. The left lung contributed notably less, with the upper lobe reaching 23.04%, while the lower lobe dropped to 1.91%. This stark asymmetry emphasizes how particle inertia, combined with lateral gravitational effects, favors the right-sided airways.

In the dorsal orientation, the pattern remained similar, with the right lung again showing dominant deposition. RUL reached 22.1%, and RML and RLL also maintained elevated levels. The left upper lobe (23.43%) nearly equaled the RUL, suggesting dorsal positioning may partially redistribute airflow to upper lobes. However, the left lower lobe maintained minimal deposition (1.88%), indicating a consistent anatomical disadvantage for large particle access.

In the upright posture, while the overall deposition rose to 79.12%, distribution became more balanced across lobes. Nevertheless, the right lung (54.17%) again surpassed the left in deposition share. The trend illustrates how vertical posture, while moderating gravitational extremes, still allows particle inertia to shape regional outcomes.

Overall, 9 µm particles demonstrated strong lobe-dependent and orientation-sensitive deposition behavior. The total deposition remained high and consistent across all orientations (78–80%), underscoring the dominant role of inertial and gravitational forces at this size. This pattern is visualized in ***Figure 4.7***, which depicts the regional deposition distribution for 9 µm particles across the three body orientations.

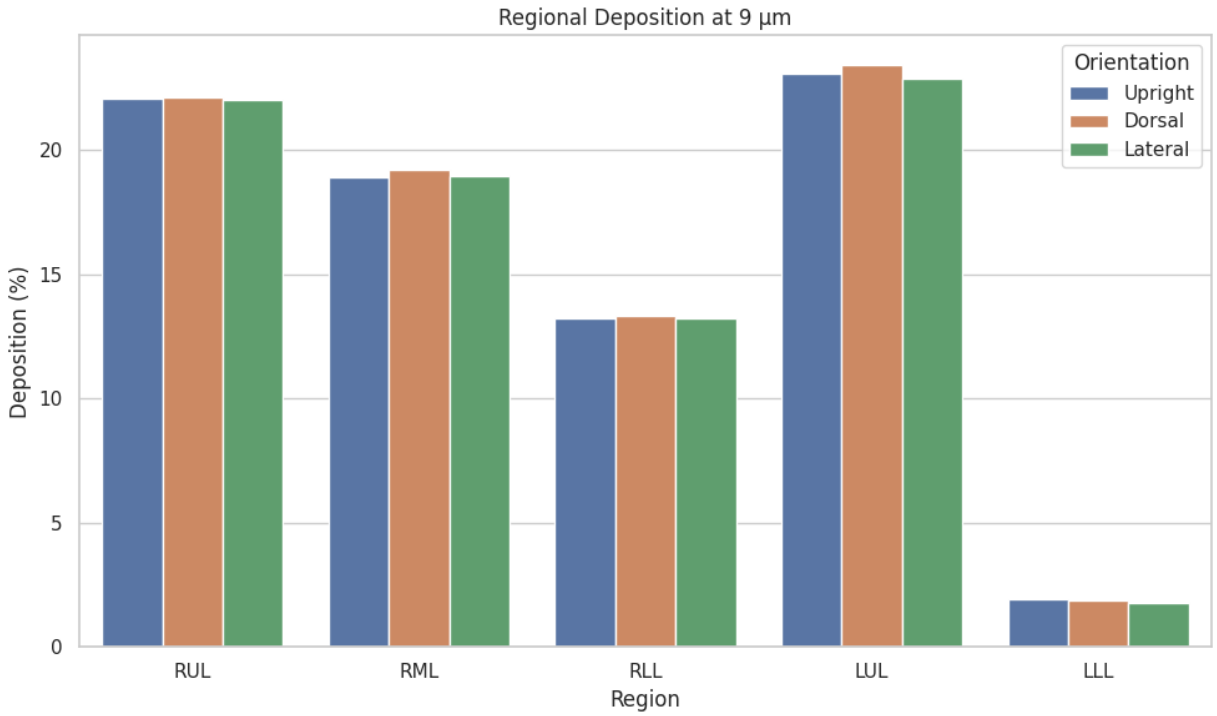


Figure 4.7*: Regional Aerosol Deposition at Different Body Orientations for Particle Size 9 µm*

At 10 µm, the deposition efficiency reached its peak values, but the change from 9 µm was modest, suggesting a plateau in the deposition response. The overwhelming influence of inertia and gravity causes particles of this size to deviate sharply from airflow and settle primarily in the proximal and upper regions of the lungs.

In the lateral position, the total deposition was highest (82.58%), with the right upper (23.72%) and middle (22.43%) lobes exhibiting the largest contributions. The left upper lobe recorded 23.37%, but the left lower lobe remained minimal (1.15%).

Similarly, the dorsal posture showed 82.55% total deposition, nearly identical to the lateral case. The upper lobes, particularly RUL (23.63%) and LUL (24.19%), dominated deposition. The left lower lobe, consistent with other cases, contributed only 1.15%.

In the upright position, deposition reached 82.53%. Right and left lung contributions were 57.55% and 24.98%, respectively, with the upper lobes again absorbing the majority of particles. As with 9 µm, the variation in distribution with orientation became minimal.

These observations are supported by ***Figure 4.8***, which illustrates the regional aerosol deposition patterns for 10 µm particles across the three body positions.

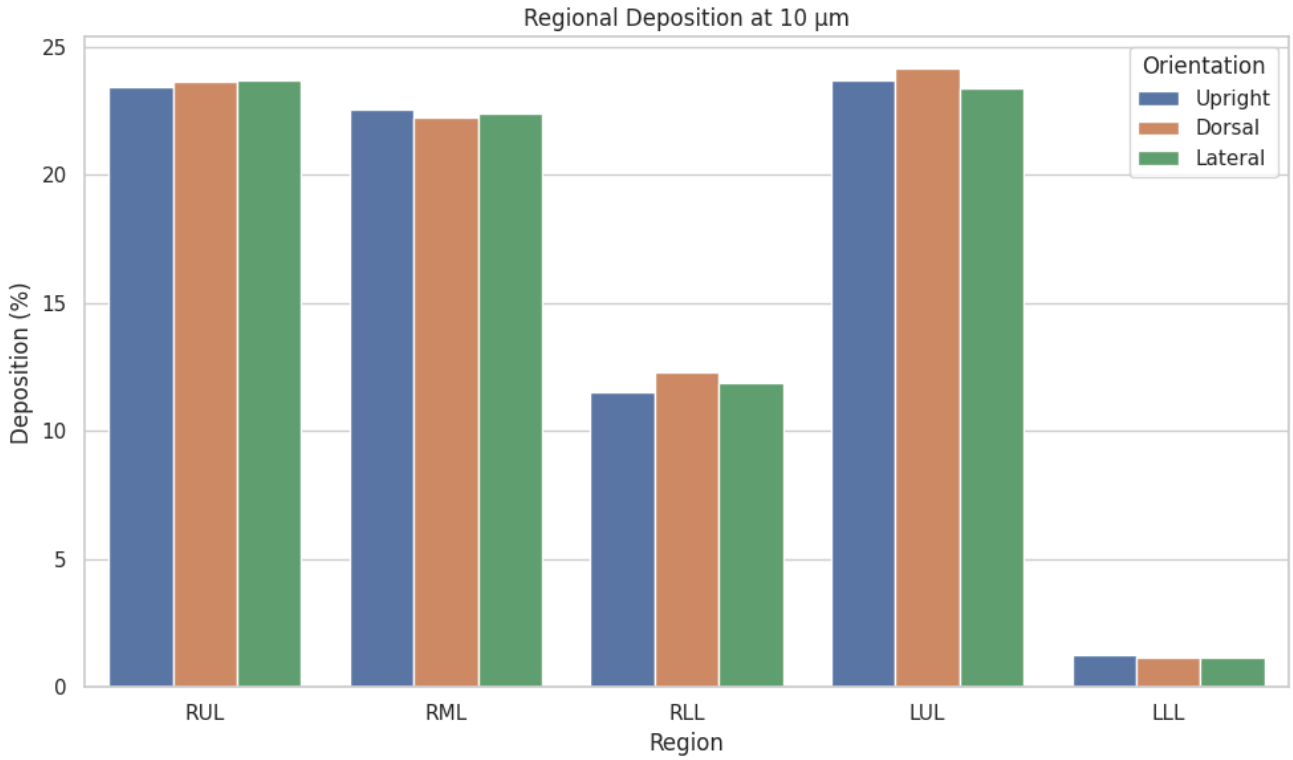


Figure 4.8: *Regional Aerosol Deposition at Different Body Orientations for Particle Size 10 µm*

Collectively, the regional distribution patterns across all body orientations and particle sizes reveal distinct and consistent trends. As particle size increases, deposition becomes increasingly localized to upper lobes, particularly on the right side, with the influence of body orientation gradually diminishing at higher sizes. While smaller particles distribute more diffusely and are sensitive to posture, larger particles concentrate in gravitationally favorable regions due to their dominant inertia. This progression from dispersal to localization highlights the complex interplay between particle dynamics and pulmonary geometry—a relationship crucial for optimizing targeted aerosol delivery in clinical and research applications.

4.4 Differences in Deposition Efficiency Across Body Orientations

In this section, the effects of body orientation transitions on regional aerosol deposition are analyzed by evaluating absolute and relative changes in deposition efficiencies between upright, dorsal, and lateral postures for different particle sizes. The analysis aims to identify specific particle sizes and lung lobes that benefit most from posture changes, providing insights for potential optimization of targeted aerosol delivery. While absolute changes directly reflect

the difference in deposition percentages, they are often small in magnitude and may appear insignificant, particularly in lobes where overall deposition is already low. However, relative changes offer a more comprehensive perspective by expressing these shifts as a percentage of the initial deposition values, thereby capturing the true impact of body orientation on regional deposition.

The absolute differences in deposition efficiency between upright and dorsal orientations are presented in ***Figure 4.9***. The left upper lobe (LUL) exhibits positive changes for all particle sizes, with the magnitude increasing as particle size increases, reaching its maximum at 10 µm (+0.49%). The left lower lobe (LLL) also shows positive changes at smaller particle sizes, specifically at 3 µm and 5 µm. On the right side, the right upper lobe (RUL) presents small positive changes for larger particle sizes (9 µm and 10 µm), while the right lower lobe (RLL) demonstrates positive changes at most particle sizes, with the largest increase observed at 10 µm (+0.79%). Minor negative changes are seen for RLL at 3 µm and 7 µm.

Overall, an orientation-induced redistribution pattern is observed, where the total left lung deposition increases when shifting from upright to dorsal, while the total right lung deposition decreases for this transition.

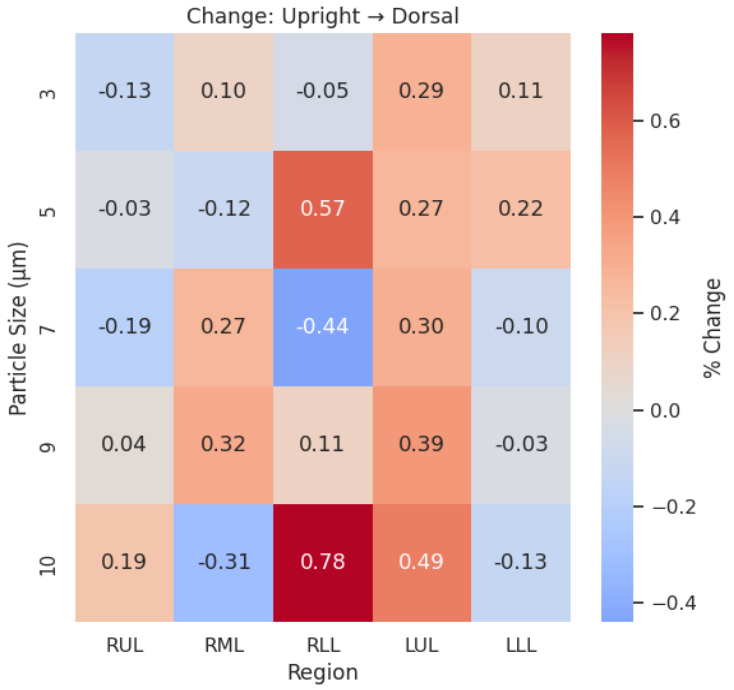


Figure 4.9*: Heatmap of absolute differences in deposition efficiency from upright to dorsal orientation across lung lobes and particle sizes*

In this study, significant relative changes were observed for this transition, with positive changes reaching up to 17.98% and negative changes reaching up to 37.14% during the upright-to-dorsal transition. These findings underscore the importance of considering both absolute and relative changes to fully comprehend how body posture can influence targeted drug delivery. These findings underscore the importance of considering both absolute and relative changes to fully comprehend how body posture can influence targeted drug delivery. The corresponding relative changes are illustrated in ***Figure 4.10***, providing a visual representation of these percentage-wise variations across lung lobes.

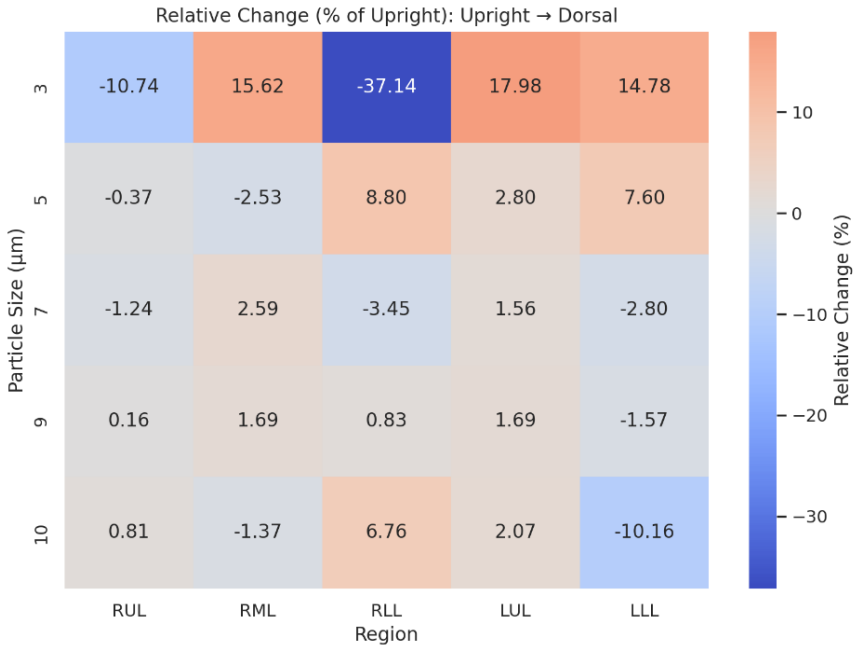


Figure 4.10: *Heatmap of relative differences in deposition efficiency from upright to dorsal orientation across lung lobes and particle sizes*

The absolute differences in deposition efficiency between upright and lateral orientations are presented in ***Figure 4.11***. The right upper lobe (RUL) shows the highest absolute increase at 7 µm (+0.44%), while the right lower lobe (RLL) shows a notable positive change at 10 µm (+0.38%). The right middle lobe (RML) exhibits positive changes for all particle sizes except at 10 µm, indicating a consistent sensitivity to posture changes across most sizes. The left lower lobe (LLL**)** shows positive changes for smaller particles, specifically at 3 µm, 5 µm, and 7 µm. Additionally, the left upper lobe (LUL) shows positive changes for 3 µm and 5 µm, though these changes are smaller in magnitude.

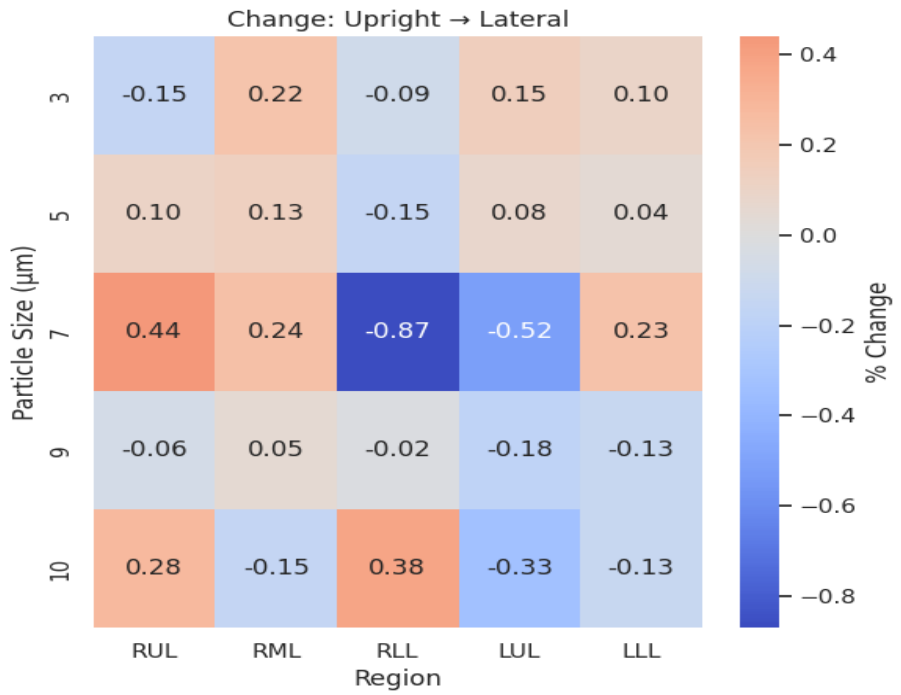


***Figure 4.11**: Heatmap of absolute differences in deposition efficiency from upright to lateral orientation across lung lobes and particle sizes*

The corresponding relative changes are illustrated in ***Figure 4.12***. The most prominent relative increase is observed in the right middle lobe (RML) at 3 µm, reaching +35%. The left lower lobe (LLL) also demonstrates a considerable relative increase of +13.95% at 3 µm, followed by the left upper lobe (LUL) with a relative increase of +8.96% at 3 µm**.** These results emphasize that, despite small absolute changes, the lateral positioning can induce substantial relative increases in certain lung regions for smaller aerosol sizes, particularly benefiting the right middle lobe and the left lung lower regions.

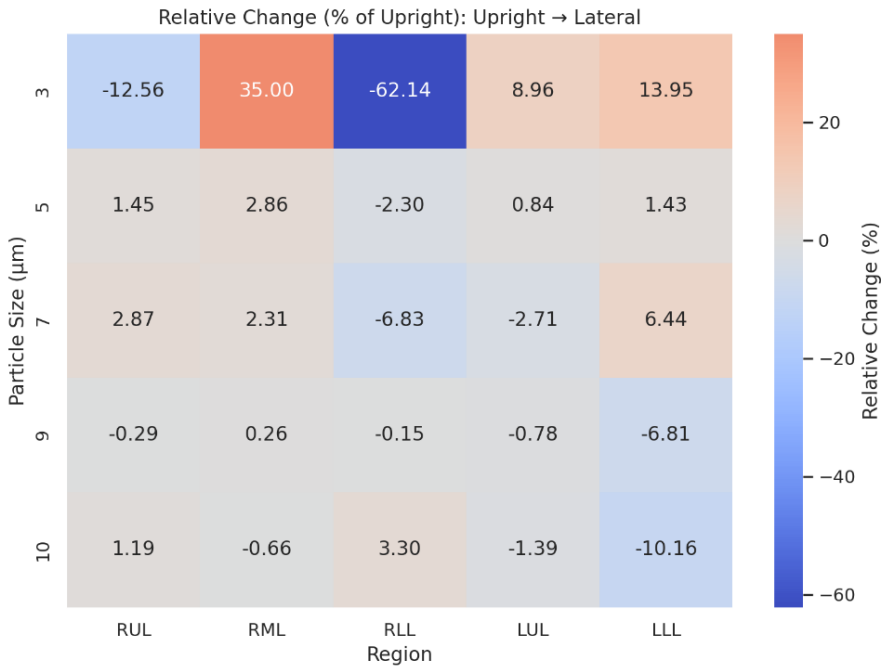


***Figure 4.12**: Heatmap of relative differences in deposition efficiency from upright to lateral orientation across lung lobes and particle sizes*

The absolute differences in deposition efficiency between dorsal and lateral orientations are presented in ***Figure 4.13***. In this transition, positive changes are generally limited and of small magnitude. The right upper lobe (RUL) exhibits the highest positive change at 7 µm (+0.36%), while the right lower lobe (RLL) shows no positive changes at any particle size. The right middle lobe (RML) shows small positive changes across sizes but remains low overall. For the left lower lobe (LLL)**,** a minor positive change is observed only at 7 µm (+0.33%), while the left upper lobe (LUL) shows no positive change across any particle size in this transition.

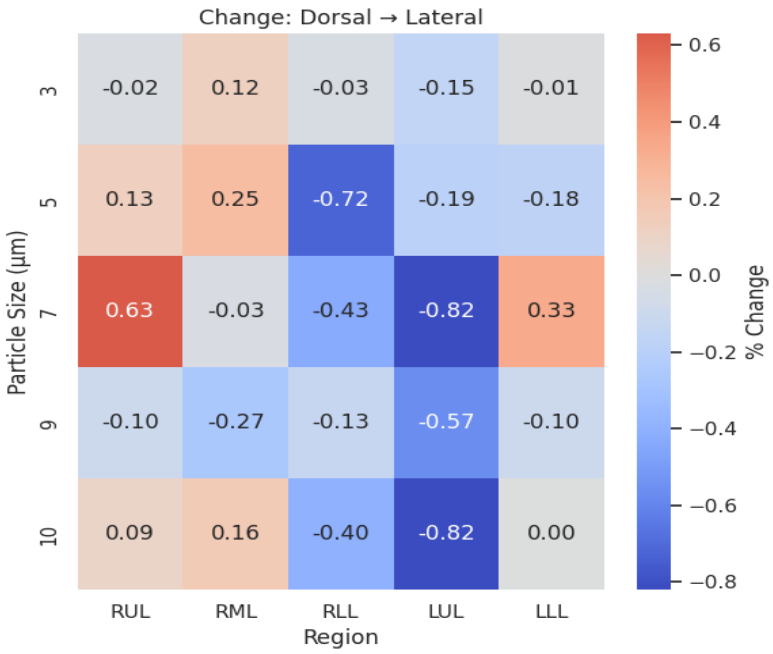


***Figure 4.13**: Heatmap of absolute differences in deposition efficiency from dorsal to lateral orientation across lung lobes and particle sizes*

The corresponding relative changes are illustrated in ***Figure 4.14***. The most significant relative increase is found in the right middle lobe (RML)**,** reaching +16.67%. Additionally, the left lower lobe (LLL**)** shows a notable relative increase of +9.51% at 7 µm. These findings suggest that dorsal-to-lateral transition induces only minimal deposition enhancements overall, with modest benefits appearing primarily in the right middle lobe and left lower lobe at specific particle sizes**.**

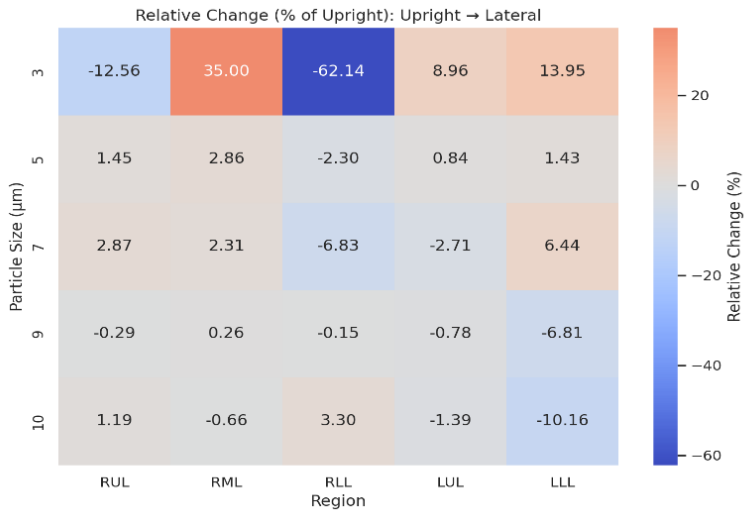


***Figure 4. 14**: Heatmap of relative differences in deposition efficiency from upright to lateral orientation across lung lobes and particle sizes*

Overall, the posture-induced changes in regional deposition efficiency reveal that although absolute differences are often small, relative changes can be significant for certain lobes and particle sizes. Smaller particles (particularly at 3 μm) demonstrate the highest sensitivity to orientation shifts, with the right middle lobe (RML) and left lower lobe (LLL) frequently showing notable relative increases. The observed variations underscore the importance of considering both absolute and relative deposition changes when evaluating the influence of body posture on targeted aerosol delivery.

4.5 Dominant Orientation for Regional Deposition

To further summarize the influence of body posture on regional aerosol deposition, the dominant orientation for each lung region and particle size is identified and presented in ***Figure 4.15***. This representation highlights, for each combination of particle size and lobe, which body position results in the highest deposition efficiency.

The analysis reveals several notable trends. For smaller particles (3 μm and 5 μm), the lateral position tends to dominate deposition in the right middle lobe (RML) and right upper lobe (RUL), whereas the dorsal position shows dominance in several other lobes, including LUL and LLL. At 7 μm**,** deposition patterns begin to shift, with dorsal positioning emerging as dominant across multiple lobes, particularly in the left lung. For larger particles (9 μm and 10 μm), the dorsal orientation becomes increasingly dominant for most lung regions, except for some lobes such as RML and LLL, where upright positioning shows the highest deposition. These results demonstrate that optimal body posture for maximizing aerosol deposition is not uniform but highly dependent on both the particle size and the target lung region. This highlights the potential to fine-tune inhalation therapy strategies by considering posture in conjunction with particle size to improve targeted delivery outcomes.

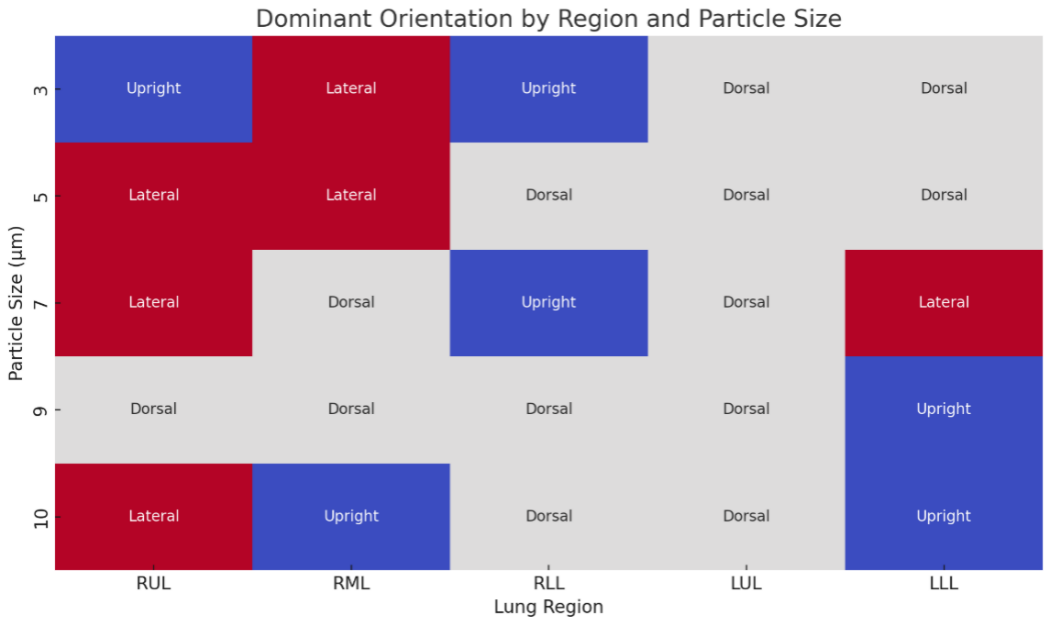


***Figure 4. 15**: Dominant body orientation for maximum deposition efficiency across lung lobes and particle sizes*

4.6 Discussion

This study investigated the effects of particle size and body orientation on regional aerosol deposition using a realistic human lung model and transient inhalation profile. The results provide several meaningful insights into aerosol behavior in the respiratory system, while also revealing limitations and trade-offs associated with the modeling choices.

The most consistent finding across all orientations was the strong dependence of deposition efficiency on particle size. Deposition increased non-linearly with size, with the most significant gains observed between 3 µm and 7 µm, beyond which a plateauing behavior emerged. This trend reflects the growing influence of inertial impaction and gravitational sedimentation as particle mass increases. Such size-dependent behavior is a well-established phenomenon and has been reported in a wide range of studies using both idealized and anatomical models.

In addition, the results showed that the right lung consistently had higher deposition than the left lung across all particle sizes and body positions. This matches what is commonly found in other studies and is likely due to natural differences in lung anatomy. The right lung has a larger volume and straighter airways, which makes it easier for particles to travel there. While we cannot make direct comparisons with previous studies because this study uses a unique combination of realistic lung shape, breathing pattern, and body position, the overall trends are similar to what is reported in existing research.

Despite the valuable findings, this study has several limitations that must be acknowledged. One key limitation is the assumption of a constant breathing profile across all body orientations.

In reality, posture can influence lung compliance and respiratory mechanics, potentially altering the inhalation flow rate and distribution. However, given the focus on gravitational and inertial effects and the relatively small expected impact of posture on the breathing waveform, this assumption is considered a reasonable simplification.

Another important limitation is the exclusion of the mouth-throat and laryngeal regions from the simulation domain. These upper airway sections are known to cause significant particle losses due to inertial impaction, especially for larger aerosols. As a result, the total deposition efficiencies reported here are not representative of complete respiratory tract deposition. Nonetheless, this modeling choice provides a strategic benefit: by bypassing the upper airway losses, the simulation allows a larger fraction of particles to reach the tracheobronchial tree, enabling clearer observation of how gravity and airflow dynamics affect deposition in the lower lungs.

This compromise offers insights that would otherwise be masked by upstream losses. Moreover, considering that excessive deposition in the mouth-throat region reduces the effectiveness of inhaled drugs, this study can offer guidance for the development of advanced inhalation devices. If aerosol delivery systems can be engineered to bypass or minimize upper airway deposition, the findings of this study would become highly relevant for optimizing drug delivery to targeted regions of the lung.

In summary, this study demonstrates how particle size and body posture interact to shape aerosol deposition patterns in the lungs. The findings confirm trends widely observed in the literature, such as the size-dependent increase in deposition efficiency and the dominance of the right lung in deposition, while also introducing a novel perspective by evaluating posture effects using realistic geometry and breathing. The insights gained here have implications for both respiratory drug delivery and inhalation exposure assessments, and they highlight the potential benefits of integrating posture control and device optimization into therapeutic strategies.

Chapter 05

Conclusion

This study investigated the impact of body orientation and particle size on aerosol deposition in a realistic human lung model, utilizing a realistic aerosol breathing profile. Simulations were performed for upright, dorsal, and lateral postures with particle sizes ranging from 3 µm to 10 µm.

The results showed that deposition efficiency increases significantly with particle size, with the most rapid increase observed between 3 µm and 7 µm, after which the rate of increase slows down. Although the overall deposition did not vary greatly across body orientations, regional deposition patterns showed notable changes. The right lung consistently received more aerosol than the left lung in all postures and across all particle sizes. In addition, the upper lobes of both lungs demonstrated higher deposition than the lower lobes, especially for larger particles. These findings suggest that body orientation can influence the distribution of inhaled particles within the lungs, particularly for smaller particles. This insight could be useful for optimizing targeted drug delivery, especially if inhalation devices can be designed to reduce losses in the upper airway and direct more aerosol into specific lung regions.

While the exclusion of mouth-throat region limits the accuracy of total deposition values, it allowed clearer observation of how particle dynamics interact with lung geometry and gravity. Overall, this study provides a foundation for future research aimed at improving aerosol delivery strategies through posture control and particle design. Further work could include complete airway geometry, variable breathing conditions, and experimental validation to enhance the applicability of the results.

References

[1] E. R. a. E. R. W. Weibel, "Principles and methods of morphometry," *Morphometry of the human lung*, pp. 9-39, 1963.

[2] M. M. N. L. Y. O. S. a. A. F. Estaji, "Aerosol dosimetry in the whole conducting zone of a murine left-lung using CF-PD and LSFM images," *Journal of Aerosol Science*, vol. 181, p. 106425, 2024.

[3] S. A. O. K. M. Y. Z. A. T. A. S. S. A. e. a. Nannu Shankar, "Cellular responses of lung cells cultured at an air-liquid interface are influenced by spatial nanoparticle deposition patterns in an in vitro aerosol exposure system," *Aerosol Science and Technology* , pp. 1-12, 2024.

[4] A. M. H. a. P. R. Aboelezz, "An Investigation Into the Impact of Simplified Lung Airway Models on Respirable Dust Particle Deposition Using CFD and Wind Tunnel Testing," *In Fluids Engineering Division Summer Meeting*, vol. 88131, 2024.

[5] "High-Flow Nasal Aerosol Therapy; Regional Aerosol Deposition and Airway Responsiveness.," *Journal of Aerosol Medicine and Pulmonary Drug Delivery*, vol. 37, pp. 338-345, 2024.

[6] "Aerosol Inhalation of Gene Delivery Therapy for Pulmonary Diseases," *Biomolecules*, vol. 14.8, p. 904, 2024.

[7] W. D. e. a. Bennett, "Regional deposition and retention of particles in shallow, inhaled boluses: effect of lung volume," *Journal of applied physiology* , pp. 168-173, 1999.

[8] G. S. K. Z. J. B. C. K. J. H. W. S. WD Bennett, "Regional deposition and retention of particles in shallow, inhaled boluses: effect of lung volume," *Journal of applied physiology*, 1999.

[9] S. Verbanck, "Implications of left-to-right lung ventilation heterogeneity.," *Journal of Applied Physiology*, pp. 1150-1151, 2000.

[10] J. Y. Z. X. C. Y. C. Y. Z. a. Z. J. Huang, "Droplet deposition dynamics in a realistic three-dimensionally printed human upper airway: An in vitro study.," *Physics of Fluids*, 2024.

[11] M. P. D Kundu, "Asymmetric lung increases particle filtration by deposition," *Scientific Reports*, 2023.

[12] Y. a. Y.-S. C. Zhou, "Particle deposition in a cast of human tracheobronchial airways.," *Aerosol Science and Technology*, pp. 492-500, 2005.

[13] R. a. W. H. Winkler-Heil, "Modeling particle deposition in the Balb/c mouse respiratory tract," *Inhalation toxicology*, 180-191.

[14] J. e. a. Wedel, "Anatomy matters: The role of the subject-specific respiratory tract on aerosol deposition—A CFD study," *Computer Methods in Applied Mechanics and Engineering*, p. 115372, 2022.

[15] J. K. e. a. Mutuku, "Influence of Bifurcation Morphology on Exercise-Induced PAH Deposition in the Lungs: A Computational Modeling Approach for Air Quality Research.," *Biomechanics and Modeling in Mechanobiology* , pp. 1-18, 2025.

[16] H. e. a. Combs, "Design and fabrication of a three-dimensional asymmetric neonate lung model to study surfactant transport in airways.," *Innovation and Emerging Technologies*, p. 2450006, 2024.

[17] H. e. a. Xiao, "Multi-scale modeling of aerosol transport in a mouth-to-truncated bronchial tree system.," *Computers in Biology and Medicine* , p. 109292, 2024.

[18] A. M. H. a. P. R. Aboelezz, "An Investigation Into the Impact of Simplified Lung Airway Models on Respirable Dust Particle Deposition Using CFD and Wind Tunnel Testing.," *In Fluids Engineering Division Summer Meeting*, vol. 88131, 2024.

[19] H. J. Z. a. L. L. Ziang, "Framework for lung CT image segmentation based on UNet++," *arXiv preprint arXiv*, 2025.

[20] M. e. a. Gouveia, "Comparing 2D and 3D Feature Extraction Methods for Lung Adenocarcinoma Prediction Using CT Scans: A Cross-Cohort Study," *Applied Sciences*, p. 1148, 2025.

[21] J. e. a. Yang, "Fast3R: Towards 3D Reconstruction of 1000+ Images in One Forward Pass," *arXiv preprint arXiv*, 2025.

[22] H. e. a. Sadafi, "Validation of computational fluid dynamics models for airway deposition with SPECT data of the same population," *Scientific Reports*, vol. 14, no. 1, 2024.

[23] G. e. a. Tian, "Validating CFD predictions of pharmaceutical aerosol deposition with in vivo data.," *Pharmaceutical research*, vol. 32, pp. 3170-3187, 2015.

[24] B. a. K. R. L. Ma, "CFD simulation of aerosol deposition in an anatomically based human large–medium airway model," *Annals of biomedical engineering*, vol. 37, pp. 271-285, 2009.

[25] A. e. a. Laycock, "Knock-out mouse models and single particle ICP-MS reveal that SP-D and SP-A deficiency reduces agglomeration of inhaled gold nanoparticles in vivo without significant changes to overall lung clearance.," *Nanotoxicology*, pp. 1-22, 2025.

[26] P. G. S. C. K. a. C.-L. L. Koullapis, "Computational fluid dynamics (CFD) simulations of aerosol deposition in the lungs.," *Ninth International Symposium on Turbulence and Shear Flow Phenomena*, 2015.

[27] M. J. Oldham, "Challenges in validating CFD-derived inhaled aerosol deposition predictions," *Inhalation Toxicology*, vol. 18, pp. 781-786, 2006.

[28] G. e. a. Tian, "Validating CFD predictions of pharmaceutical aerosol deposition with in vivo data," *Pharmaceutical research*, vol. 32, pp. 3170-3187, 2015.

[29] M. M. Rahman, "Numerical study of nanoscale and microscale particle transport in realistic lung models with and without stenosis," *International Journal of Multiphase Flow*, 2021.

[30] A. N. W. D. S. M. &. D. W. López, "CFD study of Jet Impingement Test erosion using Ansys Fluent® and OpenFOAM®," *Computer Physics Communications*, 197.

[31] A. B.-P. R. A.-O. R. &. F.-T. A. Pandal-Blanco, "Implementation of a specific boundary condition for a simplified symmetric single-path CFD lung model with OpenFOAM," *Biomechanics and Modeling in Mechanobiology*, vol. 18, no. 6, p. 1759–1771, 2019.

[32] W. &. Vågsæther, "Comparison of OpenFoam and ANSYS Fluent. Compitational Fluid Dynamic Simulation of Gas-Gas Single Phase Mixing with and without Static Mixer," *IEEE,* 2016.

[33] C.-N. D. F. &. v. W. B. Xiao, "Fully-coupled pressure-based finite-volume framework for the simulation of fluid flows at all speeds in complex geometries," *Journal of Computational Physics,* p. 91–130, 2017.

[34] G. C. K. R. P. &. S. B. K. Cheng, "High fidelity field simulations using density and pressure based approaches," *Applied Numerical Mathematics,* vol. 55, no. 3, p. 264–282, 2005.

[35] L. S. W. &. D. M. Mangani, "Comparing the performance and accuracy of a pressure-based and a density-based coupled solver," 2016.

[36] K. e. al., " A next-generation discontinuous galerkin fluid dynamics solver with application to high-resolution lung airflow simulations.," *IEEE International Conference on High Performance Computing, Data, and Analytics,* 2021.

[37] K. e. al., " Computational fluid dynamics (CFD) Simulations of aerosol deposition in the lungs," 2015.

[38] N. K. P. P. &. A. A. Nowak, "Computational fluid dynamics simulation of airflow and aerosol deposition in human lungs," *Annals of Biomedical Engineering,* vol. 31, no. 4, p. 374–390, 2003.

[39] K. K. R. N. D.-K. &. I. K. Kuga, "Effect of transient breathing cycle on the deposition of micro and nanoparticles on respiratory walls," *Computer Methods and Programs in Biomedicine,* 2023.

[40] M. E. H. A. G. &. A. O. Kiasadegh, "Transient numerical simulation of airflow and fibrous particles in a human upper airway model," *Journal of Aerosol Science,* 2020.

[41] Z. C. K. a. C. S. K. Zhang, "Cyclic micron-size particle inhalation and deposition in a triple bifurcation lung airway model," *Journal of Aerosol Science,* vol. 33, 2002.

[42] A. e. al, "Dry powder inhaler aerosol deposition in a model of tracheobronchial airways: Validating CFD predictions with in vitro data," *International Journal of Pharmaceutics,* 2020.

[43] L. T. &. L. P. W. Holbrook, "Validating CFD predictions of highly localized aerosol deposition in airway models: In vitro data and effects of surface properties," *Journal of Aerosol Science,* 2013.

[44] N. e. al., "Inertial and gravitational effects on aerosol deposition in the conducting airways," *Journal of Aerosol Science,* 2018.

[45] C. Darquenne, "Aerosol deposition in the human lung in reduced gravity," *Journal of Aerosol Medicine and Pulmonary Drug Delivery,* vol. 27, no. 3, p. 170–177, 2014.

[46] X. F. Y. Z. W. S. B. &. T. F. Chen, "Numerical investigation of particle deposition in a triple bifurcation airway due to gravitational sedimentation and inertial impaction.," *Powder Technology,* 2018.

[47] Y. Y. Y. G. Y. G. Y. &. K. Y. Yu, "Aerosol deposition in circular tubes with simultaneous consideration of diffusion and sedimentation.," *Journal of Aerosol Science,* 2021.

[48] W. e. al, "A 3D Monte Carlo Simulation for Aerosol Deposition onto Horizontal Surfaces by Combined Mechanisms of Brownian Diffusion and Gravity Sedimentation," *Atmosphere,* vol. 13, no. 9, 2022.

[49] A. B. J. P. &. F. J. J. Tsuda, " Effects of alveolated duct structure on aerosol kinetics. II. Gravitational sedimentation and inertial impaction," *Journal of Applied Physiology,* vol. 76, no. 6, 1994.

[50] O. e. al, "Particle Deposition in Human Lung Airways: Effects of Airflow, Particle Size, and Mechanisms," *Aerosol and Air Quality Research,* vol. 20, no. 12, 2020.

[51] "A Numerical Simulation of the Airflow and Aerosol Particle Deposition in a Realistic Airway Model of a Healthy Adult.," *Journal of Pharmaceutical Sciences,* vol. 111, no. 11, p. 3130–3140, 2022.

[52] M. S. S. S. C. S. E. &. G. Y. Islam, "Numerical investigation of diesel exhaust particle transport and deposition in up to 17 generations of the lung airway," 2016.

[53] M. C. Y. &. S. S. Sommerfeld, "Potential and constraints for the application of CFD combined with Lagrangian particle tracking to dry powder inhalers.," *European Journal of Pharmaceutical Sciences,* vol. 128, p. 299–324, 2019.

[54] M. R. M. M. M. Z. M. &. F. S. Saidi, "Comparison between Lagrangian and Eulerian approaches in predicting motion of micron-sized particles in laminar flows," *Atmospheric Environment,* vol. 89, p. 199–206, 2014.

[55] J. S. A. &. J. T. Xiao, "Development and Validation of Two-Way Fluid-Particle Coupling in Turbulent Flows for a CFD Code," 2013.

[56] C. C. S. P. G. &. A. A. Venditti, "Comparison between one- and two-way coupling approaches for estimating effective transport properties of suspended particles undergoing Brownian sieving hydrodynamic chromatography," *Physics of Fluids,* vol. 34, no. 4, 2022.

[57] B. &. A. S. Soni, "2.6.1 Steady versus Unsteady Airflow Conditions in Aerosol Deposition," 2013.

[58] A. P. K. J. S. O. J. M. C. F. &. A. A. Farghadan, " Particle transport and deposition correlation with near-wall flow characteristic under inspiratory airflow in lung airways.," *Computers in Biology and Medicine,* 2020.

[59] P. P. M. N. &. A. A. Kakade, "Computational fluid dynamics simulation of airflow and aerosol deposition in human lungs," in *International Conference of the IEEE Engineering in Medicine and Biology Society*, 2002.

[60] R. K. K. Kizuka, "Regional Deposition of Inhaled Nano- to Microscale Particles in Realistic Upper Respiratory Tract Model Under Steady and Transient Breathing Conditions," *springer Nature,* p. 1673–1676, 2023.

[61] A. R. E. A. R. S. B. &. A. M. Esmaeili, " Numerical simulation of ellipsoidal particles deposition in the human nasal cavity under cyclic inspiratory flow," *Journal of The Brazilian Society of Mechanical Sciences and Engineering,* vol. 42, no. 5, p. 1–13, 2020.

[62] L. e. al., "CFD Guided Optimization of Nose-to-Lung Aerosol Delivery in Adults: Effects of Inhalation Waveforms and Synchronized Aerosol Delivery.," *Pharmaceutical Research,* 2020.

[63] M. Z. M. M. R. ,. K. D. Arman Mirzaaghaian, "Numerical simulation of targeted drug delivery to different regions of realistic human lung model under realistic aerosol breathing condition," *Powder Technology,* vol. 444, 2024.

[64] A. C. F. &. A. A. Farghadan, "Topological analysis of particle transport in lung airways: Predicting particle source and destination.," *Computers in Biology and Medicine,* 2019.

[65] "A Numerical Simulation of the Airflow and Aerosol Particle Deposition in a Realistic Airway Model of a Healthy Adult," *Journal of Pharmaceutical Sciences,* vol. 111, no. 11, p. 3130–3140, 2022.

[66] G. H. R. R. V. A. C. C. &. B. A. Spasov, " A Critical Analysis of the CFD-DEM Simulation of Pharmaceutical Aerosols Deposition in Upper Intra-Thoracic Airways: Considerations on Aerosol Transport and Deposition," *Pharmaceutics,* 2024.

[67] P. W. T. G. K.-H.-D. N. &. H. Longest, "Validating Whole-Airway CFD Predictions of DPI Aerosol Deposition at Multiple Flow Rates," *Journal of Aerosol Medicine and Pulmonary Drug Delivery,* vol. 29, no. 6, p. 461–481, 2016.

[68] L. L. X. L. G. C. &. G. J. A. S. Augusto, "A cfd study of deposition of pharmaceutical aerosols under different respiratory conditions," *Brazilian Journal of Chemical Engineering,* vol. 33, no. 3, p. 549–558, 2016.

[69] B. P. O. T. &. O. G. Asgharian, "A modeling study of the effect of gravity on airflow distribution and particle deposition in the lung. Inhalation Toxicology," *Inhalation Toxicology,* vol. 18, p. 473–481, 2006.

[70] P. S. F. S. J. O. B. &. K. S. C. Koullapis, "Towards whole-lung simulations of aerosol deposition: A model of the deep lung," *Journal of Aerosol Science,* 2020.

[71] C. L. W. J. E. F. J. M. C. R. A. &. G. R. W. Darquenne, "Total and regional deposition of inhaled aerosols in supine healthy subjects and subjects with mild-to-moderate COPD," *Journal of Aerosol Science,* 2016.

[72] C. N. D. C. &. P. G. K. Mills, " Mode shift of an inhaled aerosol bolus is correlated with flow sequencing in the human lung," *Journal of Applied Physiology,* vol. 92, no. 3, p. 1232–1238, 2002.

[73] L. P. F. L. C. B. D. C. G. A. M. R. M. A. &. D. d. A. A. Alcoforado, "nfluência da variação dos decúbitos laterais na deposição pulmonar de aerossol Influence of change in lateral decubitus on pulmonary aerosol deposition," 2011.

[74] R. C. Z. K. L. B. W. D. P. G. K. &. D. C. Sá, "Regional Ventilation Is the Main Determinant of Alveolar Deposition of Coarse Particles in the Supine Healthy Human Lung During Tidal Breathing," *Journal of Aerosol Medicine and Pulmonary Drug Delivery,* vol. 30, no. 5, p. 322–331, 2017.

[75] S. L. &. B. J. D. Sneddon, "Persistent apex to base gradients of aerosol deposition in rats," *Respiration Physiology,* vol. 46, no. 2, p. 113–124, 1981.

[76] C. B. M. G. O. J. M. B. E. C. O. I. M. S. M. &. P. G. K. Darquenne, "Increase in relative deposition of fine particles in the rat lung periphery in the absence of gravity," *ournal of Applied Physiology*, vol. 117, 2014.

[77] R. B. N. C. P. R. M. L. &. D. C. Theunissen, "Experimental Investigation of Aerosol Deposition in Alveolar Lung Airways," 2006.

[78] S. H. E. A. &. L. C.-L. Miyawaki, "Numerical simulations of aerosol delivery to the human lung with an idealized laryngeal model, image-based airway model, and automatic meshing algorithm," *Computers & Fluids*, vol. 148, 2017.

[79] M. Hindle, "Aerosol drug delivery," *Production and Processes*, 2008.

[80] P. M. J. P. &. L. E. Diot, "Aerosols: a re-emerging treatment," *Revue De Pneumologie Clinique*, vol. 54, p. 125–134, 1998.

[81] Y. S. Cheng, "Modeling aerosol drug delivery." In Optimization of aerosol drug delivery," *Dordrecht: Springer Netherlands*, 2003.

[82] F. e. al, " Budesonide/formoterol MDI with co-suspension delivery technology in COPD: the TELOS study," *European Respiratory Journal*, vol. 52, 2018.

[83] Ostrovski, "Targeted Drug Delivery to Upper Airways Using a Pulsed Aerosol Bolus and Inhaled Volume Tracking Method," *Flow Turbulence and Combustion*, vol. 102, p. 73–87, 2019.

[84] G. e. al, "The (re)emergence of aerosol delivery: Treatment of pulmonary diseases and its clinical challenges," *Journal of Controlled Release*, vol. 379, p. 421–439, 2025.

[85] R. d. G. J. P. S. &. K. S. Xu, "Towards optimized drug delivery in simplified and patient-specific lung geometries," 2023.

[86] P. W. T. G. W. R. &. H. M. Longest, "Comparing MDI and DPI Aerosol Deposition Using In Vitro Experiments and a New Stochastic Individual Path (SIP) Model of the Conducting Airways," *Pharmaceutical Research*, vol. 29, p. 1670–1688, 2012.

[87] M. P. O. G.-B. M. I. K. Y. L. Y. &. T. J. Yousefi, "CFD simulation of aerosol delivery to a human lung via surface acoustic wave nebulization," *Biomechanics and Modeling in Mechanobiology*, vol. 16, p. 2035–2050, 2017.

[88] J. K. V. &. S. H. Suggett, "Dry Powder Inhalers (DPIs) vs Metered Dose Inhaler (MDI) with valved spacer: Using Functional Respiratory Imaging (FRI) to assess modelled lung deposition in a COPD patient," *Airway Pharmacology and Treatment*, 2022.

[89] K. &. Chen, "Effect of Inhaling Patterns on Aerosol Drug Delivery: CFD Simulation," 2008.

[90] B. F. Y. &. F. C. A. Bartlett, "Computer modeling of aerosol particle transport through lung mucosa," *bioRxiv*, 2021.

[91] E. L. K. E. L. &. F. C. A. Peterman, "Evaluating Regional Pulmonary Deposition using Patient-Specific 3D Printed Lung Models," *ournal of Visualized Experiments*, 2020.

[92] Y. Feng, "Create the Individualized Digital Twin for Noninvasive Precise Pulmonary Healthcare," 2018.

[93] J. Z. Y. C. X. F. Y. R. X. Y. M. &. D. T. Wang, "Targeted delivery of inhalable drug particles in a patient-specific tracheobronchial tree with moderate COVID-19: A numerical study," *Powder Technology,* 2022.

[94] J. K. v. S. P. Š. M. H. M. C. Y. &. R. J. Wedel, "Anatomy matters: The role of the subject-specific respiratory tract on aerosol deposition — A CFD study," *Computer Methods in Applied Mechanics and Engineering,* 2022.

[95] A. R. &. Z. P. Tahavvor, "Numerical Simulation of Transient Air Flow and Particle Deposition in a Lung and Bronchus of a Human Respiratory System," 2020.

Publications

[1] Turag Dev and Prasanjit Das, *"Numerical Study of the Impact of Body Orientation on Aerosol Deposition in a Realistic Lung Model Under Realistic Breathing Condition*," in **3rd International Conference on Mathematical Analysis and Application in Modelling 2024 (ICMAAM-2024)**, Chattogram, Bangladesh, Dec. 2024.

Full_Thesis_Turag_Dev.pdf

ORIGINALITY REPORT

16%	12%	13%	6%
SIMILARITY INDEX	INTERNET SOURCES	PUBLICATIONS	STUDENT PAPERS

PRIMARY SOURCES

1	Submitted to Chittagong University of Engineering and Technology Student Paper	1%
2	Arman Mirzaaghaian, Ming Zhao, Md. Mizanur Rahman, Kejun Dong. "Numerical simulation of targeted drug delivery to different regions of realistic human lung model under realistic aerosol breathing condition", Powder Technology, 2024 Publication	<1%
3	www.mdpi.com Internet Source	<1%
4	ouci.dntb.gov.ua Internet Source	<1%
5	ir.uiowa.edu Internet Source	<1%
6	eprints.qut.edu.au Internet Source	<1%
7	www.hindawi.com Internet Source	<1%
8	dspace.vutbr.cz Internet Source	<1%
9	Anthony J. Hickey, Heidi M. Mansour. "Inhalation Aerosols - Physical and Biological Basis for Therapy", CRC Press, 2019 Publication	<1%